MICRORNAS AND MESSENGER RNAS IN CYCLIC STRETCH INDUCED AORTIC VALVE PATHOGENESIS

A Dissertation
Presented to
The Academic Faculty

by

Md Tausif Salim

In Partial Fulfillment
of the Requirements for the Degree
Doctor of Philosophy in the
School of Chemical and Biomolecular Engineering

Georgia Institute of Technology
May 2021

MICRORNAS AND MESSENGER RNAS IN CYCLIC STRETCH INDUCED AORTIC VALVE PATHOGENESIS

Approved by:

Ajit P. Yoganathan, PhD
School of Chemical and Biomolecular Engineering
Georgia Institute of Technology

Mark R. Prausnitz, PhD
School of Chemical and Biomolecular Engineering
Georgia Institute of Technology

Hanjoong Jo, PhD
Wallace H. Coulter Department of Biomedical Engineering
Georgia Institute of Technology and Emory University

Julie A. Champion, PhD
School of Chemical and Biomolecular Engineering
Georgia Institute of Technology

Lakshmi P. Dasi, PhD
Wallace H. Coulter Department of Biomedical Engineering
Georgia Institute of Technology and Emory University

Date Approved: [April 29, 2021]

To my parents, my wife Aysha and late Dr. Nerem

ACKNOWLEDGEMENTS

First, I would like to express my gratitude to Dr. Y for giving me the opportunity to conduct research in CFM lab. I would like to convey my gratitude to Shiva for helping me sort out problems (both personal and professional) in an objective fashion. I would like to thank Joan for being my mentor and helping me sort out all my research problems. I would like to thank Nico for helping me with all the research work. I am extremely grateful to Dr. Jo for allowing me to work in his lab. I am very grateful to late Dr. Nerem for giving me helpful tips in terms of career planning. I would like to thank Dr. Dasi for joining my thesis committee after the passing of Dr. Nerem. I would like to express my gratitude to Drs. Prausnitz and Champion for being so helpful and supportive. I am extremely grateful to all CFM lab members. I wouldn't be here without my parents whose hardwork and sacrifices enabled me to reach this point in my life. Last but not the least, I would like to thank my wife Aysha for always being there for me.

TABLE OF CONTENTS

LIST OF TABLES

LIST OF FIGURES

LIST OF SYMBOLS AND ABBREVIATIONS

AV	Aortic valve
ECM	Extracellular matrix
HAVEC	Human aortic valve endothelial cell
HAVIC	Human aortic valve interstitial cell
HUVEC	Human umbilical vein endothelial cell
MSC	Mesenchymal stem cell
PAV	Porcine aortic valve
PAVIC	Porcine aortic valve interstitial cell
RT-qPCR	Real-time quantitative polymerase chain reaction
VEC	Valvular endothelial cell
VIC	Valvular interstitial cell
VSMC	Vascular smooth muscle cell

SUMMARY

Calcific aortic valve disease (CAVD) is one of the most prevalent valvular diseases among the elderly population. Unfortunately, there are no therapeutic drugs available to treat this disease. Since calcified aortic valves (AVs) have distinct miRNA and gene expression profiles compared to healthy AVs, microRNA (miRNA) and messenger RNA (mRNA) based therapies hold a lot of promise as potential drugs. In this regard, mechanosensitivity of miRNAs and mRNAs can serve as a critical criterion in identifying the most effective candidates, as it has been shown that altered mechanical environment plays a key role in AV pathogenesis. To this day, majority of the studies have focused on disturbed flow-induced changes in miRNA and mRNA expression in relation to CAVD. However, identification and functional description of stretch-sensitive miRNAs and mRNAs in CAVD are poorly studied. Hence, this work aimed to identify and functionally describe miRNAs and mRNAs that are stretch-sensitive in AV. The overall hypothesis of this dissertation was that mechanical stretch-sensitive miRNAs and mRNAs play a significant role in AV calcification. To test this hypothesis, the following aims were proposed: (1) investigate the effects of physiological (10%) and pathological (15%) cyclic stretch on miRNA expression in AV, and (2) investigate the effects of physiological (10%) and pathological (15%) cyclic stretch on mRNA expression in AV. An *ex vivo* experimental approach was adopted by cyclically stretching porcine aortic valve (PAV) tissue in an *ex vivo* stretch bioreactor. RT-qPCR was used to assess the relative expression of miRNAs and mRNAs at 10% and 15% stretch. In addition, osteogenic medium was used to induce calcification in PAV tissue. In specific aim 1, it was found that pathological

stretch upregulated miR-21-5p expression in PAV tissue compared to the physiological level. On the other hand, the expression of miR-181a, miR-181b, miR-199a-3p and miR-214 was downregulated in PAV tissue by pathological stretch compared to the physiological level. Further functional studies on miR-214 revealed that miR-214 overexpression could inhibit PAV calcification via downregulation of ATF4 expression. In specific aim 2, it was found that pathological stretch downregulated YAP1 and UBE2C mRNA expression, while it did not have any effect on the mRNA expression of SOX9, ASH2L, ROR2 and ATP1A2. When the effect of cyclic stretch on VHL and HIF1A (that constitute one of the downstream pathways of UBE2C) mRNA expression was evaluated, it was observed that pathological stretch did not significantly affect VHL and HIF1A mRNA expression. Furthermore, it was found that HIF1 inhibitor PX-478 significantly reduced PAV collagen turnover and calcification under pathological stretch. These implied that HIF1A could promote AV disease in a stretch-independent manner, while UBE2C might have more prominent stretch-sensitive downstream pathways other than VHL/HIF1A. Overall, the research work presented in this dissertation increased our understanding of the role of pathological stretch in promoting AV disease via the regulation of miRNA and mRNA expression.

CHAPTER 1. INTRODUCTION

Heart valve diseases are prevalent in more than 13.2% of the elderly population aged greater than 75 years old (Nkomo *et al*., 2006). Aortic stenosis (AS) is one of the most prevalent heart valve diseases, affecting more than 3.4% of the elderly population (Osnabrugge *et al*., 2013). When untreated, the mortality rate is about 25% per year after the onset of severe symptoms (angina, syncope, heart failure, etc.) (Ross *et al*., 1968). AS is characterized by pathological narrowing of the aortic valve (AV) opening during systole, resulting in increased pressure gradient across the valve. The narrowing of AV opening is caused by significantly thicker and stiffer AV leaflets. The higher thickness and stiffness in AV leaflets arise from pathological fibrosis and calcification of AV tissue that take place over a period of several years. Unfortunately, despite its high prevalence, there is no clear understanding of the underlying mechanism of AS pathogenesis and disease progression (Leopold *et al*., 2012).

Given the high prevalence and mortality associated with AS, there is substantial interest in developing new and more effective treatment options for these patients. However, there are currently no therapeutic drugs available to treat AS and the only treatment options are either surgical or transcatheter AV replacement (Smith *et al*., 2011; Leon *et al*., 2016). Hyperlipidemia is considered to be one of the major risk factors of calcific aortic valve disease (CAVD) (Rajamannan *et al*., 2011) and it was believed that lipid-lowering therapy (such as statin) could slow down the progression of AS. However, it was found that intensive lipid-lowering therapy could not halt the progression of CAVD or induce its regression in AS patients (Cowell *et al*., 2005). This indicated that CAVD is

highly complex and multifactorial in nature, which requires in-depth understanding of the underlying mechanism involving all contributing factors.

From a mechanistic perspective, AV controls the unidirectional flow of oxygenated blood from the left ventricle into the aorta. During each cardiac cycle, AV leaflets experience different types of mechanical forces, such as tensile stress, bending stress, shear stress, etc. (Balachandran *et al*., 2011). In healthy AVs, each of these mechanical forces remain within the physiological range. However, any chronic deviation from the physiological level may function as mechanical triggers for AV pathogenesis. For example, AV leaflets experience lower (physiological) level of tensile stretch under normotensive condition; however, under hypertensive condition, these leaflets undergo increased level of tensile stretch (Yap *et al*., 2010). Elevated mechanical stretch has been shown to induce pathological extracellular matrix (ECM) remodeling and calcification in porcine aortic valve (PAV) leaflets (Balachandran *et al*., 2009; Balachandran *et al*., 2010). Similarly, low, oscillatory shear stress (characteristic of disturbed flow) has been shown to promote pathological ECM remodeling and calcification in PAV leaflets (Sucosky *et al*., 2009; Rathan *et al*., 2011). Considering that hypertension is one of the major risk factors of CAVD (Rajamannan *et al*., 2011), it is not surprising that mechanical forces play such a critical role in AV pathogenesis and disease progression.

Over the past two decades, microRNA (miRNA) and messenger RNA (mRNA) based drugs have been considered as potential therapeutics for different diseases, such as cancer (Rupaimoole *et al*., 2017; Sahin *et al*., 2014). For example, mRNA-based technology has been used very recently to develop vaccines for coronavirus disease 2019 (COVID-19) (Polack *et al*., 2020; Baden *et al*., 2021). This indicates that miRNA and mRNA-based

therapies hold a lot of promise for other diseases as well. Especially, miRNA and mRNA-based drugs have emerged as exciting candidates for CAVD treatment (Hutcheson *et al*., 2014; Van der Ven *et al*., 2017). However, since CAVD is highly complex and multifactorial in nature, it is crucial to identify key miRNA and mRNA targets that play a significant role in AV pathogenesis. To this end, mechanosensitive miRNAs and mRNAs may be the ideal therapeutic targets for CAVD, given that mechanical forces play a critical role in AV pathogenesis (as described above). Tensile stretch, along with shear stress, is one of the major mechanical forces experienced by AV leaflets during each cardiac cyclic. Although significant deviation in either of these mechanical cues can promote AV pathogenesis, it has been shown that elevated mechanical stretch induces significantly higher AV calcification compared to low, oscillatory shear stress (Rathan, 2016). Despite that, most of the studies to date have focused on the identification of shear-sensitive miRNAs and mRNAs and their functional relations to CAVD (Rathan *et al*., 2016; Heath *et al*., 2018; Fernandez Esmerats *et al*., 2019). Therefore, it will be crucial to develop an in-depth understanding of the functional roles of stretch-sensitive miRNAs and mRNAs in CAVD. The work presented in this dissertation aims to investigate the effect of physiological and pathological cyclic stretch on different miRNA and mRNA expression in relation to CAVD. In addition, the mechanistic roles of selected miRNA and mRNA candidates in CAVD will be evaluated. For these studies, an *ex vivo* experimental approach using PAV leaflets will be employed. The research findings will help in enhancing our mechanistic understanding of AV pathogenesis and disease progression from mechanobiological point of view. Ultimately, these may help in identifying effective therapeutic targets for CAVD in the future.

CHAPTER 2. BACKGROUND

2.1 The Heart and The Cardiac Cycle

The heart is a major organ of the human body. It pumps oxygenated blood returning from the lungs to the rest of the body and deoxygenated blood from the right side of the heart to the lungs. A normal heart has four chambers – the left and right atria, and the left and right ventricles (Figure 2.1a).

The right (deoxygenated) and left (oxygenated) sides of the heart are separated by a muscular wall called the septum. The right atrium collects deoxygenated blood from the vena cavae and pumps it via the right ventricle and the pulmonary arteries to the lungs, where the blood is oxygenated. The oxygenated blood returns to the left atrium via the pulmonary veins and is pumped to the systemic circulation when the left ventricle contracts during systole.

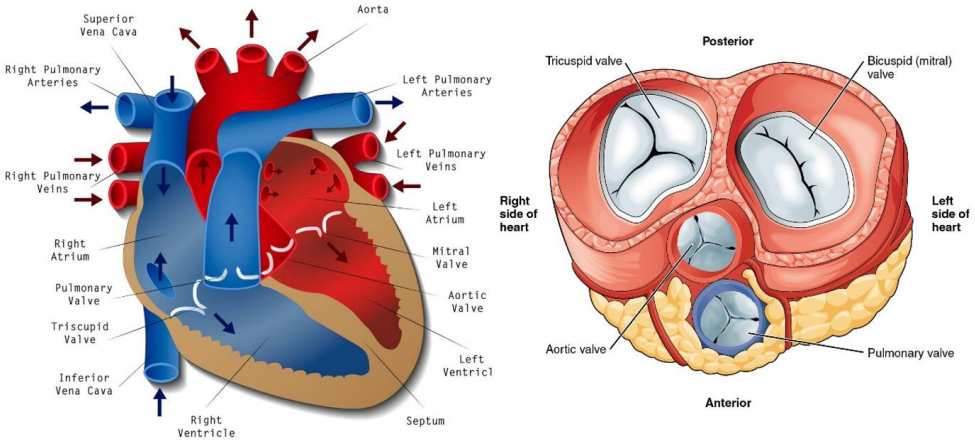

(a) Four chambers (b) Heart valves

Figure 2.1 - Anatomy of the heart.

The heart has four valves (Figure 2.1b): two on each side to maintain unidirectional flow of blood through the heart. These valves can be classified into two types based on their anatomical location: atrioventricular valves (mitral and tricuspid valve) and semilunar or outflow tract valves (aortic and pulmonary valve). The atrioventricular valves have chordae tendinae that attach to papillary muscles on the ventricular walls. This structural feature is absent in the outflow tract valves.

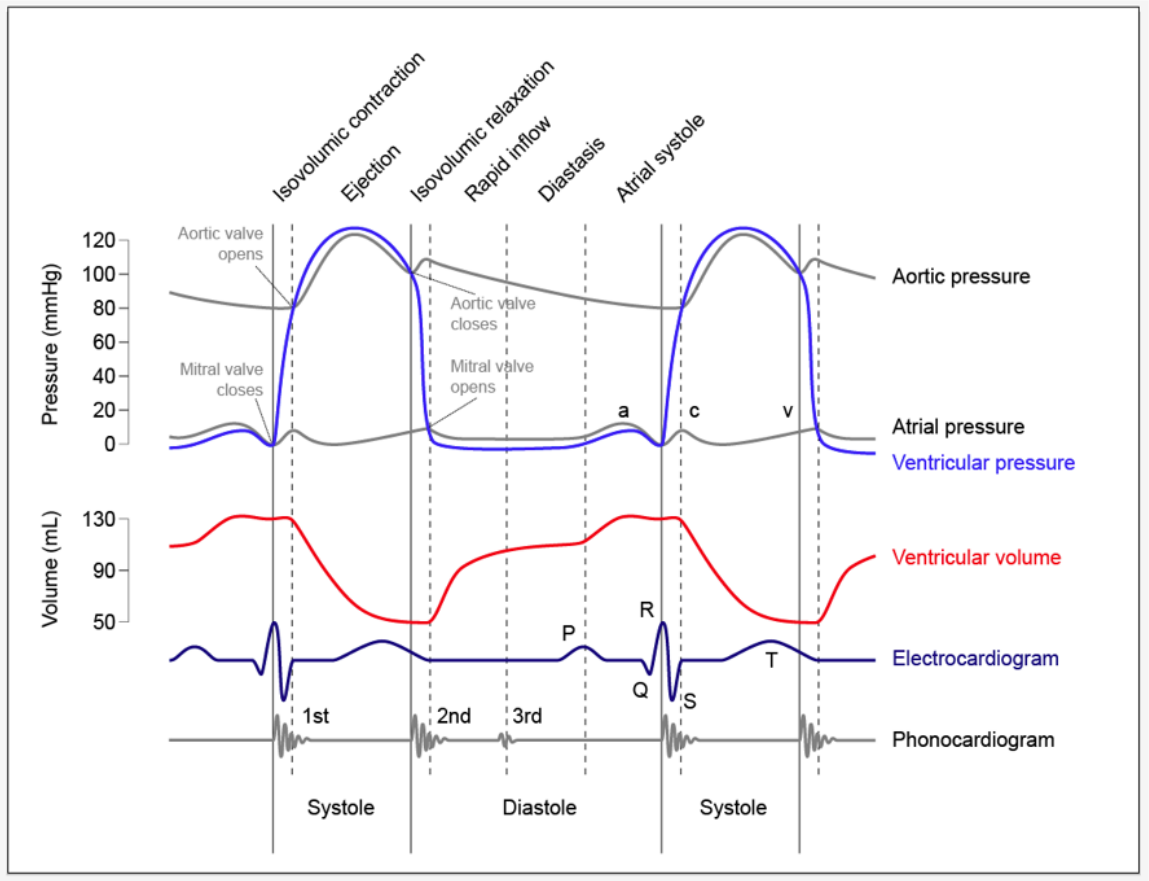

Figure 2.2 – Cardiac cycle.

A normal cardiac cycle can be divided into several distinct phases (Figure 2.2). During atrial contraction, blood is ejected from the atria into the ventricles resulting in a rise in ventricular pressure. A fourth heart sound may be heard at this juncture. At the onset of systole, ventricular isovolumic contraction occurs with the closing of the atrioventricular

valves first followed by all the valves. During this stage, the ventricular volume remains constant. In the rapid ejection phase, as soon as the pressure in the left ventricle exceeds the pressure in the aorta, the aortic valve opens and blood flows rapidly from the left ventricle into the aorta. Following rapid ejection, the rate of outflow from the ventricle decreases, and the ventricular and aortic pressures start to decrease in the reduced ejection phase.

At the end of systole, during the isovolumic relaxation phase, the ventricular ejection decreases to zero. The left ventricle pressure falls below the pressures in the aorta and pulmonary artery, which causes the aortic and pulmonary valves to close (beginning of diastolic phase). Once the ventricular pressure falls below the atrial pressure the atrioventricular valves open and rapid ventricular filling begins. During this period, the flow of blood from the aorta to the peripheral arteries continues, and the aortic pressure slowly decreases. This rapid ventricular filling phase is followed by the reduced ventricular filling phase in which a large portion of filling occurs.

2.2 The Aortic Valve (AV)

The aortic valve (AV) is situated at the aortic root and regulates blood flow from the left ventricle into the aorta. As shown in Figure 2.3, it consists of three semilunar cusps or leaflets, which are attached to a fibrous annulus embedded within the left ventricle and the septum. Two adjacent leaflets are attached at the commissures and there is an elliptical depression behind each leaflet called the sinus of Valsalva. The left and right sinuses contain ostia that lead into the left and right main coronary arteries. The third sinus does not feed a coronary artery and is called a non-coronary sinus.

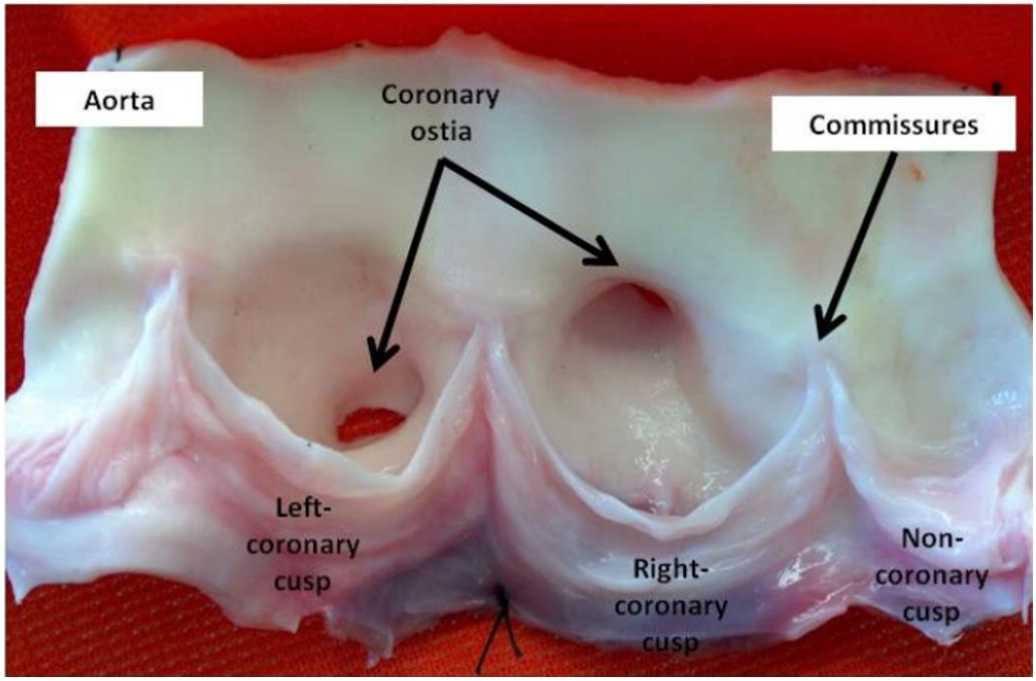

Figure 2.3 – Excised porcine AV (Balachandran *et al*., 2010).

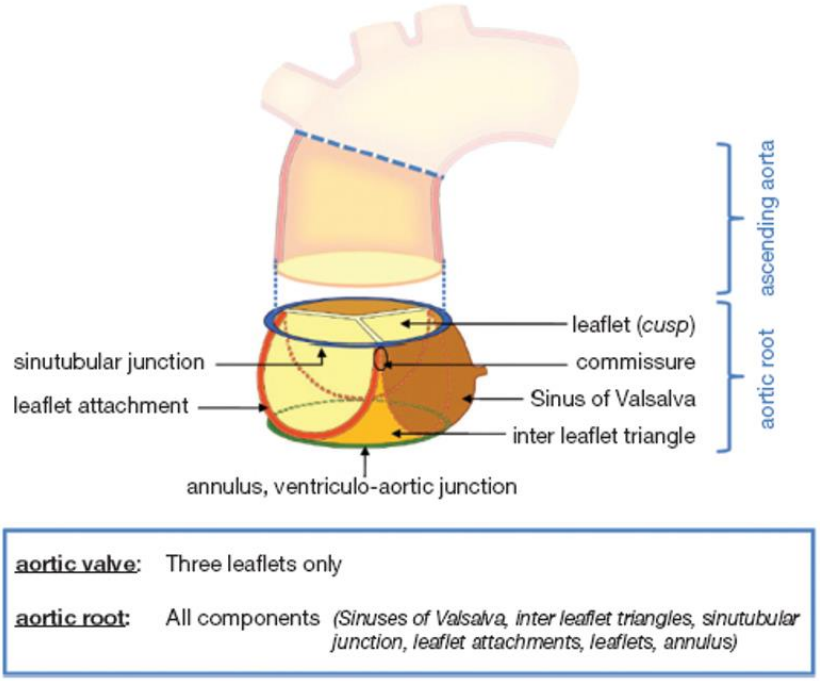

Figure 2.4 – Aortic root anatomy (Charitos *et al*., 2013).

Based on their respective anatomical positions, the three AV leaflets are thereby named the left coronary cusp (LCC), the right coronary cusp (RCC) and the non-coronary

cusp (NCC). The basal regions of the leaflets are attached to the sinuses of Valsalva, whereas the sinotubular junction (STJ) connects the sinuses to the aorta (Figure 2.4). Hence, the three leaflets, in combination with the sinuses of Valsalva, form the functional unit of the aortic valve.

2.3 Structure of the AV Leaflet

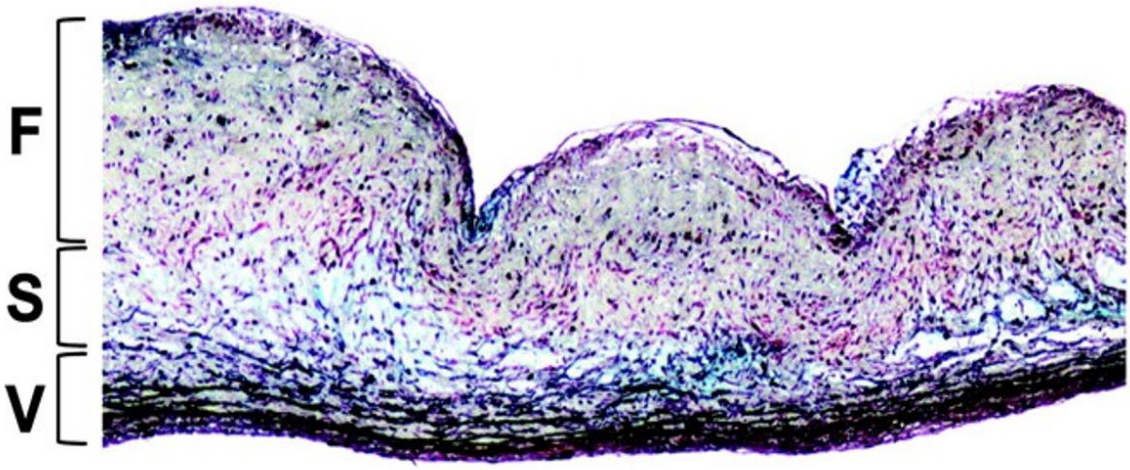

Figure 2.5 – Normal porcine AV leaflet stained with Movat pentachrome, demonstrating the trilaminar structure [F = Fiborsa, S = Spongiosa, and V = Ventricularis] (Chen *et al*., 2011).

The AV leaflets are lined with one layer of endothelial cells (ECs) on both the aortic (leaflet surface facing the aorta) and ventricular (leaflet surface facing the left ventricle) sides. In the interior region, the leaflets are populated with interstitial cells (ICs), which represent the most abundant cell type in AV. Each leaflet consists of three distinct layers, namely, the fibrosa, the spongiosa and the ventricularis. The fibrosa and the ventricularis are located immediately below the endothelial layer on the aortic and ventricular surfaces of the leaflet, respectively. The spongiosa lies between the fibrosa and the ventricularis (Figure 2.5).

The fibrosa provides the major load-bearing capacity of the valve leaflet (Wiltz *et al*., 2013). It is mainly composed of circumferentially oriented collagen fibers, which are interconnected with radially aligned elastin fibers. The ventricularis, on the other hand, primarily consists of elastin fibers. Elastin helps with restoring the crimped state of collagen fibers via its recoil action. The spongiosa is mainly composed of glycosaminoglycans and proteoglycans. It works as a lubricating layer between the fibrosa and the ventricularis to promote flexibility. It also dampens the vibrations arising from a closing valve and prevents delamination.

2.4 AV Cell Biology

The cells of the aortic valve can be broadly categorized into two classes:

(i) Endothelial cells (ECs): Cells that line the surface of AV leaflets, and

(ii) Interstitial cells (ICs): Cells that populate the interior region of AV leaflets.

Homeostasis of both cell types is required to maintain physiological functioning of AV. Pathological alteration in one cell type can induce similar adverse alteration in the other cell type, which would eventually lead to AV disease (Figure 2.6).

2.4.1 Endothelial Cells

Valvular endothelial cells (VECs) form a monolayer on the aortic and ventricular surfaces of the aortic valve. Interestingly, the preferential orientation of these cells is perpendicular to the direction of blood flow (Deck *et al*., 1986), which contrasts with the parallel alignment of vascular endothelial cells (Langille *et al*., 1981). These imply a significant difference in the mechanical stresses experienced by the valvular and vascular

endothelial cells (Butcher *et al*., 2004), which is further emphasized by their distinct transcriptional profiles (Butcher *et al*., 2006).

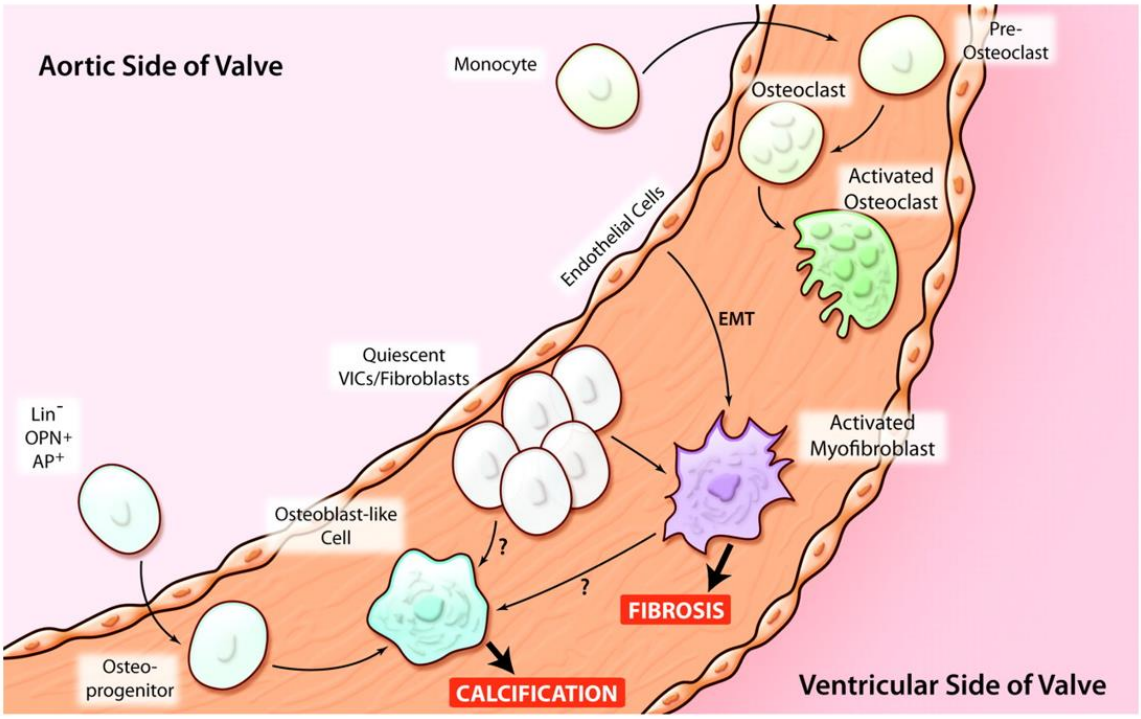

Figure 2.6 – Pathological alteration in either cell type (endothelial or interstitial) can lead to AV disease (Miller *et al*., 2011).

In a co-culture model, VECs have been shown to promote a more quiescent phenotype of valvular interstitial cells (VICs) (Butcher *et al*., 2006). Pathological alteration in extracellular matrix (ECM) composition prompts VECs to undergo endothelial-to-mesenchymal transformation (EndMT) (Dahal *et al*., 2017), leading to AV disease. Additionally, endothelial nitric oxide synthase (eNOS) has been shown to protect against aortic valve fibrosis (El Accaoui *et al*., 2014).

Oscillatory shear stress, as experienced by VECs on the fibrosa side, causes upregulation of EndMT genes (Mahler *et al*., 2014). While EndMT represents an essential process during embryogenesis, it is believed that dysregulated EndMT contributes to the initiation

and progression of AV disease (Chakraborty *et al*., 2010). Interestingly, Rathan *et al*. (2011) showed that exposure of fibrosa to low oscillatory shear stress results in much higher AV calcification compared to the physiological level.

VECs have been also found to exhibit side-specificity in gene expression under shear stress conditions (Holliday *et al*., 2011), emphasizing the significantly different shear stress profiles on the fibrosa and ventricularis sides of AV in vivo (Kvitting *et al*., 2004; Markl *et al*., 2005). These side-specific and shear-dependent transcriptional profiles may underlie the observed preferential AV calcification on the fibrosa side (Chen *et al*., 2011).

2.4.2 Interstitial Cells

Valvular interstitial cells (VICs) represent the majority of cell population in aortic valve. These cells are heterogeneous in nature, comprising of specific cell phenotypes (such as smooth muscle cell, fibroblast and myofibroblast). Interstitial cells (ICs) play a crucial role in maintaining the physiological function of aortic valve through the regulation of extracellular matrix (ECM) protein synthesis and extracellular matrix remodeling (Taylor *et al*., 2003). However, under pathological conditions (such as hemodynamic stress), these cells transform into an abnormally activated state from the regular quiescent state and promote the initiation and progression of aortic valve disease (Liu *et al*., 2007).

Interestingly, VICs have been shown to suppress endothelial-to-mesenchymal transformation (EndoMT) (Shapero *et al*., 2015) and calcification (Hjortnaes *et al*., 2015) of valvular endothelial cells (VECs). Hence, it is evident that VICs regulate the physiological function of VECs via cell-cell interactions.

VICs exhibit significantly different gene expression profiles under different pressure conditions (Warnock *et al*., 2011), matrix elasticity (Ma *et al*., 2017), stiffness (Mabry *et al*., 2016), etc., representing varying degree of myofibroblastic activation. Therefore, mechanical forces have a predominant role in modulating the phenotypic switch of interstitial cells.

Several genes have been reported to suppress calcification of VICs, such as Interleukin-37 (IL-37) (Zeng *et al*., 2017), Klotho (Li *et al*., 2017), Autophagy Related 7 (ATG7) (Deng *et al*., 2017), etc. On the other hand, genes like Neurotrophin 3 (NTF3) (Yao *et al*., 2017), Dipeptidyl Peptidase 4 (DPP4) (Choi *et al*., 2017), High Mobility Group Box 1 (HMGB1) (Shen *et al*., 2017), etc. promote VIC calcification. So, these highlight the complex nature of VIC function and its pathological activation and progression toward aortic valve calcification.

2.5 AV Tissue Mechanics and Hemodynamics

AV tissues exhibit viscoelasticity and highly non-linear stress-strain behavior (Billiar *et al*, 2000; Billiar *et al*, 2000). The internal configuration of the fiber network in AV continuously undergoes strain-induced changes, which involve straightening of highly crimped collagen fibers and rotation of these fibers toward the axis of stretch (Sacks *et al*., 2007). The AV leaflets experience tensile and bending stresses during the cardiac cycle (Figure 2.7). Interestingly, majority of the stresses and strains occur during diastole and early systole. The total stresses, as a combination of bending and membrane stretching, were found to be in the order of 50 kPa during systole and 500 kPa during diastole. These

result into a 10% leaflet stretching in the circumferential direction from peak systole to peak diastole (Thubrikar *et al*., 1986; Thubrikar *et al*., 1986; Thubrikar *et al*., 1979).

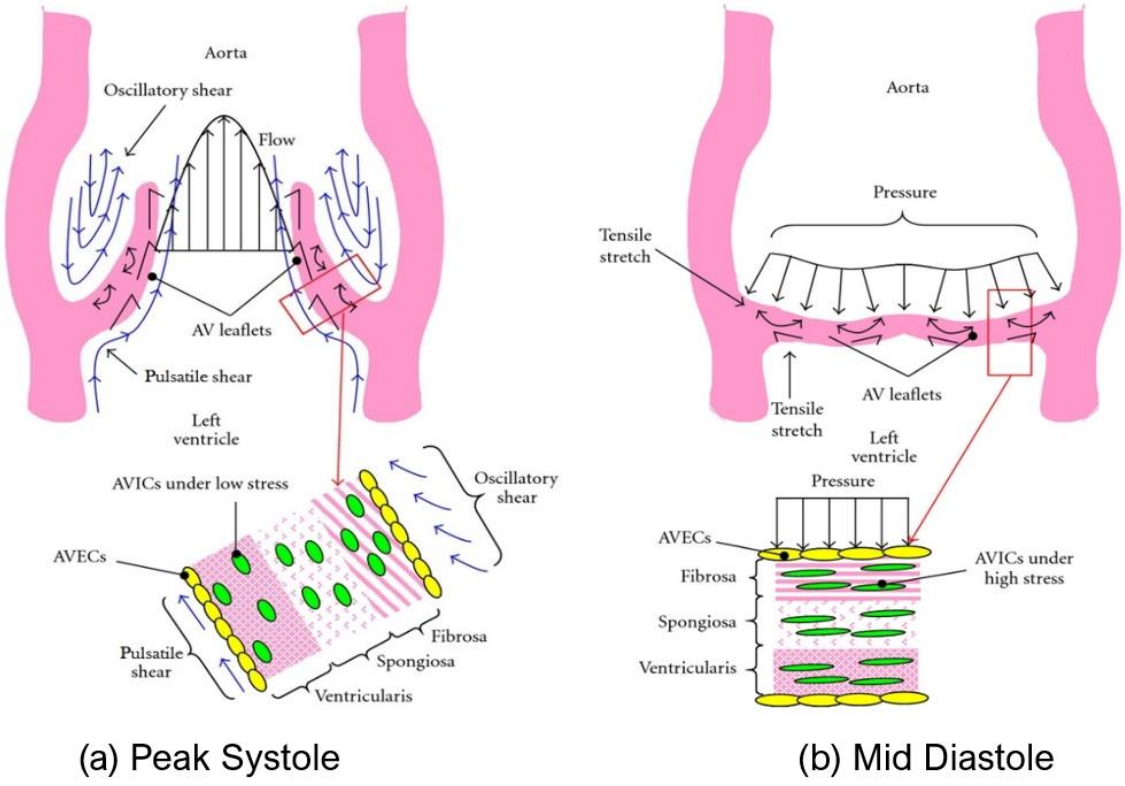

Figure 2.7 – Mechanical forces experienced by AV (Balachandran *et al*., 2011).

In addition, the fibrosa and ventricularis sides of AV experience bidirectional oscillatory shear stress and unidirectional pulsatile shear stress, respectively (Balachandran *et al*., 2011) (Figure 2.7). The peak value of the unidirectional pulsatile shear stress was found to be around 80 dyne/cm^2, whereas the one for the bidirectional oscillatory shear stress was ± 10 dyne/cm^2 (Rathan *et al*., 2016; Yap *et al*., 2012; Yap *et al*., 2012; Rathan *et al*., 2011; Ge *et al*., 2009; Cao *et al*., 2016).

To ensure healthy functioning of AV, it is highly important that all mechanical forces lie within respective physiological ranges. Any significant deviation from the physiological

range may initiate sustained pathological responses at the cellular and tissue levels, ultimately leading to AV disease.

2.6 Effect of Mechanical Stretch on AV

Elevated cyclic stretch (15%) was found to induce increased extracellular matrix (ECM) remodeling in AV by upregulating the expression of Matrix Metalloproteinase 2 and 9 (MMP-2 and -9), Cathepsin S, Cathepsin K, etc. (Balachandran *et al*., 2009). In addition, cellular proliferation and apoptosis in AV was significantly higher under 15% stretch (Balachandran *et al*., 2009). Interestingly, higher cyclic stretch (15%) also resulted in increased AV calcification compared to the physiological level (10%), including upregulation of calcification-related genes, such as Bone Morphogenetic Protein-4 (BMP-4), Runt related Transcription Factor 2 (RUNX2), Osteocalcin, etc. (Balachandran *et al*., 2010). Hence, pathologically high cyclic stretch (15%) contributes to AV pathogenesis by promoting adverse ECM remodeling and calcification, as opposed to the maintenance of AV homeostasis by physiological stretch (10%).

2.7 AV Stenosis and Treatment Options

Aortic valve (AV) stenosis or aortic stenosis (AS) is characterized by narrowing of the valve opening during systole (Figure 2.8, top row), resulting in a larger pressure gradient between the left ventricle and the aorta. Under this condition, the left ventricle must work harder to overcome the increased afterload caused by the stenotic AV. This is like attaching smaller and smaller nozzles to the end of a garden hose. The narrowing from the nozzle slows the forward flow of water and results in progressive pressure build-up within the garden hose (Figure 2.8, bottom row).

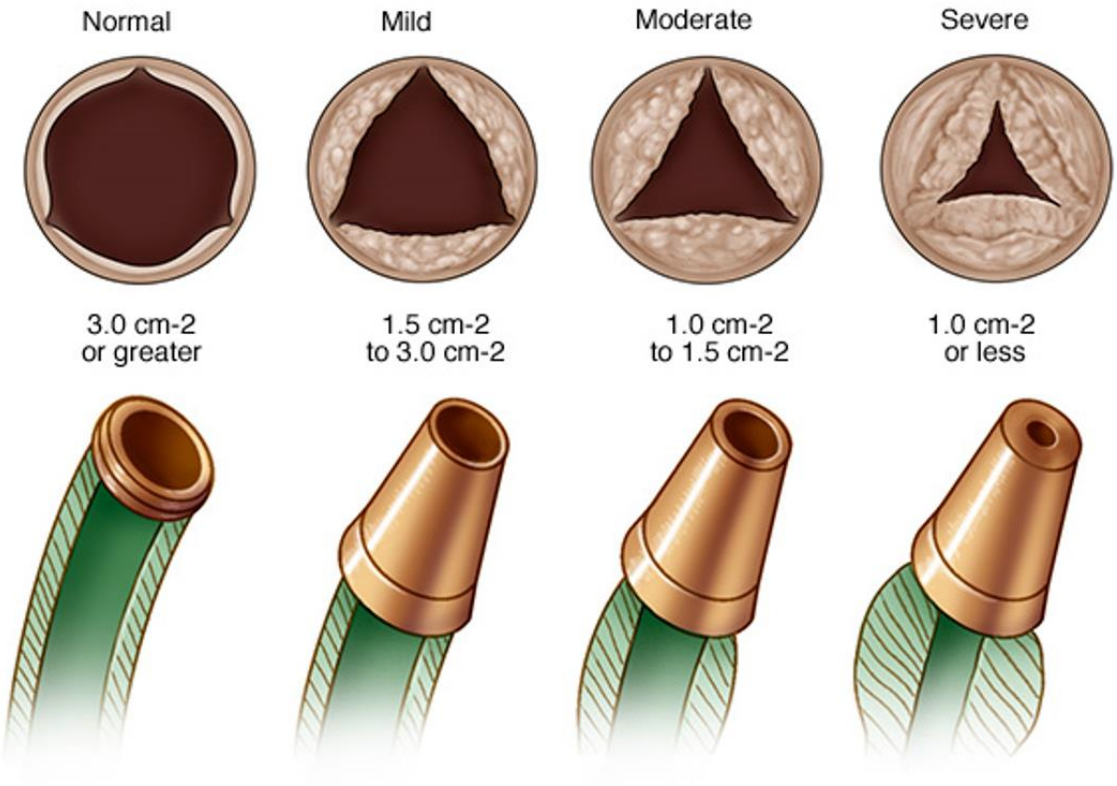

Figure 2.8 – AV Stenosis (Mayo Clinic*)*.

The main reason behind the occurrence of AS is thickening and calcification of AV leaflets, preferentially on the fibrosa side (Figure 2.9). Normally, the pressure gradient across a healthy aortic valve is only a few mm Hg. However, with progressive narrowing of AV opening, the pressure gradient increases gradually. A mild stenosis is characterized by a pressure gradient of around 20 mm Hg. When the pressure gradient ranges between 20- and 40-mm Hg, it is indicated as moderate stenosis. A case of severe stenosis happens when the pressure gradient is higher than 40 mm Hg (Cleveland Clinic).

In a recent study, Osnabrugge *et al*. (2013) found that more than 12% of the elderly population (age ≥ 75 years) are diagnosed with AS, with more than 3% representing the severe case. In addition to that, severe AS has a worse prognosis than many metastatic

cancers (*New Heart Valve*). Hence, this disease poses a significant burden on the elderly population.

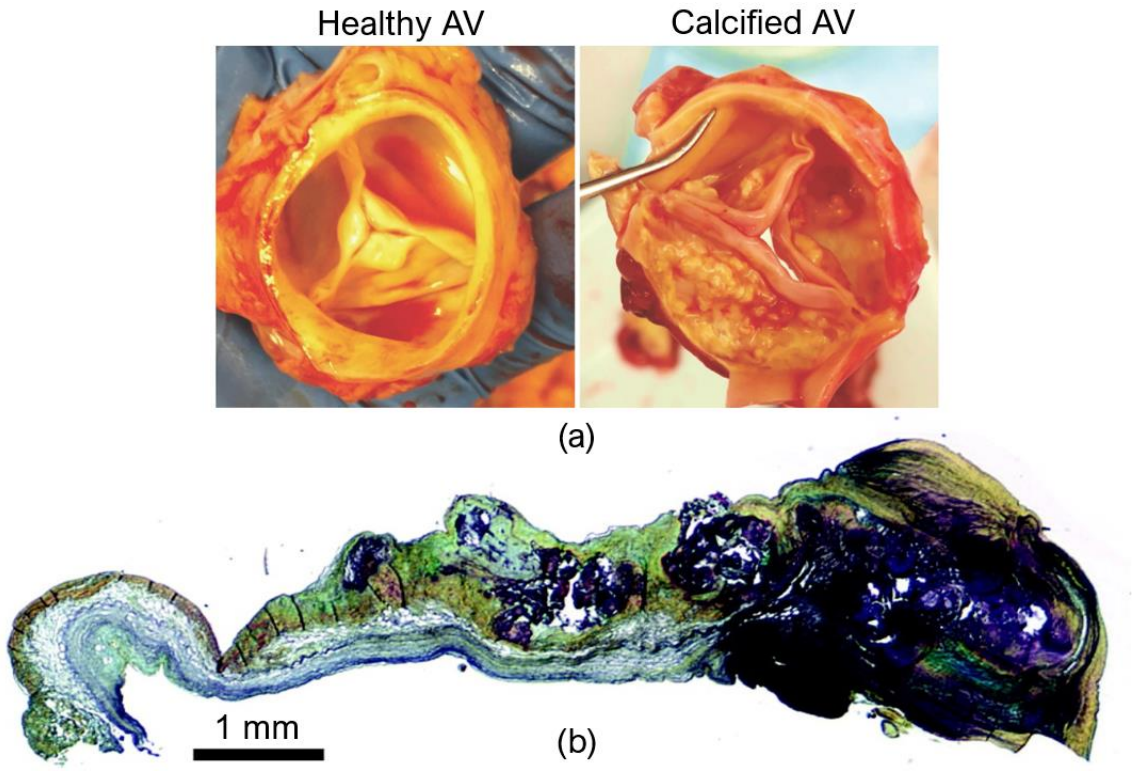

Figure 2.9 – (a) Healthy and calcified AV (St. Hilaire Laboratory, University of Pittsburgh, Pittsburgh, PA), (b) Movat pentachrome stain of a calcified AV, demonstrating maladaptive ECM remodeling and calcification (purple) (Chen *et al.*, 2011).

At present, there are no therapeutic drugs available to treat AS. The only available treatment options are either surgical aortic valve replacement (SAVR) or transcatheter aortic valve replacement (TAVR). SAVR is the gold standard for treating severe AS in operable patients, whereas TAVR offers a minimally invasive, catheter-based treatment option for inoperable high-risk and intermediate-risk AS patients (Leon *et al*., 2016; Kodali *et al*., 2012; Smith *et al*., 2011). There are two different types of prosthetic heart valves available for SAVR (Figure 2.10): (i) mechanical (generally used in younger AS patients) and (ii) bioprosthetic (generally used in older AS patients). On the other hand, there are

two FDA-approved transcatheter heart valves used in TAVR, namely the Edwards SAPIEN 3 and Medtronic EvolutPro valves (Figure 2.11).

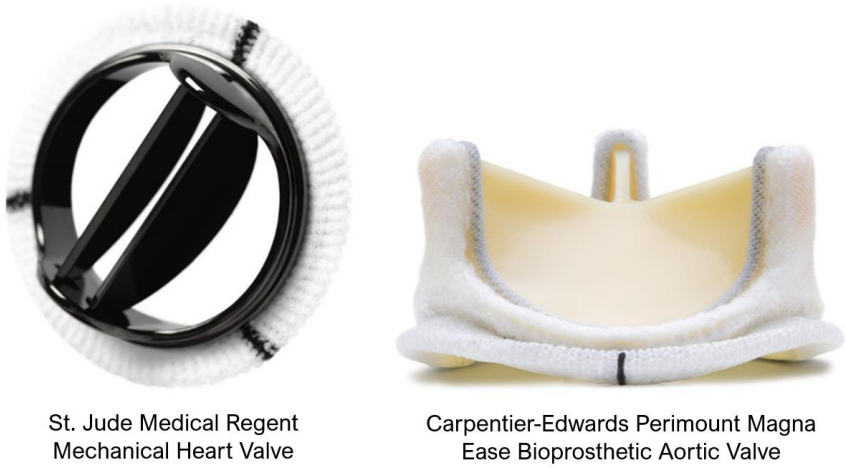

Figure 2.10 – Surgical aortic valves.

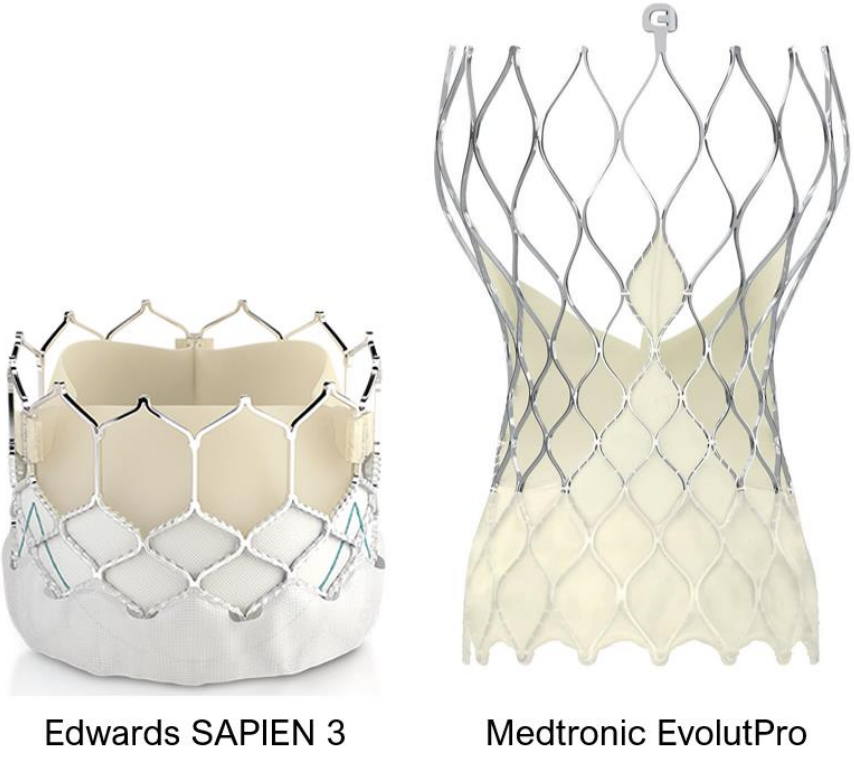

Figure 2.11 – Transcatheter Aortic Valves.

2.8 MicroRNAs and Messenger RNAs in Cardiovascular Diseases

microRNAs are small (~ 22 nucleotides in length) non-coding RNAs that modulate gene expression by silencing their targets (Ha *et al*., 2014). Since the discovery of the first microRNA (lin-4) in 1993 (Lee *et al*., 1993), these have been implicated in nearly all developmental and pathological processes (Sun *et al*., 2010). Due to their role in modulating gene expression, microRNAs have been widely considered as a potential therapeutic option for different diseases, such as cancer (Rupaimoole *et al*., 2017; Shah *et al*., 2016).

Many microRNAs have been found to be involved with cardiovascular diseases (McManus *et al*., 2015; Romaine *et al*., 2013; Quiat *et al*., 2013). The following figure outlines several microRNAs that have been implicated in cardiovascular diseases (Olson *et al*., 2014).

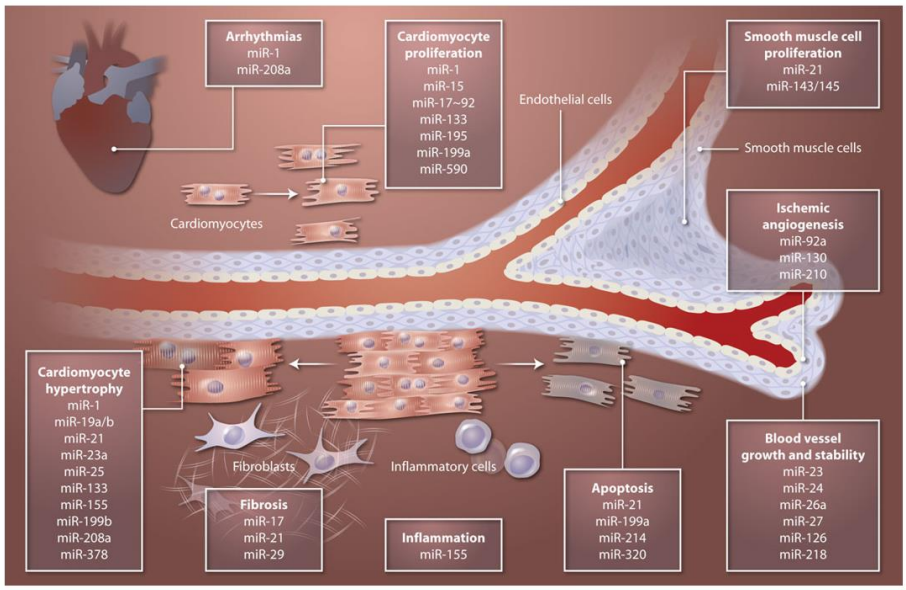

Figure 2.12 – microRNA in cardiovascular diseases (Olson *et al*., 2014).

For example, Zhou *et al*. (2018) identified several microRNAs that have been implicated in heart failure, acute myocardial infarction, and arrhythmia. Some of these microRNAs, such as miR-21 and miR-133, are involved with multiple pathologies (Figure 2.13).

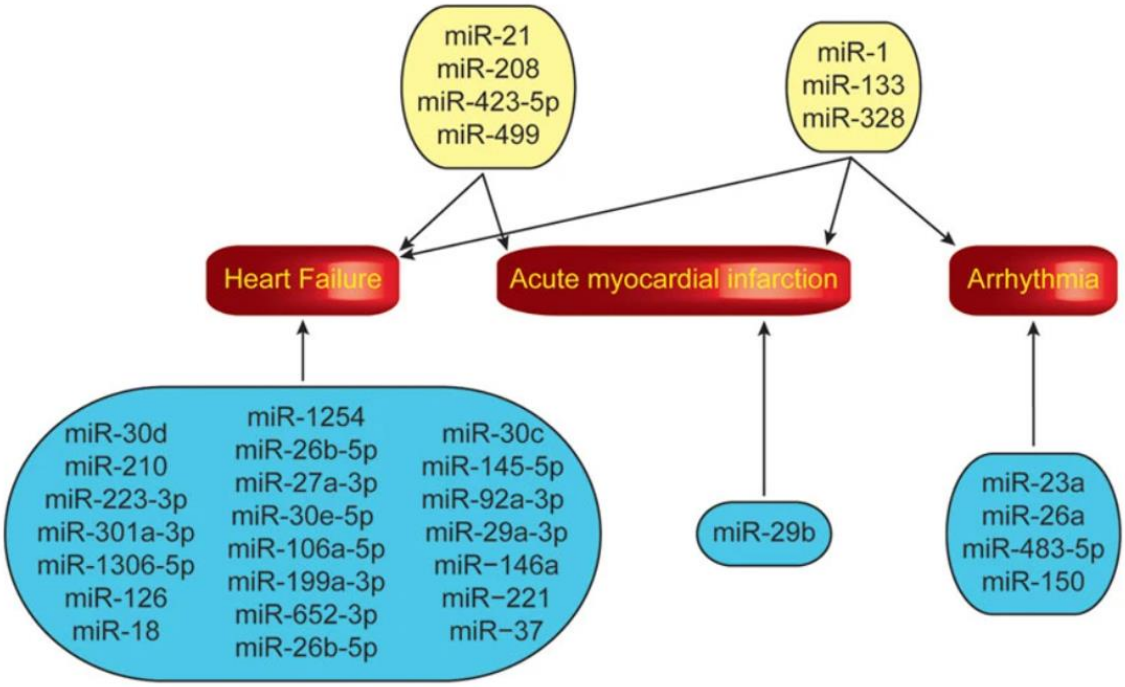

Figure 2.13 – microRNAs involved in heart failure, myocardial infarction and arrhythmia (Zhou *et al*., 2018).

Due to their fundamental role in regulating cellular processes by modulating gene expression, microRNAs can play a key role in the pathogenesis and progression of CAVD. Consequently, microRNA-based drugs are considered to be one of the potential therapeutic options for treatment of CAVD.

Similar to microRNAs, messenger RNA (mRNA) or gene-based therapeutics are considered as another potential treatment option for CAVD. Hundreds of genes have been implicated in CAVD over the past decades (Figure 2.14). Some of these genes include

osteogenic transcription factors such as Transforming Growth Factor-β (TGF-β) and Runt-Related Transcription Factor 2 (RUNX2), which are involved in the calcification process. On the other hand, some genes, such as Tumor Necrosis Factor-α (TNF-α) and Matrix Metalloproteinases (MMPs), are more associated in the earlier inflammatory and fibrotic stages of CAVD. However, most of these genes are located at the downstream end of the major signaling pathways that regulate CAVD pathogenesis. Consequently, it is crucial to identify genes that are located at the upstream end of the significant signaling pathways that modulate AV fibrosis and calcification.

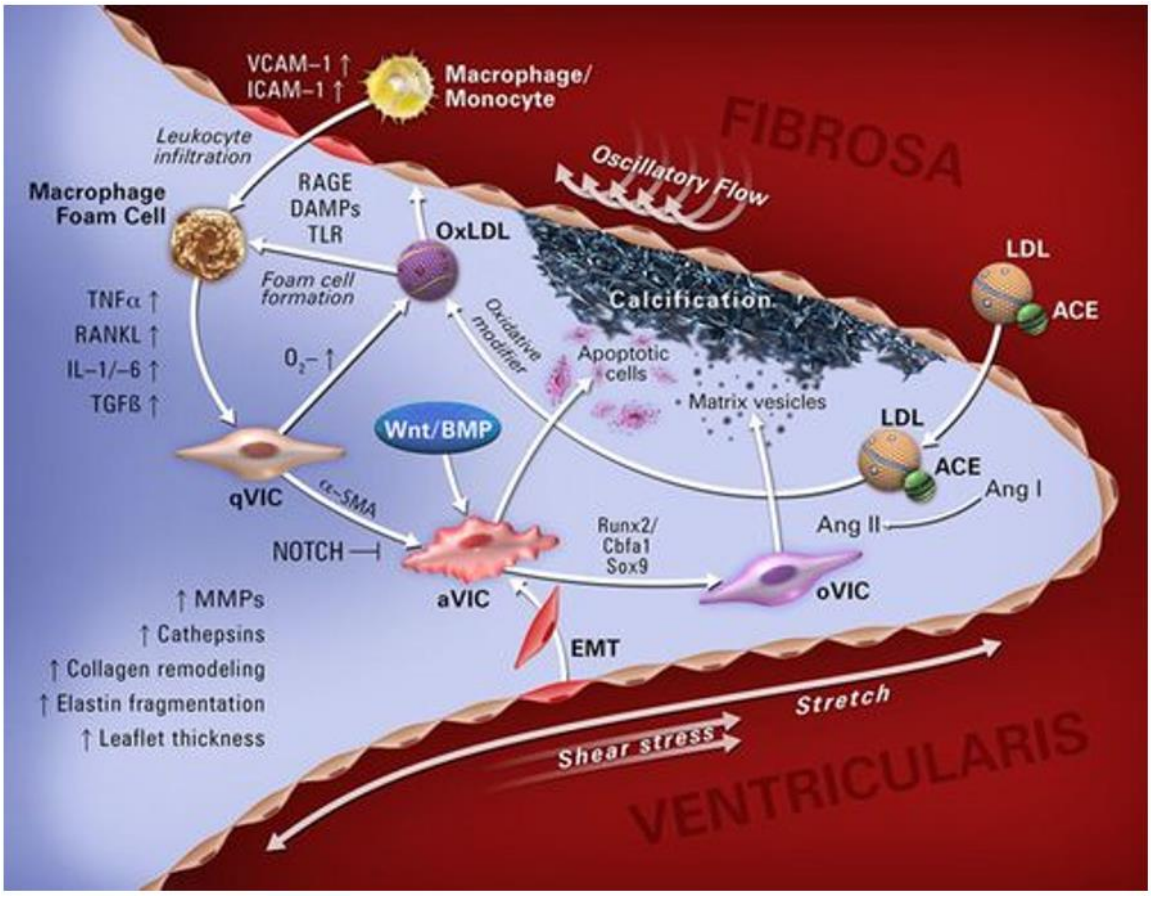

Figure 2.14 – Different mechanisms in CAVD (Yutzey *et al.*, 2014).

2.9 Rationale for Thesis Research

The AV experiences different types of mechanical forces during each cardiac cycle, such as tensile stress, bending stress, shear stress, etc. (Balachandran *et al*., 2011). In healthy AV leaflets, each of these mechanical forces remain within their respective physiological ranges. However, chronic (or pathological) deviation in these mechanical forces can result in AV fibrosis and calcification. Since tensile stretch is one of the major mechanical forces experienced by AV (Balachandran *et al*., 2011) and elevated stretch induces significantly higher AV calcification (Balachandran *et al*., 2010), stretch-sensitive microRNAs and mRNAs can play a significant role in AV pathogenesis. Hence, this dissertation will focus on investigating the role of stretch-sensitive microRNAs and mRNAs in the pathogenesis of CAVD.

CHAPTER 3. HYPOTHESIS AND SPECIFIC AIMS

Aortic valve (AV) stenosis is one of the most prevalent heart valve diseases in the elderly population and is characterized by a pathological narrowing of the valve opening (Osnabrugge *et al*., 2013). The main reason behind the narrowing of AV opening during systole is the fibrosis and calcification of AV leaflets (Chen *et al*., 2011). Previously, it was believed that AV stenosis is a result of an age-related tissue degeneration process. However, extensive mechanobiological research in the last two decades has shown that mechanical forces play a significant role in the initiation and progression of AV fibrosis and calcification, implying that AV stenosis is not a mere manifestation of age-related *passive* degeneration. Rather, this disease results from an active pathological process spanning several years (Rajamannan *et al*., 2011). The AV experiences different types of mechanical force during each cardiac cycle, such as tensile stress, bending stress, shear stress, etc. (Balachandran *et al*., 2011). For the healthy functioning of AV leaflets, each of these mechanical forces should remain within their respective optimal (or physiological) ranges. Any chronic (or pathological) deviation in these mechanical forces promote AV pathogenesis, resulting in AV fibrosis and calcification. Elevated mechanical stretch and low, oscillatory shear stress have been shown to promote AV pathogenesis, leading to AV fibrosis and calcification *ex vivo* (Balachandran *et al*., 2009; Balachandran *et al*., 2010; Sucosky *et al*., 2009; Rathan *et al*., 2011).

Currently, there are no therapeutic drugs available to treat calcific AV disease and the only treatment options are either surgical or transcatheter AV replacement (Smith *et al*., 2011; Leon *et al*., 2016). In the pursuit of effective therapeutics to treat calcific AV

disease, manipulation of microRNA (miRNA) and messenger RNA (mRNA) expression levels have recently emerged as exciting candidates (Hutcheson *et al*., 2014; Van der Ven *et al*., 2017). In this approach, identification of effective miRNA and mRNA candidates is a critical first step. To this end, mechanosensitive miRNAs and mRNAs are promising, given that perturbations to mechanical stimuli, such as stretch and shear, play a major role in the AV calcification process. So far, several studies have focused on the identification of shear-sensitive miRNAs and mRNAs and their functional relations to calcific AV disease (Rathan *et al*., 2016; Heath *et al*., 2018; Fernandez Esmerats *et al*., 2019). However, stretch-sensitive miRNAs and mRNAs relevant to calcific AV disease remain to be identified or functionally described. Considering that elevated mechanical stretch induces significantly higher AV calcification compared to low, oscillatory shear stress (Rathan, 2016), it will be important to understand the role of stretch-sensitive miRNAs and mRNAs in calcific AV disease.

The main hypothesis of this dissertation is that mechanical stretch-sensitive miRNAs and mRNAs play a significant role in AV calcification. To test this hypothesis, the following aims are proposed:

3.1 Specific Aim 1

The objective of specific aim 1 is to investigate the effects of physiological (10%) and pathological (15%) cyclic stretch on microRNA (miRNA) expression in AV. Freshly obtained porcine aortic valve (PAV) leaflets are cyclically (1 Hz) stretched at the physiological (10%) and pathological levels (15%) using an *ex vivo* stretch bioreactor system. Next, the expression levels of AV calcification-specific miRNAs are evaluated by

real-time quantitative polymerase chain reaction (RT-qPCR). Finally, overexpression of specific miRNA is performed using miRNA mimic to assess its effect on PAV calcification.

3.2 Specific Aim 2

The objective of specific aim 2 is to investigate the effects of physiological (10%) and pathological (15%) cyclic stretch on messenger RNA (mRNA) expression in AV. Freshly obtained PAV leaflets are cyclically (1 Hz) stretched at the physiological (10%) and pathological levels (15%) using an *ex vivo* stretch bioreactor system. Next, the expression levels of AV calcification-specific mRNAs are evaluated by RT-qPCR. Finally, inhibition of specific mRNA is performed using pharmacological inhibitor to assess its effect on PAV calcification.

Completion of the abovementioned research will enhance our mechanistic understanding of AV calcification process. In addition, this may help in identifying novel therapeutic targets for calcific AV disease in the future.

CHAPTER 4. METHODS

4.1 Stretch Bioreactor System

The stretch bioreactor system used in this dissertation was previously designed and validated in the Cardiovascular Fluid Mechanics Laboratory (Balachandran, 2010). The following figure indicates the main features of the stretch bioreactor.

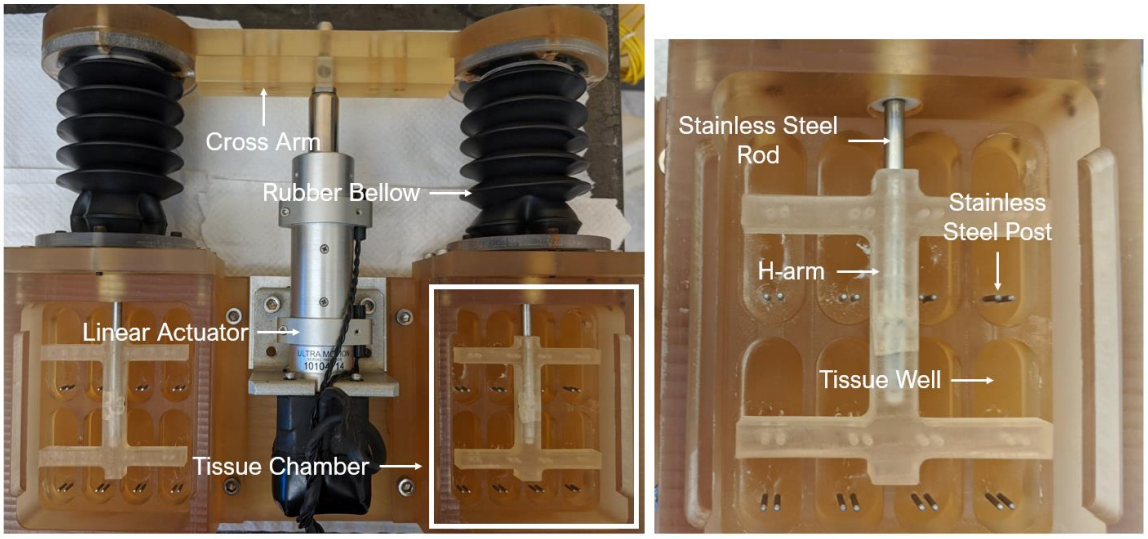

Figure 4.1 – Stretch bioreactor.

Briefly, the bioreactor has two identical chambers, each containing 8 wells for culturing 16 tissues at the same time (one tissue sample per well). Each well can contain approximately 5 mL of culture medium. There are two stainless steel posts in each well – one stationary and the other mobile. The stationary post is fixed to the bottom surface of each well, whereas the moving post is mounted from an H-shaped arm that is coupled to a rigid, stainless steel rod. This stainless-steel rod is further coupled to a cross-arm and a linear actuator (part no. D-A.083-HT17-2-2NO-ES-BR/RC4, ULTRA MOTION, Cutchogue, NY). The motion of the linear actuator is controlled by a ST5-Si stepper motor

drive (APPLIED MOTION, Watsonville, CA), which is connected to a laptop. Appropriate stretch program (10% or 15% stretch, Si Programmer™, APPLIED MOTION) is downloaded from the laptop to the motor drive to initiate a cyclic stretch experiment. This whole setup is depicted in the following diagram:

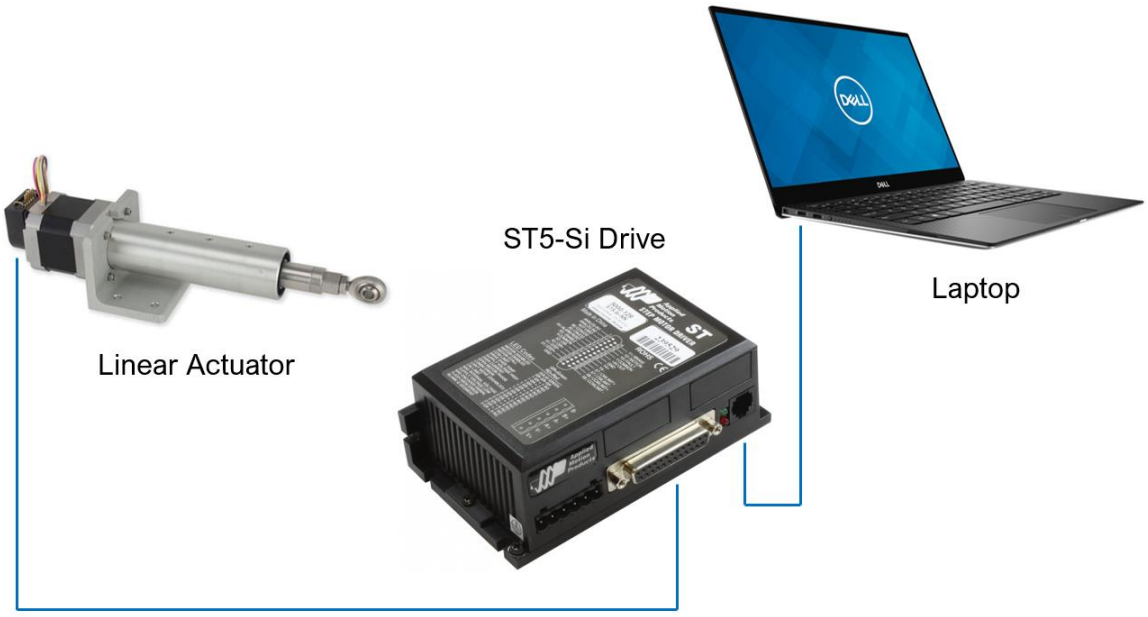

Figure 4.2 – Setup of the stretch bioreactor system.

In addition, each chamber of the bioreactor is always covered with a transparent lid, while the stainless-steel rods are covered with rubber bellows on the outside of the bioreactor. These provide the necessary environmental sealing to ensure sterile operation.

The stretch bioreactor system is made of polysulfone (most of the parts) and polycarbonate (chamber lids) for biocompatibility. Prior to each stretch experiment, the bioreactor is ethylene-oxide sterilized in a 12-hour (or 24-hour) cycle to prevent contamination.

4.2 Workflow of *Ex Vivo* Stretch Experiment

The following diagram outlines the workflow for setting up and running an *ex vivo* stretch experiment:

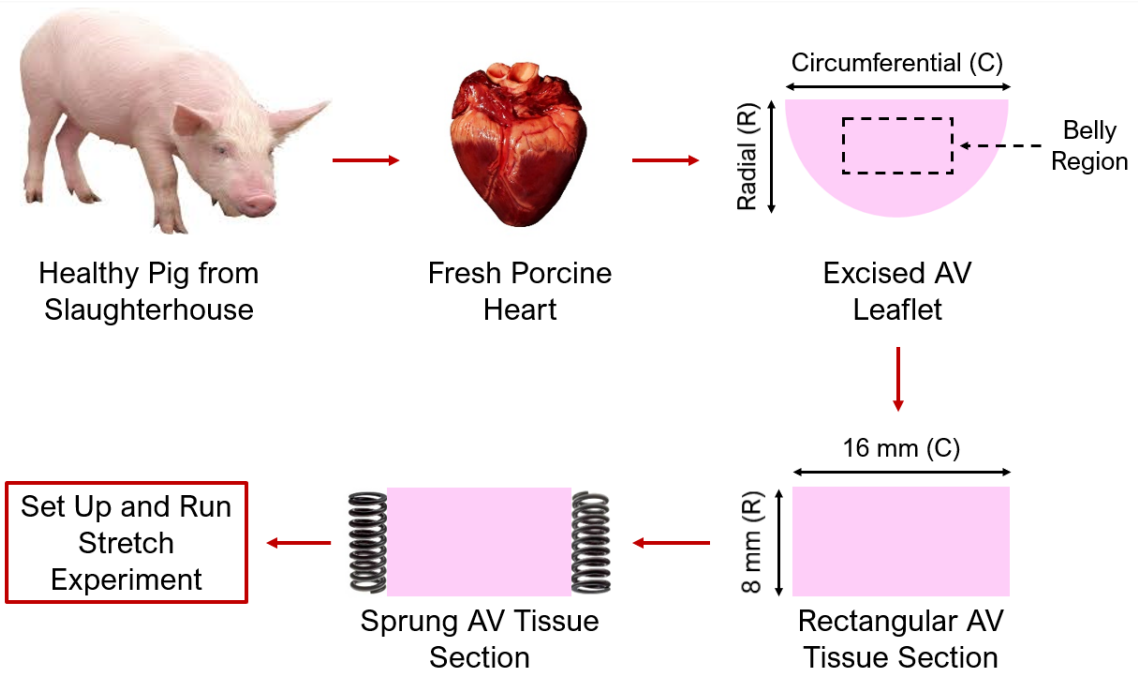

Figure 4.3 – Workflow for setting up a stretch experiment.

Each of the above steps is described in detail below:

4.2.1 Harvesting of Porcine Aortic Valve (PAV) Tissue

Healthy porcine hearts are obtained immediately (within 10 – 15 minutes) after slaughter from a local abattoir (Holifield Farms, Covington, GA). The three porcine aortic valve (PAV) leaflets from each heart are excised using a surgical scissor and stored in a 50-mL tube containing sterile, DNase/RNase-free ice-cold Dulbecco's Phosphate-Buffered Saline (DPBS) solution on-site. After excising the required number of PAV leaflets, these are transported back to the laboratory (transportation time does not exceed 1 hour). All

tools (metallic tray, forceps, surgical scissors) used in the harvesting process are sterilized in an autoclave.

4.2.2 Stretch Experiment Setup

Upon arriving in the laboratory, excised PAV leaflets are transferred to petri dishes containing sterile, DNase/RNase-free ice-cold DPBS solution inside a Class II Biological Safety Cabinet. From thereon, all the following steps are carried out inside the safety cabinet. A rectangular section of 16 mm (in the circumferential direction) by 8 mm (in the radial direction) is cut from the belly region of each PAV leaflet tissue using a surgical blade and stored in sterile, DNase/RNase-free ice-cold DPBS solution. Next, two stainless steel springs (part no. 9663K16, MCMASTER-CARR, Elmhurst, IL) are manually inserted (an optimum of four turns or insertions) on either side (circumferential direction) of each tissue section so that the tissue section covers at least half the inner diameter of the spring.

After completion of the springing step, the tissue sections are statically kept in sterile regular culture medium. Next, 5 mL of regular or osteogenic culture medium (depending on the type of experiment) is added to each well of the stretch bioreactor. Then, each sprung tissue section is mounted between the stationary and moving posts of one of the bioreactor wells. Once all the sprung tissue sections are mounted inside the wells of the bioreactor, the moving post is incrementally moved away from the stationary post to a final position where the distance between two posts is 19 mm (as measured by slide callipers). This distance approximately corresponds to an unstretched initial condition for each tissue section.

After that, the appropriate stretch program is downloaded from the laptop to the ST5-Si stepper motor drive that controls the linear actuator of the bioreactor and the program is thereby executed to start the cyclic stretch experiment at 60 cycles/minute.

Next, it is quickly checked (both visually and quantitatively by slide callipers) whether all the tissue sections are being cyclically stretched in an appropriate manner. Finally, the stretch bioreactor system is carefully transferred from the biological safety cabinet to a humidified CO_2 incubator. Throughout the duration of the stretch experiment, the following operating conditions are maintained inside the incubator:

Table 4.1 – CO_2 incubator operating conditions.

Operating Variable	Operating Condition
Chamber Temperature	37°C
CO_2 Concentration	5%

It is ensured that all tools (tweezers, scalpel handle, surgical blades, springs, allen key) and the stretch bioreactor system (including the moving posts and assembly screws) are sterilized by ethylene oxide (Anprolene AN74j Sterilizer, ANDERSEN PRODUCTS, Haw River, NC) beforehand. Additionally, aseptic techniques are strictly followed, and 70% ethanol and RNase AWAY decontaminant solution (catalog no. 53225-514, VWR, Radnor, PA) are used to maintain sterile RNase-free conditions.

4.2.3 Replacing Culture Medium

Over the course of a stretch experiment, the culture medium is replaced every 2 – 3 days. It is ensured that the 2 – 200 µL and 50 – 1000 µL pipet tips are autoclaved beforehand. In addition, aseptic techniques are strictly followed, and 70% ethanol and RNase AWAY decontaminant solution are used to maintain sterile RNase-free conditions.

4.2.4 Tissue Sample Collection after Completion of Stretch Experiment

After completion of the experiment, the stretch bioreactor system is carefully transferred from the CO_2 incubator to the biological safety cabinet. Next, PAV tissue samples are taken out of the bioreactor and washed three times in sterile DNase/RNase-free ice-cold DPBS solution to remove the residual culture medium adhering to the tissues. Then, the portions of each tissue section connected to the springs are discarded and only the middle portion is kept for further analyses.

If the tissue samples are to be used for RT-qPCR, then each of these samples is transferred to an autoclaved RNase/DNase-free 1.7 mL microcentrifuge tube, followed by snap-freezing using liquid nitrogen and storage in –80°C freezer. On the other hand, if the tissue samples are to be used for qualitative (Von Kossa and Alizarin Red stains) and quantitative (Arsenazo assay) assessment of calcification, one-third of each tissue sample (in the radial direction) is excised along the circumferential direction, embedded in Optimum Cutting Temperature (OCT) compound, and stored in –80°C freezer. The remaining portion of the tissue sample is transferred to an autoclaved RNase/DNase-free 1.7 mL microcentrifuge tube, snap-frozen in liquid nitrogen and stored in –80°C freezer.

All tools (tweezers, scalpel handle, surgical blades) and microcentrifuge tubes are autoclaved beforehand. Additionally, aseptic techniques are strictly followed, and 70% ethanol and RNase AWAY decontaminant solution are used to maintain sterile RNase-free conditions.

4.3 Formulations of Different Tissue Culture Media

Two types of culture medium are used in static or stretch experiments: regular and osteogenic medium. The regular medium is used to maintain normal cell viability of PAV tissues over the course of an experiment, whereas the osteogenic medium is used to accelerate the process of PAV calcification by adding specific chemicals that promote osteogenesis. Both media formulations were previously developed and validated in the Cardiovascular Fluid Mechanics Laboratory (Balachandran, 2010).

4.3.1 Formulation of Regular Culture Medium

The formulation of regular medium is outlined in the following table:

Table 4.2 – Regular culture medium.

Component	Stock Concentration	Required Concentration	Required Amount or Volume in 1L Medium
Dulbecco's Modified Eagle Medium (DMEM) [THERMO FISHER	–	13.36 g/L	13.36 g

Table 4.2 Continued

SCIENTIFIC catalog no. 12100061]			
Bovine Calf Serum [FISHER SCIENTIFIC catalog no. SH3007203]	–	10% (by volume)	100 mL
Sodium Bicarbonate [SIGMA ALDRICH catalog no. S5761]	–	3.7 g/L	3.7 g
Ascorbic Acid [SIGMA ALDRICH catalog no. A7631]	10 mg/mL (in ultrapure water)	50 mg/L	5 mL
HEPES Buffer [FISHER SCIENTIFIC catalog no. BP299-1]	–	2.5% (by volume)	25 mL
Non-essential Amino Acid Solution [SIGMA ALDRICH catalog no. M7145]	100x	1% (by volume)	10 mL

Table 4.2 Continued

Antibiotics [FISHER SCIENTIFIC catalog no. SV3007901]	100x	1% (by volume)	10 mL
Ultrapure Water [Synergy System, EMD MILLIPORE]	–	–	As needed for 1 L final volume

The final pH of the medium is adjusted between 7.2 and 7.4 using 1N NaOH (SIGMA ALDRICH catalog no. S2770) or 1N HCl (SIGMA ALDRICH catalog no. H9892) while thoroughly mixing by a Nuova^{TM} stirring hotplate (THERMO FISHER SCIENTIFIC). Eventually, the medium is sterile filtered using a 0.1-µm vacuum filter unit (VWR catalog no. 89220-698) and stored in 4°C fridge. It is ensured that the 1 L glass bottle into which the above listed components are added is autoclaved. Additionally, aseptic techniques are strictly followed, and 70% ethanol and RNase AWAY decontaminant solution are used to maintain sterile RNase-free conditions.

4.3.2 Formulation of Osteogenic Culture Medium

The osteogenic medium is simply the regular medium supplemented with specific chemicals that induce osteogenic differentiation, as outlined below:

Table 4.3 – Osteogenic culture medium.

Component	Stock Concentration	Required Concentration	Required Volume in 1 L Medium
Sodium Phosphate Monobasic Monohydrate [FISHER SCIENTIFIC catalog no. S369-500]	100 mM (in ultrapure water)	3.8 mM	38 mL
β-Glycerophosphate [SIGMA ALDRICH catalog no. G9422]	100 mM (in ultrapure water)	1 mM	10 mL
Dexamethasone [SIGMA ALDRICH catalog no. D4902]	2.5 mM (in 100% ethanol)	10 µM	4 mL
Transforming Growth Factor-β1 (TGF-β1) [SIGMA ALDRICH catalog no. T5050]	1 µg/mL (in 4 mM HCl containing 1 mg/mL BSA)	1 ng/mL	1 mL

All components are sterile-filtered using a 0.2 µm syringe filter (FISHER SCIENTIFIC catalog no. 09-719C). The stock solution of sodium phosphate is stored in 4°C fridge, whereas β-glycerophosphate and dexamethasone solutions are stored in –20°C freezer and TGF-β1 solution in –80°C freezer.

4.4 Workflow for Real-Time Quantitative Polymerase Chain Reaction (RT-qPCR)

The detection and relative quantification of miRNA or mRNA in tissue samples is accomplished using RT-qPCR. The entire process is comprised of several steps, as outlined in the following diagram:

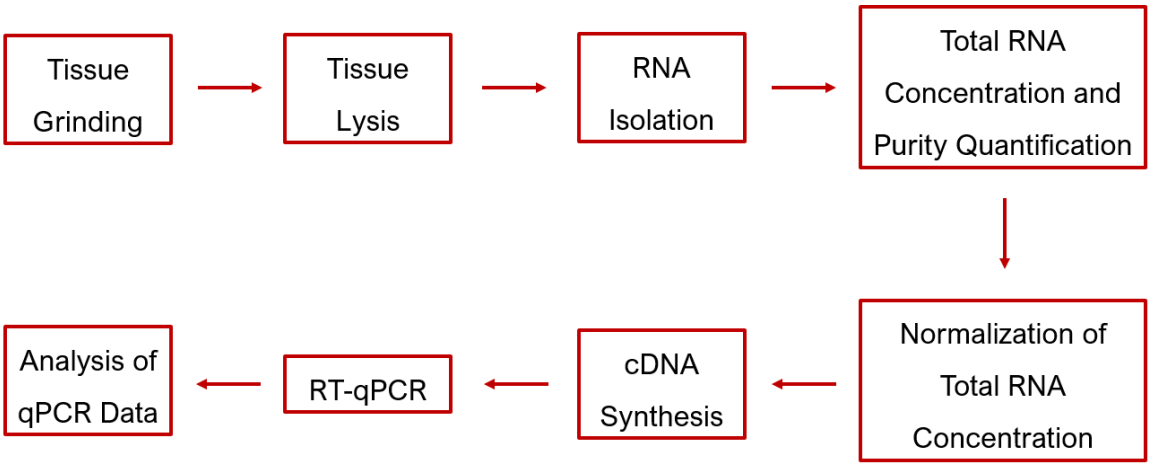

Figure 4.4 – Workflow diagram for RT-qPCR.

Each of the above steps is described in detail below:

4.4.1 Tissue Grinding

Before starting the tissue grinding process, the countertop area and all the material surfaces that come in contact with the tissue sample are thoroughly wiped by RNase

AWAY decontaminant solution. First, PAV tissue sample from static or stretch experiments is placed in a mortar. Then, liquid nitrogen is added from a Dewar flask to completely immerse the tissue sample inside the mortar. After that, a pestle is used to gradually apply a twisting downward motion on the tissue sample, thereby slowly grinding it to a fine powder form. Throughout the entire process, it is ensured that the tissue sample is always immersed in liquid nitrogen.

4.4.2 Tissue Lysis

Immediately after grinding the tissue sample to a fine powder form, more liquid nitrogen is added to the mortar to form a slurry-like mixture. The mixture is then transferred to an autoclaved RNase-free 1.7 mL microcentrifuge tube via a funnel. The remaining liquid nitrogen inside the microcentrifuge tube evaporates within the next 5 – 10 seconds. To lyse the grinded tissue sample, 1 mL of QIAzol lysis reagent (QIAGEN catalog no. 79306) is added to the microcentrifuge tube using a 1000 µL pipettor. During this step, it is ensured that the 50 – 1000 µL pipet tips being used are autoclaved. Subsequently, proper mixing of the powdered tissue sample and the lysis reagent is ensured using a vortex mixer (DADE catalog no. S8223-1), followed by a static reaction time of 1 minute. Throughout the entire process, the microcentrifuge tube is kept on ice. After this step, the process of RNA isolation can be started right away or the microcentrifuge tube containing the powdered tissue sample/lysis reagent mixture can be stored in –80°C freezer for RNA isolation later.

4.4.3 RNA Isolation

Before starting the process of RNA isolation, it is ensured that the 50 – 1000 µL and 2 – 200 µL pipet tips, and the 1.7 mL microcentrifuge tubes are autoclaved. RNA isolation is accomplished by using the Direct-zol™ RNA MiniPrep Plus RNA isolation kit from ZYMO RESEARCH (catalog no. R2072).

First, all microcentrifuge tubes containing the powdered tissue sample/lysis reagent mixtures are centrifuged in a Sorvall™ Legend™ Micro 21R microcentrifuge at 13,000xg for 10 minutes. After that, the supernatant tissue lysate (almost 1 mL) is collected equally into two autoclaved RNase-free 1.7 mL microcentrifuge tubes. Then, 500 µL of 100% molecular biology-grade ethanol (SIGMA ALDRICH catalogue no. E7023) is added to each of those tubes. After thorough mixing using a vortex mixer, 750 µL of the mixture is transferred into a Zymo-Spin™ IIICG Column (provided in the kit) in a Collection Tube (provided in the kit), which is centrifuged at 13,000xg for 30 seconds. The flow-through is subsequently discarded, and the step is repeated three more times using the same Spin Column and Collection Tube to elute the full 2 mL mixture of tissue lysate and 100% ethanol.

400 µL of RNA Wash Buffer (provided in the kit) is then added to the Spin Column, and the Spin Column-Collection Tube assembly is centrifuged at 13,000xg for 30 seconds. After discarding the flow-through, an 80 µL mixture of DNase I and DNA Digestion Buffer (both provided in the kit) is added to the column using a 100 µL pipettor, followed by an incubation period of 15 minutes at room temperature (20 – 25°C). The mixture contains 10 µL DNase I solution and 70 µL DNA Digestion Buffer.

Subsequently, 400 µL of Direct-zol™ RNA PreWash (provided in the kit) is added to the Spin Column, and the Spin Column-Collection Tube assembly is centrifuged at 13,000xg for 30 seconds, followed by disposal of the flow-through. This step with Direct-zol™ RNA PreWash is repeated one more time. Then, 700 µL of RNA Wash Buffer is added to the Spin Column, and the Spin Column-Collection Tube assembly is centrifuged at 13,000xg for 1 minute to ensure complete removal of the wash buffer.

Following this step, the Spin Column is carefully transferred to an autoclaved RNase-free 1.7 mL microcentrifuge tube. To elute the isolated RNA, 50 µL DNase/RNase-Free Water (provided in the kit) is directly added to the column matrix, and the Spin Column-Microcentrifuge Tube assembly is centrifuged at 13,000xg for 2 minutes. The spin column is subsequently discarded, and the flow-through collected in the microcentrifuge tube contains the RNA isolated from the powdered tissue sample. The total RNA concentration and RNA purity of the sample can be immediately quantified using a NanoDrop 2000/2000c UV-Vis spectrophotometer (THERMO FISHER SCIENTIFIC) or the RNA sample can be stored in –80°C freezer for total RNA concentration and purity quantification later.

4.4.4 Total RNA Concentration and RNA Purity Quantification

The total RNA concentration and purity of the isolated RNA from a PAV tissue sample is quantified using a NanoDrop 2000/2000c UV-Vis spectrophotometer. Prior to beginning the quantification process, the pedestals of the spectrophotometer are cleaned. To do that, 2 µL of DNase/RNase-free water is added on the surface of the bottom pedestal using a 2 µL pipettor, and the upper pedestal arm is then lowered to form a liquid column.

After letting it sit for approximately 2 – 3 minutes, the water from both the top and bottom pedestal is wiped away using Kimwipes.

At first, a reference RNA quantification is made by adding 2 µL of DNase/RNase-free water on the surface of the bottom pedestal, followed by lowering of the upper pedestal arm and clicking the Blank button in the NanoDrop program. Subsequently, the water from both the top and bottom pedestal is wiped off. Then, 2 µL of RNA sample is added on the surface of the bottom pedestal, followed by lowering of the upper pedestal arm and clicking the Measure button in the NanoDrop program. The NanoDrop program gives values for RNA concentration (in ng/µL), 260/280 ratio (ratio of absorbance at 260 nm and 280 nm) and 260/230 ratio (ratio of absorbance at 260 nm and 230 nm). The 260/280 and 260/230 ratios are primary and secondary measures, respectively, of RNA purity. In the case of handling multiple RNA samples at once, the system is Blanked after every 3 – 4 measurements. Throughout the entire process, the microcentrifuge tubes containing the RNA samples are kept on ice.

4.4.5 Normalization of Total RNA Concentration

After quantification of the total RNA concentration of all samples, required amounts of DNase/RNase-free water are added to the RNA samples to normalize their RNA concentrations to the same value. The post-normalization total RNA concentration is typically equal to that of the RNA sample which has the lowest total RNA concentration, obtained immediately after the NanoDrop measurement. Throughout the whole process, the microcentrifuge tubes containing the RNA samples should be kept on ice. After

normalization, the process of cDNA synthesis can be started right away, or the RNA samples can be stored in –80°C freezer for cDNA synthesis later.

4.4.6 cDNA Synthesis

The cDNA synthesis process is different based on whether the cDNA is to be used for miRNA or mRNA RT-qPCR. The two distinct synthesis methods are as follows:

4.4.6.1 cDNA Synthesis for miRNA RT-qPCR

In the case of miRNA, the cDNA is synthesized using the miScript II Reverse Transcription Kit (QIAGEN catalog no. 218161). At first, a reverse transcription mixture (for one reaction) is prepared as outlined in the following table. All the necessary components from the kit are thawed at room temperature (20 – 25°C) and then kept on ice throughout the whole process. When dealing with multiple RNA samples/reactions at once, the total volume of the master mixture should account for 1 – 2 more reactions than the required number.

Table 4.4 – Reverse transcription mixture for miRNA.

Component	Required Volume [µL]
5x miScript HiSpec Buffer	4
10x miScript Nucleics Mix	2
miScript Reverse Transcriptase Mix	2

After adding all the above components into an autoclaved 1.7 mL microcentrifuge tube, the tube should be gently vortexed (for thorough mixing) using a vortex mixer (VWR catalog no. 97043-562) and briefly centrifuged (for retaining residual liquid from the sides of the tube) in a minicentrifuge (VWR catalog no. 10067-588). From thereon, the master mixture should be kept on ice. Next, 12 µL of each RNA sample is added to an autoclaved 0.2 mL PCR tube (VWR catalog no. 20170-012) using a 20 µL pipettor, followed by the addition of 8 µL master mixture. Hence, the total reaction volume is 20 µL in each tube. After this, all the PCR tubes are centrifuged in the minicentrifuge and placed in the 96-well thermal cycler (BIORAD MyCycler^{TM}). Prior to the thermal cycling step, the PCR tubes are kept on ice all the time. The run method used in the thermal cycler is as follows:

a. 1st stage: Incubation at 37°C for 1 hour
b. 2nd stage: Incubation at 95°C for 5 minutes to inactivate miScript Reverse Transcriptase Mix
c. 3rd stage: Holding stage at 4°C

After completion of the reaction, the prepared cDNA can be used immediately for RT-qPCR of miRNA. Alternatively, it can be stored in 4°C fridge for short term (maximum one week) or in –20°C/–80°C freezer for long term (several months).

4.4.6.2 cDNA Synthesis for mRNA RT-qPCR

For mRNA, the cDNA is synthesized using the High-Capacity cDNA Reverse Transcription Kit (THERMO FISHER SCIENTIFIC catalog no. 4368814). At first, a reverse transcription mixture (for one reaction) is prepared as outlined in the following table. All the necessary components from the kit are thawed at room temperature (20 –

25°C) and then kept on ice throughout the entire process. When dealing with multiple RNA samples/reactions at once, the total volume of the master mixture should account for 1 – 2 more reactions than the required number.

Table 4. 5 – Reverse transcription mixture for mRNA.

Component	Required Volume [µL]
10x RT Buffer	2
25x dNTP Mix (100 mM)	0.8
10x RT Random Primers	2
Multiscribe^{TM} Reverse Transcriptase	1

After adding all the above components into an autoclaved 1.7 mL microcentrifuge tube, the tube is gently vortexed (for thorough mixing) using a vortex mixer and briefly centrifuged (for retaining residual liquid from the sides of the tube) in a minicentrifuge. From thereon, the master mixture is kept on ice. Next, 14.2 µL of each RNA sample is added to an autoclaved 0.2 mL PCR tube using a 20 µL pipettor, followed by the addition of 5.8 µL master mixture. Hence, the total reaction volume is 20 µL in each tube. After this, all the PCR tubes are centrifuged in the minicentrifuge and placed in the 96-well thermal cycler. Prior to the thermal cycling step, the PCR tubes are kept on ice all the time. The run method used in the thermal cycler is as follows:

a. 1st stage: Incubation at 25°C for 10 minutes
b. 2nd stage: Incubation at 37°C for 2 hours

c. 3rd stage: Incubation at 85°C for 5 minutes

d. 4th stage: Holding stage at 4°C

After completion of the reaction, the prepared cDNA can be used immediately for real-time qPCR of mRNA. Alternatively, it can be stored in 4°C fridge for short term (maximum one week) or in –20°C/–80°C freezer for long term (several months).

4.4.7 RT-qPCR

The process of RT-qPCR is different based on whether it is used for miRNA or mRNA detection and relative quantification. The two distinct methods are as follows:

4.4.7.1 RT-qPCR for miRNA

For the real-time quantitative polymerase chain reaction (RT-qPCR) in each well of a 96-well qPCR plate (THERMO FISHER SCIENTIFIC catalog no. 4316813) to detect and relatively quantify miRNA, the following mixture is prepared:

Table 4.6 – RT-qPCR mixture for miRNA.

Component	Stock Solution Concentration [µM]	Required Concentration in 20 µL Reaction Volume [µM]	Required Volume of Stock Solution [µL]
miRNA or U6 Primer	5	1	4

Table 4.6 Continued

miScript Universal Primer	–	–	4
SYBR Green qPCR Master Mix	–	–	10

When dealing with multiple cDNA samples/reactions at once, the total volume of the reagent mixture should account for 1 – 2 more reactions than the required number. All the necessary components are thawed at room temperature (20 – 25°C) and then kept on ice throughout the whole process. Here, U6 small nuclear RNA is used as the housekeeping gene (QIAGEN). The primer assay for the specific miRNA (forward primer) and the miScript Universal Primer (reverse primer) are obtained from QIAGEN. The PowerUp SYBR Green qPCR Master Mix is obtained from THERMO FISHER SCIENTIFIC (catalog no. A25776).

After adding all the above components into an autoclaved 1.7 mL microcentrifuge tube, the tube is gently vortexed (for thorough mixing) using a vortex mixer and briefly centrifuged (for retaining residual liquid from the sides of the tube) in a minicentrifuge. From thereon, the reagent mixture is kept on ice. In each well of the 96-well qPCR plate, 2 µL of cDNA sample is added using a 2 µL pipettor, followed by the addition of 18 µL of reagent mixture. Hence, the total reaction volume in each well is 20 µL. Each reaction is set up to have three replicates.

After preparing all the reaction wells, the qPCR plate is covered by an optical adhesive film (THERMO FISHER SCIENTIFIC catalogue no. 4360954) to prevent well-

to-well contamination and sample evaporation. Then, to collect the liquid content in each well without bubbles, the qPCR plate is spun at 2500 rpm for 1 minute in a PCR plate spinner (VWR catalog no. 89184-608). After that, the qPCR plate is placed in the StepOnePlus™ Real-Time PCR System (THERMO FISHER SCIENTIFIC catalog no. 4376600). The run method used in the PCR system is as follows:

a. Holding (initial activation) stage: Incubation at 95°C for 15 minutes
b. Cycling stage (50 cycles):
    1. Denaturation step: Incubation at 95°C for 15 seconds
    2. Annealing step: Incubation at 55°C for 30 seconds
    3. Extension step: Incubation at 70°C for 30 seconds (real-time fluorescence data are acquired during this step)
c. Melt curve stage:
    1. 1st step: Incubation at 95°C for 15 seconds
    2. 2nd step: Incubation at 60°C for 1 minute
    3. 3rd step: Incremental temperature increase (+ 0.3°C) to 95°C with a holding period of 15 seconds at each increment (real-time fluorescence data are acquired during each temperature increment of this step)

After completion of the RT-qPCR run, the qPCR plate is discarded, and the resulting data (Cycle Threshold or C_t value for each reaction well) are exported from the .eds file (StepOnePlus™ program) to an excel file for further analysis.

4.4.7.2 RT-qPCR for mRNA

For the real-time quantitative polymerase chain reaction (RT-qPCR) in each well of a 96-well qPCR plate to detect and relatively quantify mRNA, the following mixture is prepared:

Table 4.7 – RT-qPCR mixture for mRNA.

Component	Stock Solution Concentration [µM]	Required Concentration in 20 µL Reaction Volume [µM]	Required Volume of Stock Solution [µL]
Forward Primer	12.5	2.5	4
Reverse Primer	12.5	2.5	4
SYBR Green qPCR Master Mix	–	–	10

When dealing with multiple cDNA samples/reactions at once, the total volume of the reagent mixture should account for 1 – 2 more reactions than the required number. All the necessary components are thawed at room temperature (20 – 25°C) and then kept on ice throughout the whole process. Here, 18S ribosomal RNA is used as the housekeeping gene. The forward and reverse primers for 18S and all mRNAs of interest are obtained from INTEGRATED DNA TECHNOLOGIES (Coralville, IA).

After adding all the above components in an autoclaved 1.7 mL microcentrifuge tube, the tube is gently vortexed (for thorough mixing) using a vortex mixer and briefly

centrifuged (for retaining residual liquid from the sides of the tube) in a minicentrifuge. From thereon, the reagent mixture is kept on ice. In each well of the 96-well qPCR plate, 2 µL of cDNA sample and 18 of µL reagent mixture are added. Hence, the total reaction volume in each well is 20 µL. Each reaction is set up to have three replicates.

After preparing all the reaction wells, the qPCR plate is covered by an optical adhesive film to prevent well-to-well contamination and sample evaporation. Then, to collect the liquid content in each well without bubbles, the qPCR plate is spun at 2500 rpm for 1 minute in a PCR plate spinner. After that, the qPCR plate is placed in the StepOnePlus™ Real-Time PCR System. The run method used in the PCR system is as follows:

a. Holding stage:
    1. 1st step: Incubation at 50°C for 2 minutes
    2. 2nd step: Incubation at 95°C for 5 minutes
b. Cycling stage (50 cycles):
    1. Denaturation step: Incubation at 95°C for 3 seconds
    2. Annealing/Extension step: Incubation at 60°C for 30 seconds (real-time fluorescence data are acquired during this step)
c. Melt curve stage:
    1. 1st step: Incubation at 95°C for 15 seconds
    2. 2nd step: Incubation at 60°C for 1 minute
    3. 3rd step: Incremental temperature increase (+ 0.3°C) to 95°C with a holding period of 15 seconds at each increment (real-time

fluorescence data are acquired during each temperature increment of this step)

After completion of the qPCR run, the qPCR plate is discarded and the resulting data (Cycle Threshold or C_t value for each reaction well) are exported from the .eds file (StepOnePlus™ program) to an excel file for further analysis.

4.4.7.3 Designing RT-qPCR Primers for mRNA

The forward and reverse primers for a specific mRNA are designed using the NCBI Primer-BLAST website (https://www.ncbi.nlm.nih.gov/tools/primer-blast/). The input values for the most important parameters are listed in the following table:

Table 4.8 – Primer designing protocol for mRNA.

Parameter	Value	Comment
Reference Sequence (RefSeq)	Depends on the gene and the species of interest	This is obtained from the NCBI Gene website (https://www.ncbi.nlm.nih.gov/gene)
PCR Product Size	Minimum: 100	–
	Maximum: 200	
	Minimum: 58.0	–
	Optimum: 60.0	

Table 4.8 Continued

Primer Melting Temperature (T_m) [°C]	Maximum: 62.0	
	Maximum Difference: 2.0	
Exon Junction Span	Primer must span an exon-exon junction	This is the preferable option
	No preference	This is only used when the first option doesn't output any primers
Organism	Pig (*sus scrofa*)	–
Primer Size	Minimum: 18.0	These can be found under the *Advanced Parameters* section of the website
	Optimum: 20.0	
	Maximum: 24.0	
Primer GC Content (%)	Minimum: 30.0	
	Maximum: 80.0	

For all the other parameters, the default values are used. In any case, the designed primer pair is ensured to be specific for the mRNA of interest.

4.4.8 Analysis of RT-qPCR Data

The RT-qPCR data are analyzed using the ΔCT method. First, it is determined whether the standard deviation (SD) of the three C_t values of each sample reaction (housekeeping gene and specific miRNA or mRNA) is less than or equal to 0.5. In case it is higher than 0.5, the C_t value (among the three replicates) causing the high standard deviation is not considered for further analysis. After this, the average values of the three (or two) C_t values for each sample's housekeeping gene and specific miRNA or mRNA reactions are calculated. Next, the miRNA or mRNA expression in each sample is determined using one of the following formulae as appropriate:

$$miRNA\ Expression = 2^{[(Average\ C_t)_{U6} - (Average\ C_t)_{miRNA}]} \ldots\ldots (4.1)$$

$$mRNA\ Expression = 2^{[(Average\ C_t)_{18S} - (Average\ C_t)_{mRNA}]} \ldots\ldots (4.2)$$

To calculate the fold change in miRNA or mRNA expression at a specific experimental condition compared to the reference experimental condition (15% vs. 10% stretch, for example), the miRNA or mRNA expression values for all samples at the specific and reference conditions are normalized by the average value of the miRNA or mRNA expression in all samples at the reference condition. Hence, this makes the average value of miRNA or mRNA expression at the reference condition 1 and that one at the specific condition some number X, representative of the fold change.

4.5 Statistical Analysis

All statistical analyses are done using the IBM SPSS Statistics software. Statistically significant difference is achieved when the significance (p) value is less than or equal to 0.05. The first step in comparing two different groups is to check for normality of each data group using the Shapiro-Wilk test. If either one or both groups are not normally distributed ($p \leq 0.05$ in the Shapiro-Wilk test), non-parametric Mann-Whitney U test is used for statistical comparison. On the other hand, if both groups are normally distributed ($p > 0.05$ in the Shapiro-Wilk test), independent samples t-test is used for statistical comparison. In this case, equal variance assumption can be made if Levene's test gives a significance value greater than 0.05.

CHAPTER 5. SPECIFIC AIM 1 RESULTS

In this specific aim, firstly, the effect of different levels of cyclic stretch [physiological (10%) and pathological (15%)] on the relative expression of seven miRNAs of interest (miR-21-5p, miR-483-3p, miR-181a, miR-181b, miR-199a-3p, miR-122-5p, and miR-214) in relation to calcific aortic valve disease (CAVD) [Coffey *et al*., 2016; Rathan *et al*., 2016; Esmerats *et al*., 2019] was investigated. The associated findings are described in sections **5.1 – 5.7**.

5.1 Effect of Cyclic Stretch on miR-21-5p Expression in Porcine Aortic Valves (PAVs)

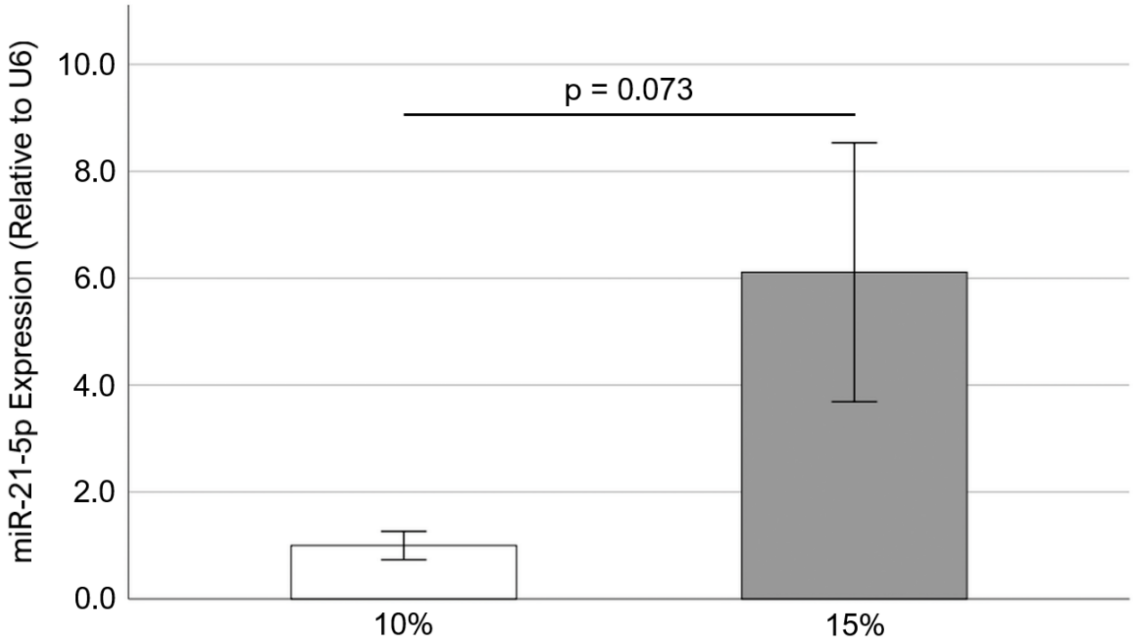

Figure 5.1 – Effect of cyclic stretch on miR-21-5p expression in PAV leaflets (n = 7 – 8). Data are presented as mean ± standard error of mean.

Freshly obtained porcine aortic valve (PAV) leaflets were cyclically (1 Hz) stretched at 10% and 15% for 2 days in regular medium. After completion of the stretch experiments,

the expression of miR-21-5p (relative to U6) was evaluated in the cyclically stretched tissue samples using RT-qPCR. It was found that there was an almost significant increase in miR-21-5p expression at 15% stretch compared to 10% (as shown in Figure 5.1).

5.2 Effect of Cyclic Stretch on miR-483-3p Expression in Porcine Aortic Valves (PAVs)

Freshly obtained porcine aortic valve (PAV) leaflets were cyclically (1 Hz) stretched at 10% and 15% for 2 days in regular medium. After completion of the stretch experiments, the expression of miR-483-3p (relative to U6) was evaluated in the cyclically stretched tissue samples using RT-qPCR. It was found that there was no significant difference in miR-483-3p expression between 10% and 15% stretch (as shown in Figure 5.2).

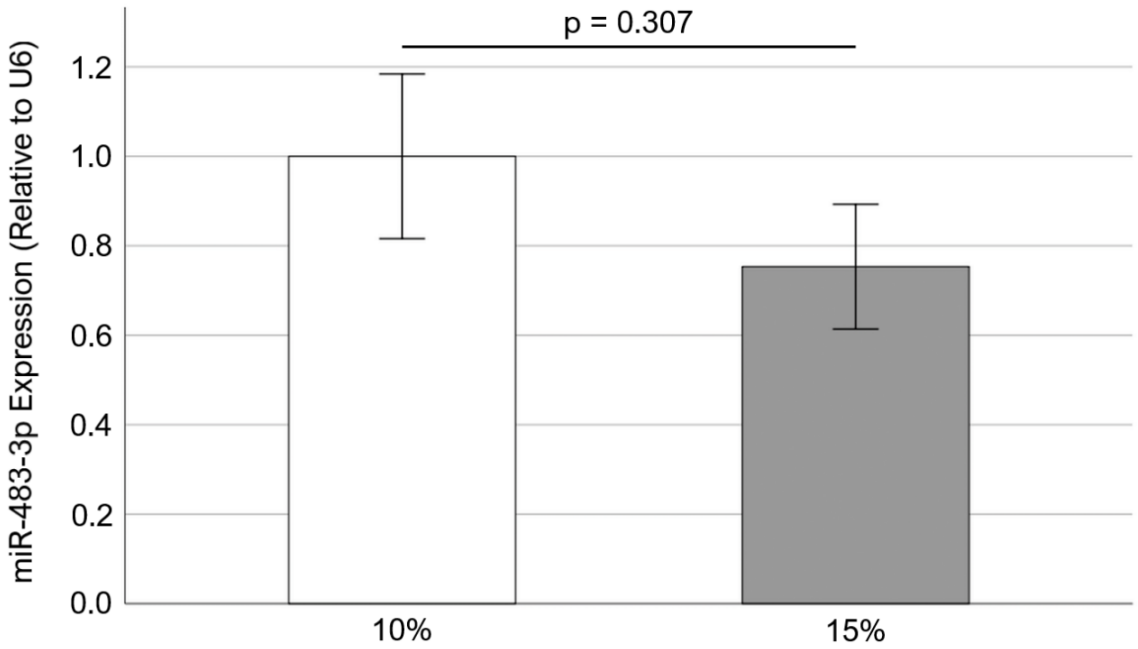

Figure 5.2 – Effect of cyclic stretch on miR-483-3p expression in PAV leaflets (n = 7 – 8). Data are presented as mean ± standard error of mean.

5.3 Effect of Cyclic Stretch on miR-181a Expression in Porcine Aortic Valves (PAVs)

Freshly obtained porcine aortic valve (PAV) leaflets were cyclically (1 Hz) stretched at 10% and 15% for 1 week in regular medium. After completion of the stretch experiments, the expression of miR-181a (relative to U6) was evaluated in the cyclically stretched tissue samples using RT-qPCR. It was found that miR-181a expression was significantly downregulated at 15% stretch compared to 10% (as shown in Figure 5.3).

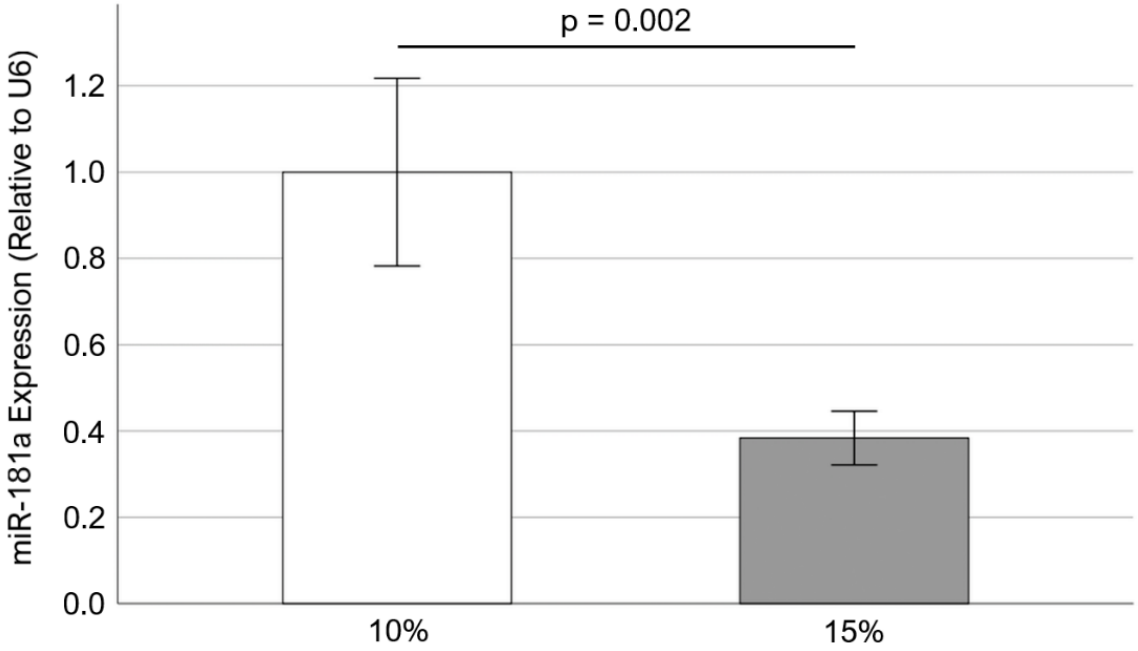

Figure 5.3 – Effect of cyclic stretch on miR-181a expression in PAV leaflets (n = 8). Data are presented as mean ± standard error of mean.

5.4 Effect of Cyclic Stretch on miR-181b Expression in Porcine Aortic Valves (PAVs)

Freshly obtained porcine aortic valve (PAV) leaflets were cyclically (1 Hz) stretched at 10% and 15% for 1 week in regular medium. After completion of the stretch experiments, the expression of miR-181b (relative to U6) was evaluated in the cyclically stretched tissue samples using RT-qPCR. It was found that miR-181b expression was significantly downregulated at 15% stretch compared to 10% (as shown in Figure 5.4).

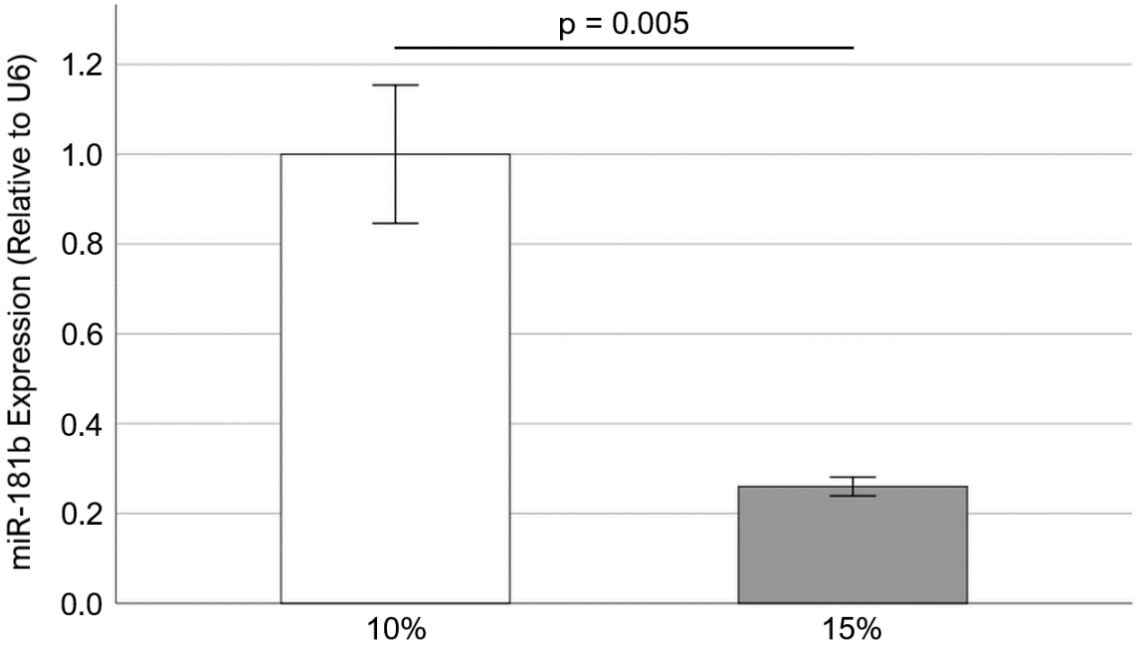

Figure 5.4 – Effect of cyclic stretch on miR-181b expression in PAV leaflets (n = 6). Data are presented as mean ± standard error of mean.

5.5 Effect of Cyclic Stretch on miR-199a-3p Expression in Porcine Aortic Valves (PAVs)

Freshly obtained porcine aortic valve (PAV) leaflets were cyclically (1 Hz) stretched at 10% and 15% for 1 week in regular medium. After completion of the stretch experiments, the expression of miR-199a-3p (relative to U6) was evaluated in the cyclically stretched tissue samples using RT-qPCR. It was found that miR-199a-3p expression was significantly downregulated at 15% stretch compared to 10% (as shown in Figure 5.5).

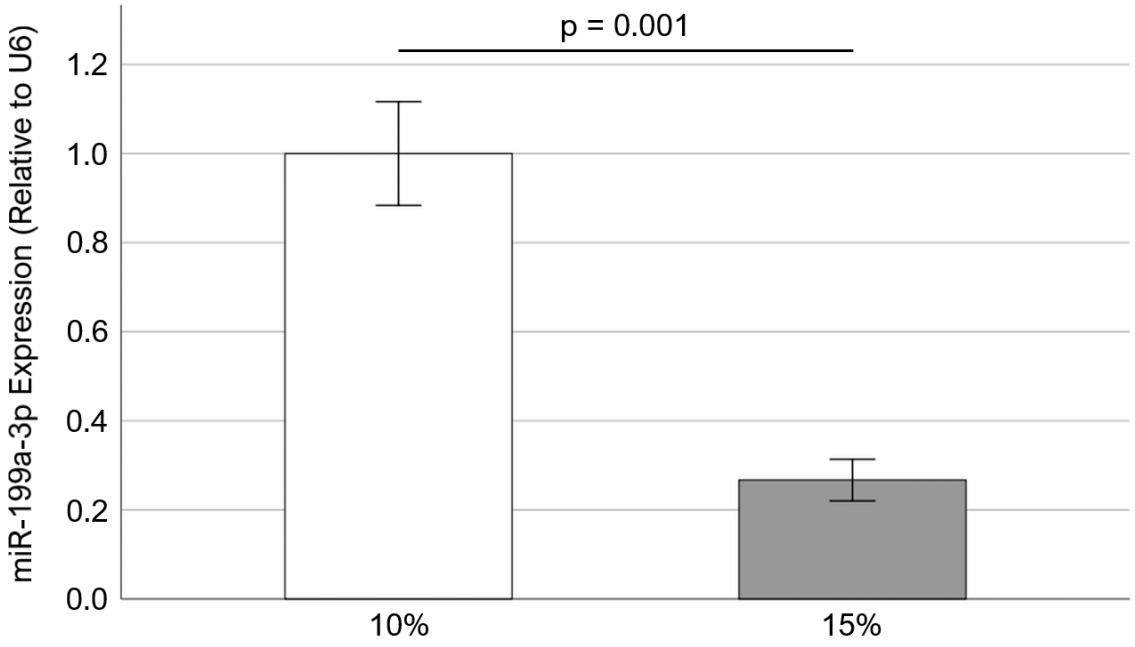

Figure 5.5 – Effect of cyclic stretch on miR-199a-3p expression in PAV leaflets (n = 6). Data are presented as mean ± standard error of mean.

5.6 Effect of Cyclic Stretch on miR-122-5p Expression in Porcine Aortic Valves (PAVs)

Freshly obtained porcine aortic valve (PAV) leaflets were cyclically (1 Hz) stretched at 10% and 15% for 1 week in osteogenic medium. After completion of the stretch experiments, the expression of miR-122-5p (relative to U6) was evaluated in the cyclically stretched tissue samples using RT-qPCR. It was found that there was no significant difference in miR-122-5p expression between 10% and 15% stretch (as shown in Figure 5.6).

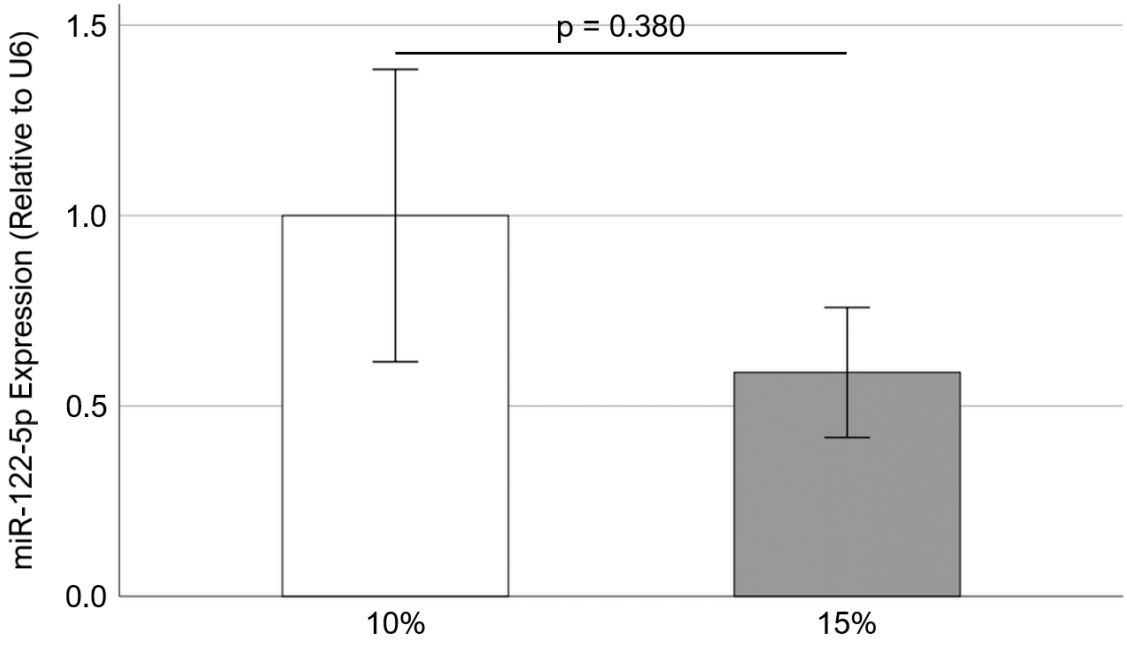

Figure 5.6 – Effect of cyclic stretch on miR-122-5p expression in PAV leaflets (n = 4 – 5). Data are presented as mean ± standard error of mean.

5.7 Effect of Cyclic Stretch on miR-214 Expression in Porcine Aortic Valves (PAVs)

Freshly obtained porcine aortic valve (PAV) leaflets were cyclically (1 Hz) stretched at 10% and 15% for 1 week in osteogenic medium. After completion of the stretch experiments, the expression of miR-214 (relative to U6) was evaluated in the cyclically stretched tissue samples using RT-qPCR. It was found that miR-214 expression was significantly downregulated at 15% stretch compared to 10% (as shown in Figure 5.7).

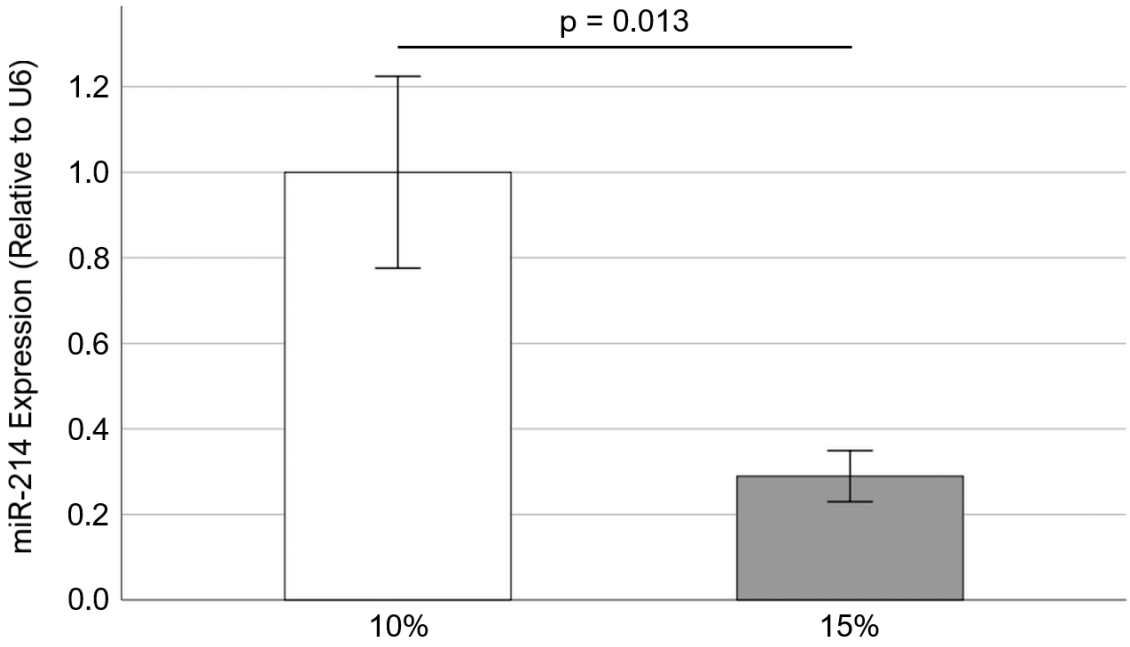

Figure 5.7. – Effect of cyclic stretch on miR-214 expression in PAV leaflets (n = 9 – 10). Data are presented as mean ± standard error of mean.

Going forward, it was decided to focus on the mechanistic role of miR-214 since:

1) miR-214 is shear-sensitive in porcine aortic valves (PAVs) [Rathan *et al*., 2016], and
2) miR-214 is differentially expressed in calcified human aortic valves [Coffey *et al*., 2016].

Given the downregulation of miR-214 expression at 15% (pathological) stretch compared to the physiological level (10%), it was hypothesized that miR-214 may have a protective role in aortic valve (AV) calcification. To test this hypothesis, firstly, the effect of miR-214 overexpression on porcine aortic valve (PAV) calcification would be examined.

5.8 miR-214 Overexpression in Porcine Aortic Valves (PAVs) under Static Culture in Osteogenic Medium

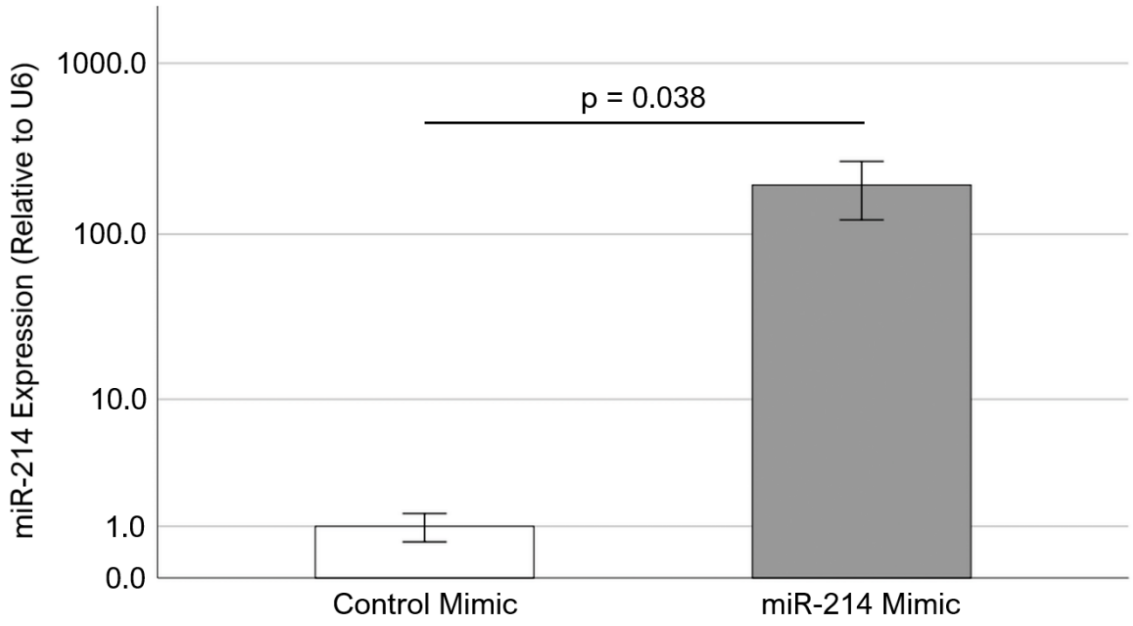

Figure 5.8 – Effect of miR-214 mimic (50 nM) on miR-214 expression in PAV leaflets after 2 weeks of static culture in osteogenic medium (n = 7 – 8). Data are presented as mean ± standard error of mean.

Freshly obtained porcine aortic valve (PAV) leaflets were cultured under static condition for 2 weeks in osteogenic medium. Overexpression of miR-214 was accomplished by using a synthetic miR-214 mimic (QIAGEN, Germantown, MD). For the control and treatment groups, the osteogenic medium was supplemented with 50 nM negative control mimic and miR-214 mimic, respectively. For both cases, Lipofectamine™

2000 (THERMO FISHER SCIENTIFIC, Waltham, MA) was used as the transfection reagent and the supplementation was done at Day 0 and Day 7. After completion of the static experiments, the expression of miR-214 (relative to U6) was evaluated in the cultured tissue samples using RT-qPCR. It was found that addition of 50 nM miR-214 mimic at Day 0 and Day 7 resulted in significant increase in miR-214 expression compared to the control case (as shown in Figure 5.8).

5.9 Effect of miR-214 Overexpression on Porcine Aortic Valve (PAV) Calcification under Static Culture in Osteogenic Medium

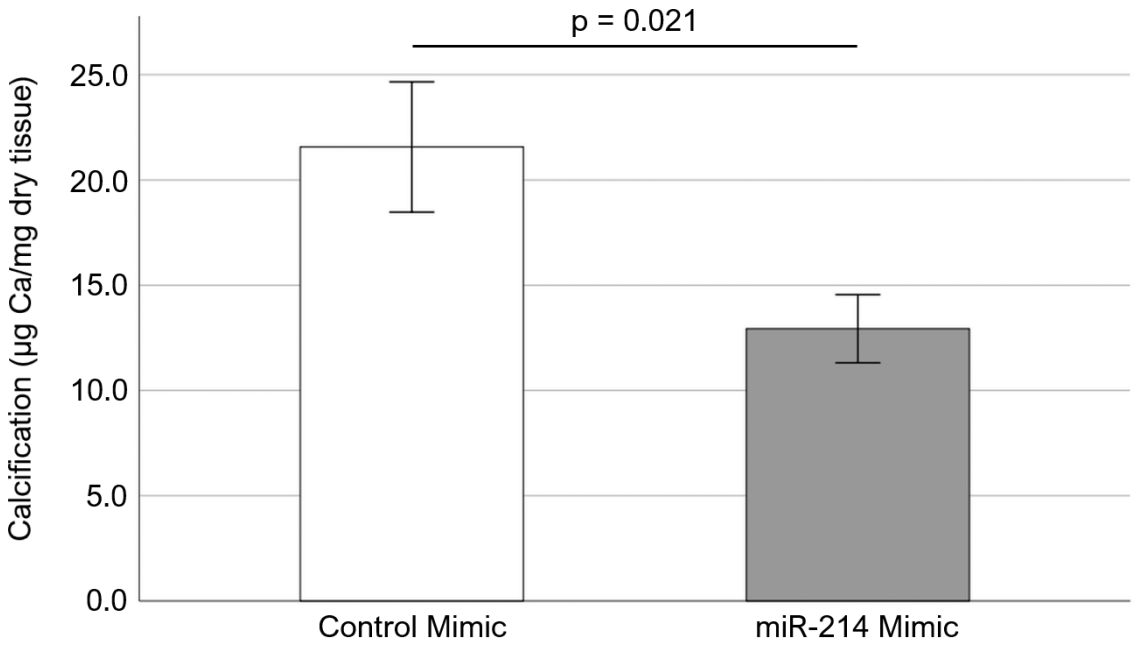

Figure 5.9.1 – Effect of miR-214 mimic (50 nM) on PAV leaflet calcification (dry basis) after 2 weeks of static culture in osteogenic medium, as determined by Arsenazo assay (n = 7 – 8). Data are presented as mean ± standard error of mean.

Freshly obtained porcine aortic valve (PAV) leaflets were cultured under static condition for 2 weeks in osteogenic medium. Overexpression of miR-214 was accomplished by using a synthetic miR-214 mimic (QIAGEN, Germantown, MD). For the

control and treatment groups, the osteogenic medium was supplemented with 50 nM negative control mimic and miR-214 mimic, respectively. For both cases, Lipofectamine™ 2000 (THERMO FISHER SCIENTIFIC, Waltham, MA) was used as the transfection reagent and the supplementation was done at Day 0 and Day 7. After completion of the static experiments, the degree of calcification in PAV leaflets was quantitatively assessed by Arsenazo assay. It was found that addition of 50 nM miR-214 mimic at Day 0 and Day 7 resulted in significant decrease in PAV leaflet calcification (dry basis) compared to the control case (as shown in Figure 5.9.1). Similar downregulation in PAV leaflet calcification can also be observed under wet basis (as shown in Figure 5.9.2).

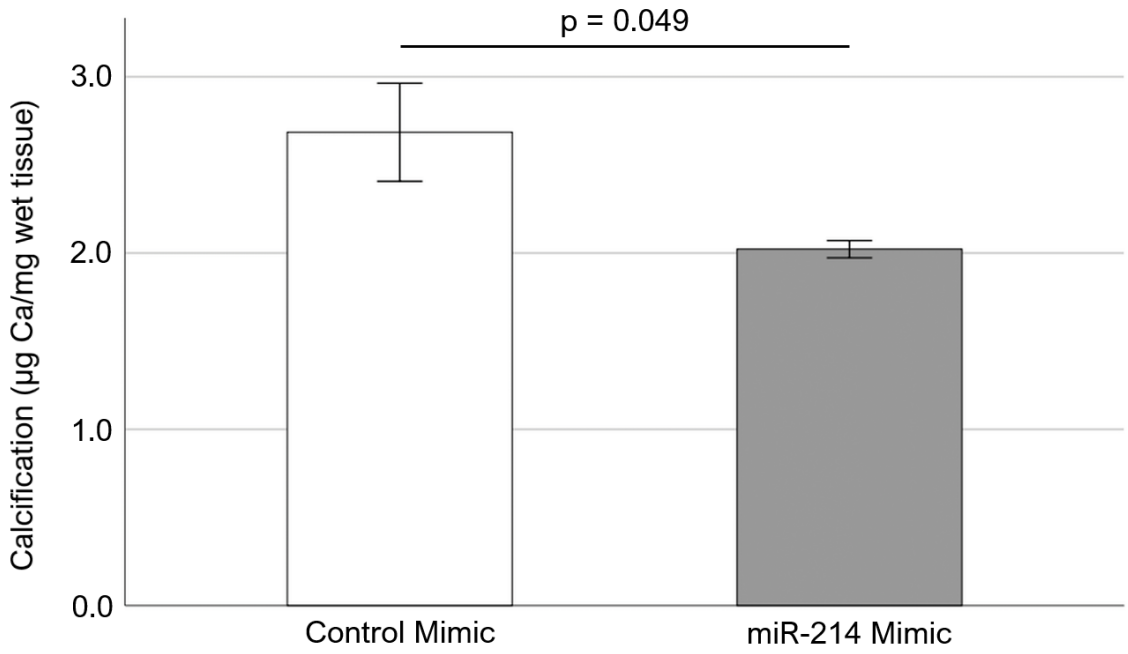

Figure 5.9.2 – Effect of miR-214 mimic (50 nM) on PAV leaflet calcification (wet basis) after 2 weeks of static culture in osteogenic medium, as determined by Arsenazo assay (n = 7 – 8). Data are presented as mean ± standard error of mean.

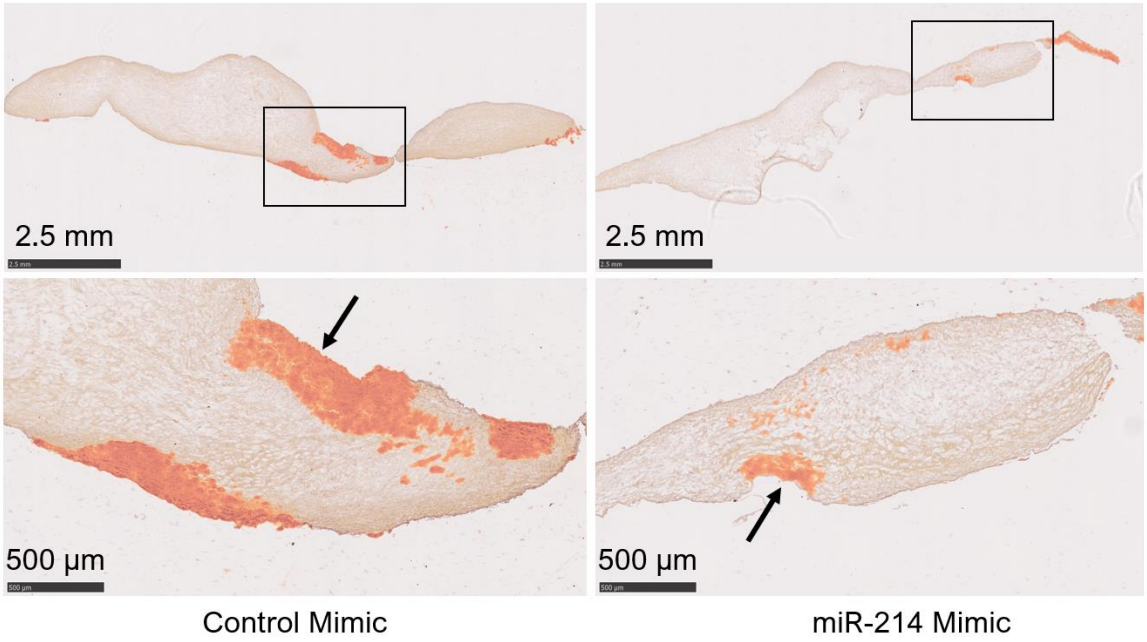

Figure 5.9.3.1 – Representative Alizarin Red staining images of PAV leaflets (top row: lower magnification, bottom row: higher magnification) after 2 weeks of static culture in osteogenic medium. Arrows indicate areas of calcification.

In addition, Alizarin Red and Von Kossa stains were performed to qualitatively assess the degree of calcification in PAV leaflets treated with negative control mimic and miR-214 mimic. Briefly, 10-µm frozen PAV tissue sections were hydrated and incubated in 2% Alizarin Red solution (2 g per 100 mL DI water; pH = 4.1 – 4.3) for 30 seconds to 1 minute. Alizarin Red binds to calcium and positive staining is identified as orange or red in color. It was found that addition of 50 nM miR-214 mimic at Day 0 and Day 7 resulted in significantly lower positive staining (i. e. calcification) in PAV leaflets compared to the control case, as shown in representative images in Figure 5.9.3.1. ImageJ software was used to further quantify the amount of positively stained area as a percentage of total tissue area in these images. It was found that indeed, addition of 50 nM miR-214 mimic at Day 0 and Day 7 resulted in significant reduction in positively stained area compared to the control case (as shown in Figure 5.9.3.2).

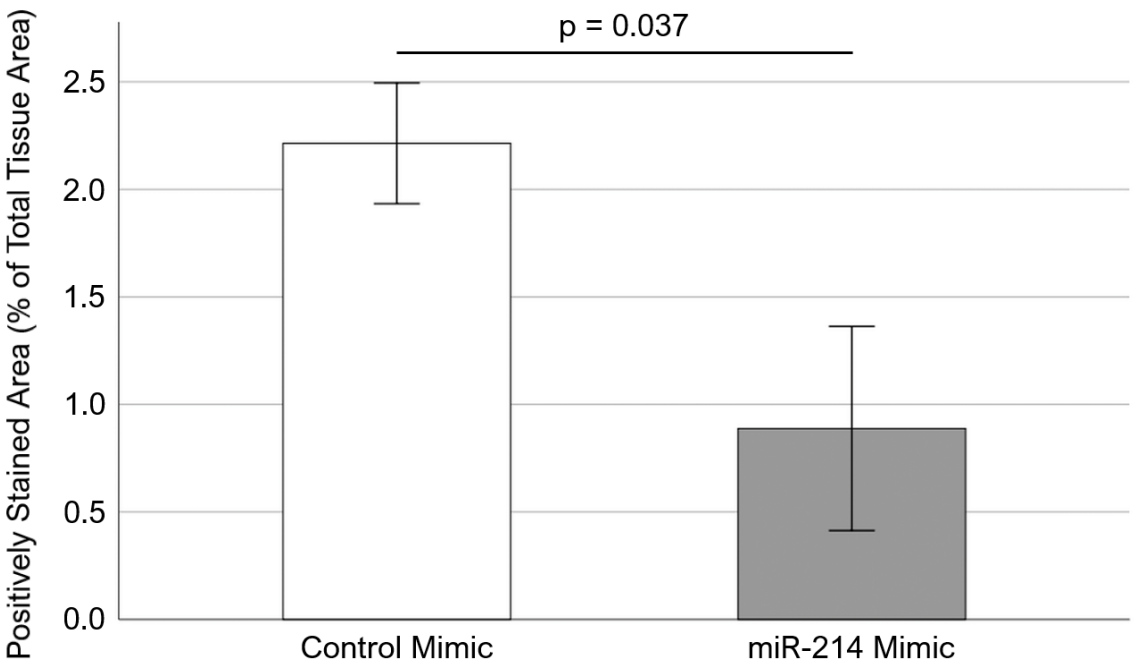

Figure 5.9.3.2 – Quantification of Alizarin Red staining images of PAV leaflets after 2 weeks of static culture in osteogenic medium (n = 6). Data are presented as mean ± standard error of mean.

For the Von Kossa stain, 10-µm frozen PAV tissue sections were hydrated and incubated in 5% silver nitrate solution (5 g per 100 mL DI water) for 1 hour under UV light. Typically, black areas (indicative of calcification) would be visible on the tissue sections after 1-hour incubation. Silver cations (Ag^{+}) react with calcium phosphate to generate this black coloration. The tissue sections were subsequently incubated in 5% sodium thiosulfate solution (5 g per 100 mL DI water) and 0.1% Nuclear Fast Red solution (0.1 g Nuclear Fast Red and 5 g aluminum sulfate per 100 mL DI water) for 5 minutes (each), respectively. It was found that addition of 50 nM miR-214 mimic at Day 0 and Day 7 resulted in lower positive staining (i. e. calcification) in PAV leaflets compared to the control case, as shown in representative images in Figure 5.9.4.1.

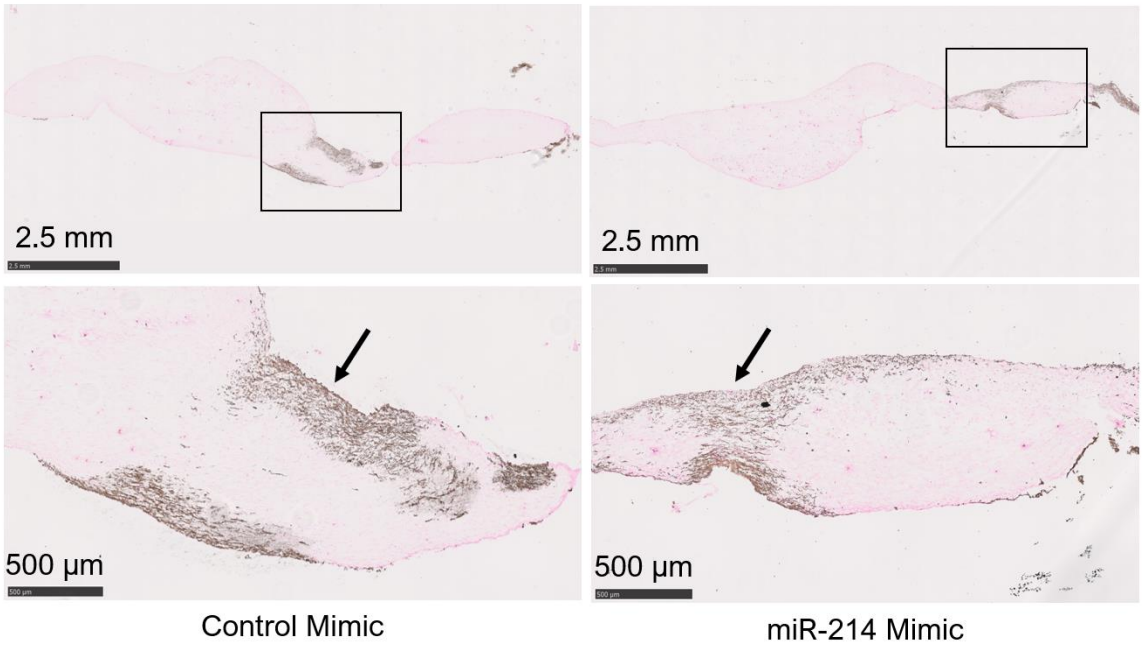

Figure 5.9.4.1 – Representative Von Kossa staining images of PAV leaflets (top row: lower magnification, bottom row: higher magnification) after 2 weeks of static culture in osteogenic medium. Arrows indicate areas of calcification.

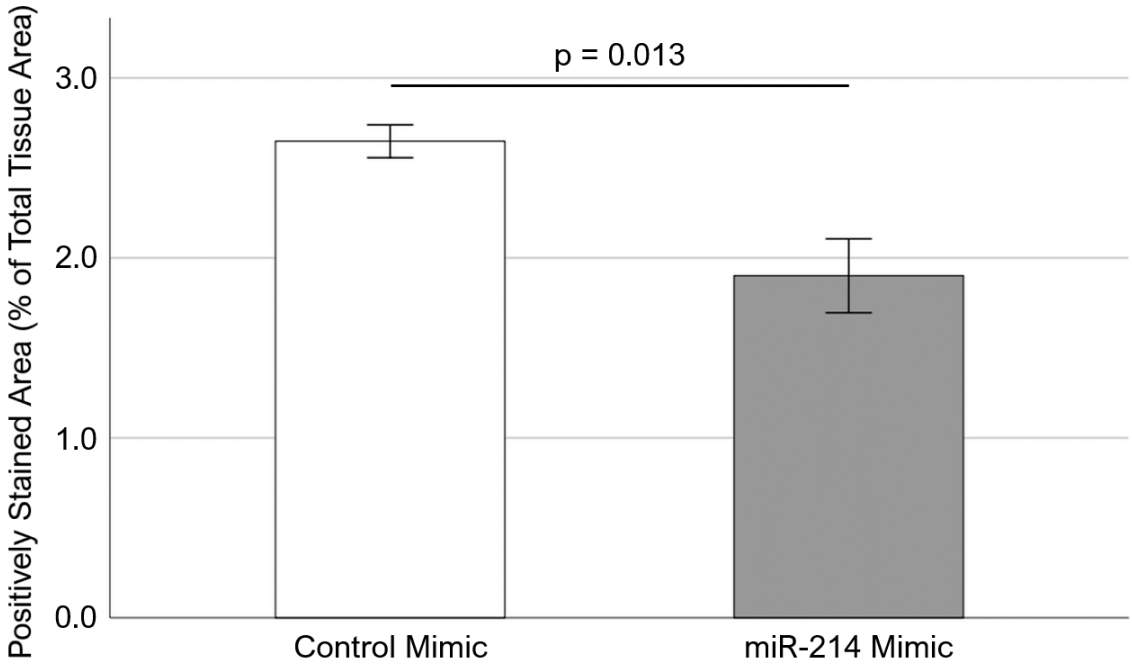

Figure 5.9.4.2 – Quantification of Von Kossa staining images of PAV leaflets after 2 weeks of static culture in osteogenic medium (n = 4 – 6). Data are presented as mean ± standard error of mean.

ImageJ software was used to further quantify the amount of positively stained area as a percentage of total tissue area in these images. It was found that indeed, addition of 50 nM miR-214 mimic at Day 0 and Day 7 resulted in significant reduction in positively stained area compared to the control case (as shown in Figure 5.9.4.2).

5.10 miR-214 Overexpression in Porcine Aortic Valves (PAVs) under Pathological (15%) Stretch in Osteogenic Medium

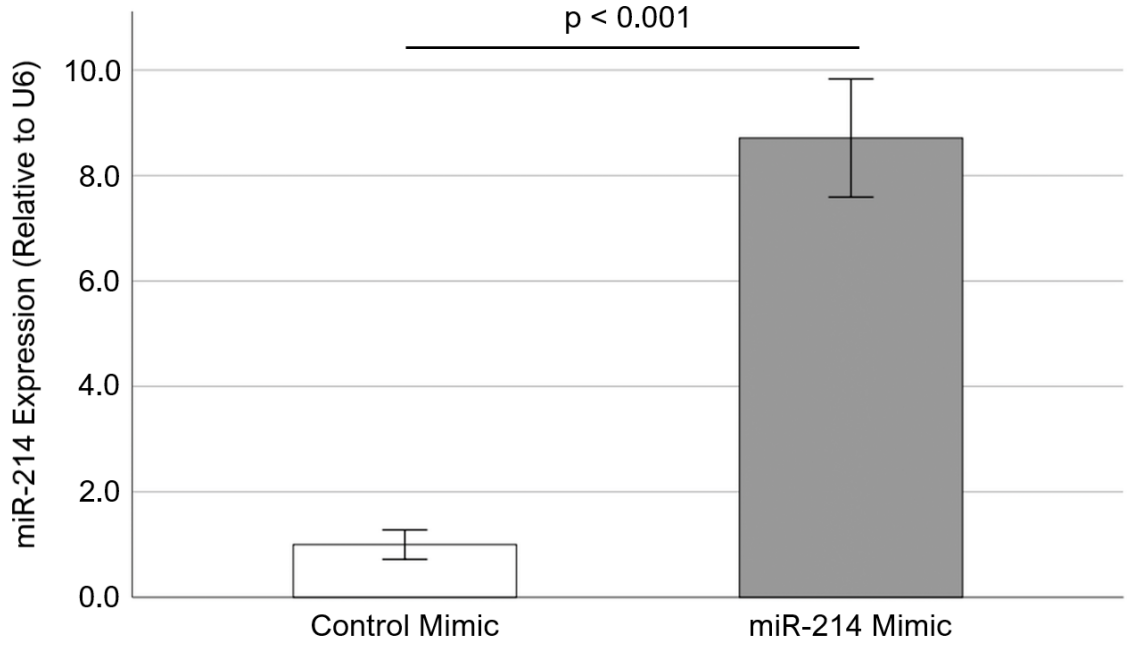

Figure 5.10 – Effect of miR-214 mimic (50 nM) on miR-214 expression in PAV leaflets after 1 week of 15% stretch in osteogenic medium (n = 6 – 7). Data are presented as mean ± standard error of mean.

Freshly obtained porcine aortic valve (PAV) leaflets were cyclically (1 Hz) stretched at 15% for 1 week in osteogenic medium. Overexpression of miR-214 was accomplished by using a synthetic miR-214 mimic (QIAGEN, Germantown, MD). For the control and treatment groups, the osteogenic medium was supplemented with 50 nM negative control mimic and miR-214 mimic, respectively. For both cases, Lipofectamine^{TM} 2000

(THERMO FISHER SCIENTIFIC, Waltham, MA) was used as the transfection reagent and the supplementation was done at Day 0. After completion of the stretch experiments, the expression of miR-214 (relative to U6) was evaluated in the cultured tissue samples using RT-qPCR. It was found that addition of 50 nM miR-214 mimic at Day 0 resulted in significant increase in miR-214 expression compared to the control case (as shown in Figure 5.10).

5.11 Effect of miR-214 Overexpression on Porcine Aortic Valve (PAV) Calcification under Pathological (15%) Stretch in Osteogenic Medium

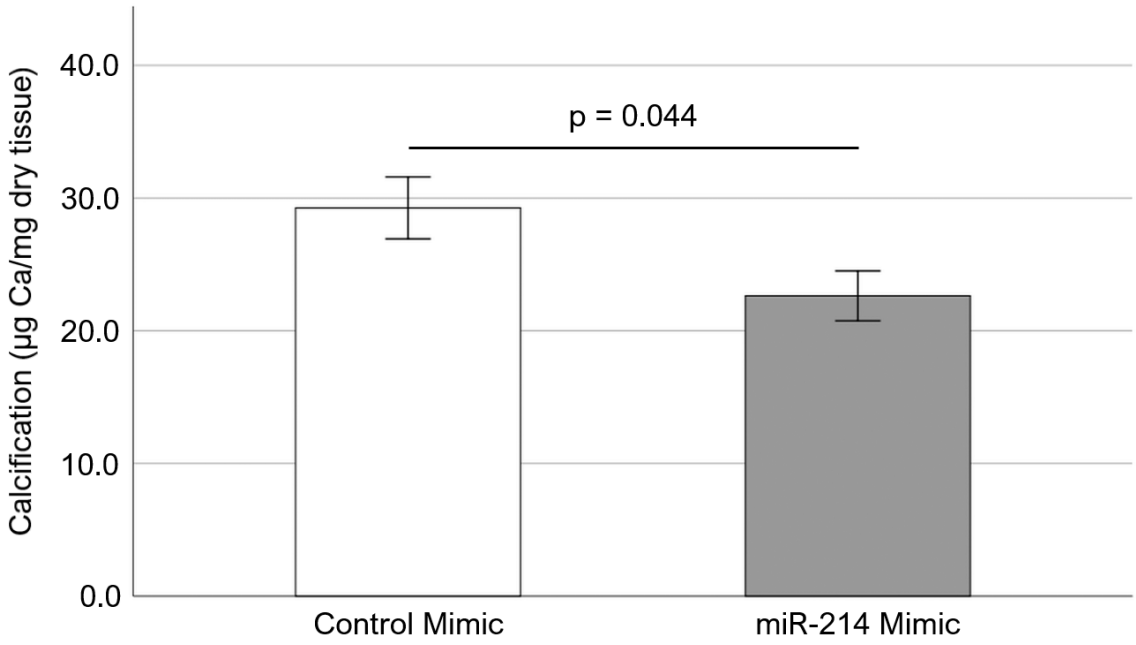

Figure 5.11.1 – Effect of miR-214 mimic (50 nM) on PAV leaflet calcification (dry basis) after 1 week of 15% stretch in osteogenic medium, as determined by Arsenazo assay (n = 8). Data are presented as mean ± standard error of mean.

Freshly obtained porcine aortic valve (PAV) leaflets were cyclically (1 Hz) stretched at 15% for 1 week in osteogenic medium. Overexpression of miR-214 was accomplished by using a synthetic miR-214 mimic (QIAGEN, Germantown, MD). For the control and treatment groups, the osteogenic medium was supplemented with 50 nM negative control

mimic and miR-214 mimic, respectively. For both cases, Lipofectamine™ 2000 (THERMO FISHER SCIENTIFIC, Waltham, MA) was used as the transfection reagent and the supplementation was done at Day 0.

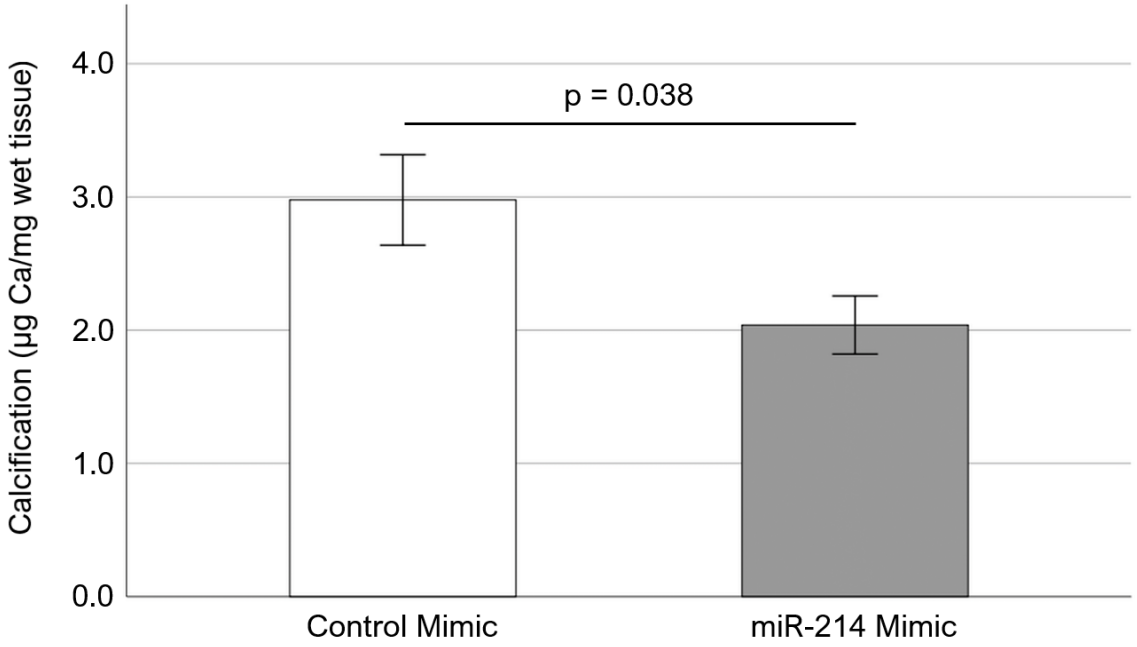

Figure 5.11.2 – Effect of miR-214 mimic (50 nM) on PAV leaflet calcification (wet basis) after 1 week of 15% stretch in osteogenic medium, as determined by Arsenazo assay (n = 8). Data are presented as mean ± standard error of mean.

After completion of the stretch experiments, the degree of calcification in PAV leaflets was quantitatively assessed by Arsenazo assay. It was found that addition of 50 nM miR-214 mimic at Day 0 resulted in significant decrease in PAV leaflet calcification (dry basis) compared to the control case (as shown in Figure 5.11.1). Similar downregulation in PAV leaflet calcification can also be observed under wet basis (as shown in Figure 5.11.2).

From the experimental results presented in sections **5.8 – 5.11**, it is evident that miR-214 has an inhibitory effect on calcification of PAV leaflets. Now, the question is: what is the underlying mechanism of this inhibitory effect?

5.12 Effect of Cyclic Stretch on TWIST1 mRNA Expression in Porcine Aortic Valves (PAVs)

Twist-Related Protein 1 (TWIST1) is a basic helix-loop-helix (bHLH) transcription factor that plays an important role in embryonic development. It has been shown that TWIST1 regulates the miR-199a/214 cluster (Lee *et al*., 2009). Overexpression of TWIST1 induced upregulation of miR-214 expression in N2a neuroblastoma cells and vice versa. Interestingly, calcified human aortic valves (AVs) were found to express lower levels of TWIST1 protein compared to healthy human AVs (Zhang *et al*., 2014). In addition, overexpression of TWIST1 in human aortic valve interstitial cells (HAVICs) significantly downregulated osteogenic differentiation of HAVICs and vice versa. This implies that TWIST1 has an inhibitory role in human AV calcification. Hence, it would be important to see how cyclic stretch modulates TWIST1 expression.

Freshly obtained porcine aortic valve (PAV) leaflets were cyclically (1 Hz) stretched at 10% and 15% for 2 days in regular medium. After completion of the stretch experiments, the expression of TWIST1 (relative to 18S) was evaluated in the cyclically stretched tissue samples using RT-qPCR. It was found that TWIST1 mRNA expression was significantly downregulated at 15% stretch compared to 10% (as shown in Figure 5.12). This indicates that the significant decrease in TWIST1 mRNA expression under pathological (15%) stretch might have caused the observed downregulation in miR-214 expression at 15% stretch (as shown in Figure 5.7).

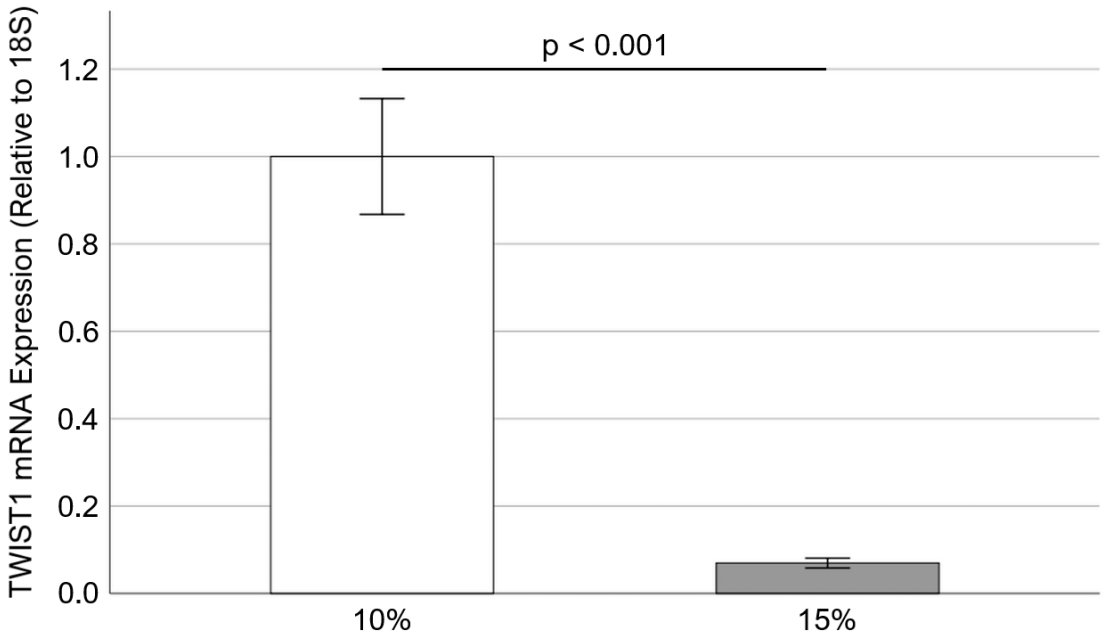

Figure 5.12 – Effect of cyclic stretch on TWIST1 mRNA expression in PAV leaflets (n = 7 – 8). Data are presented as mean ± standard error of mean.

5.13 Effect of miR-214 Overexpression on XBP1 mRNA Expression in Porcine Aortic Valves (PAVs)

X-Box Binding Protein 1 (XBP1) is a transcription factor that regulates Major Histocompatibility Complex (MHC) class II genes by binding to a promoter element referred to as an X-box. Under endoplasmic reticulum (ER) stress condition, the mRNA of this gene is processed to an active form by an unconventional splicing mechanism. Duan *et al*. (2012) showed that miR-214 directly targets XBP1 in HepG2 human hepatoma cells. In addition, Duan *et al*. (2015) found that miR-214 targets XBP1 in human umbilical vein endothelial cells (HUVECs). Hence, it is possible that miR-214 can also target XBP1 in aortic valve (AV) tissue.

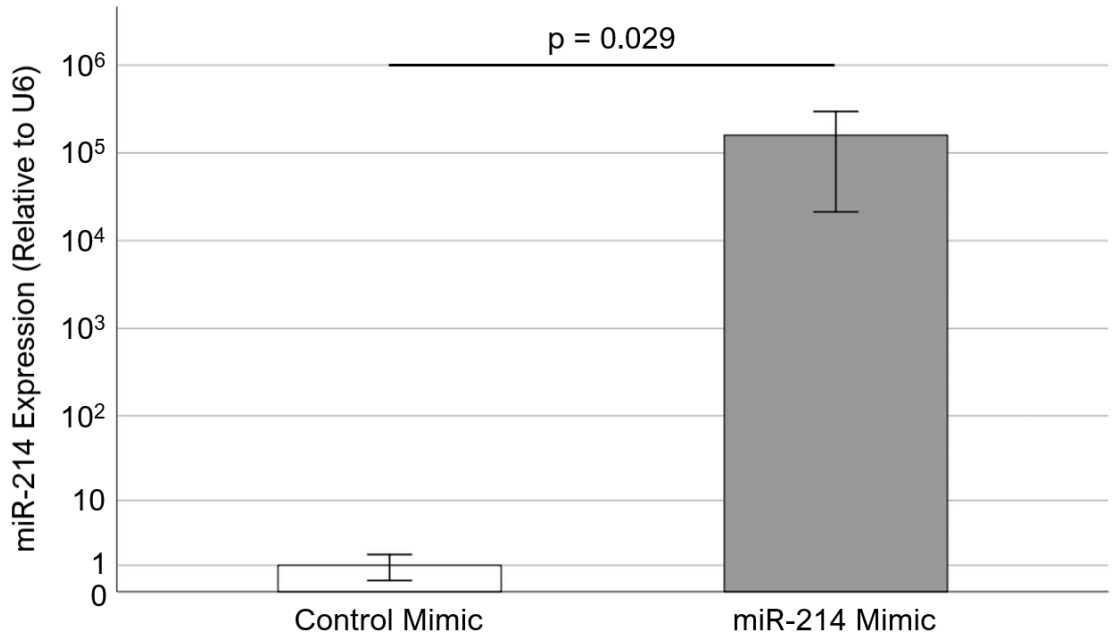

Figure 5.13.1 – Effect of miR-214 mimic (50 nM) on miR-214 expression in PAV leaflets after 2 days of static culture in osteogenic medium (n = 4). Data are presented as mean ± standard error of mean.

To test this hypothesis, freshly obtained porcine aortic valve (PAV) leaflets were cultured under static condition for 2 days in osteogenic medium. Overexpression of miR-214 was accomplished by using a synthetic miR-214 mimic (QIAGEN, Germantown, MD). For the control and treatment groups, the osteogenic medium was supplemented with 50 nM negative control mimic and miR-214 mimic, respectively. For both cases, LipofectamineTM 2000 (THERMO FISHER SCIENTIFIC, Waltham, MA) was used as the transfection reagent and the supplementation was done at Day 0. After completion of the static experiments, the expression of miR-214 (relative to U6) was evaluated in the cultured tissue samples using RT-qPCR. It was found that addition of 50 nM miR-214 mimic at Day 0 resulted in significant increase in miR-214 expression compared to the control case (as shown in Figure 5.13.1). Furthermore, the expression of XBP1 mRNA (relative to 18S) was evaluated in the cyclically stretched tissue samples using RT-qPCR.

It was found that addition of 50 nM miR-214 mimic at Day 0 did not result in a significant change in XBP1 mRNA expression compared to the control case (as shown in Figure 5.13.2). This indicates that miR-214 does not target XBP1 mRNA in PAV tissue.

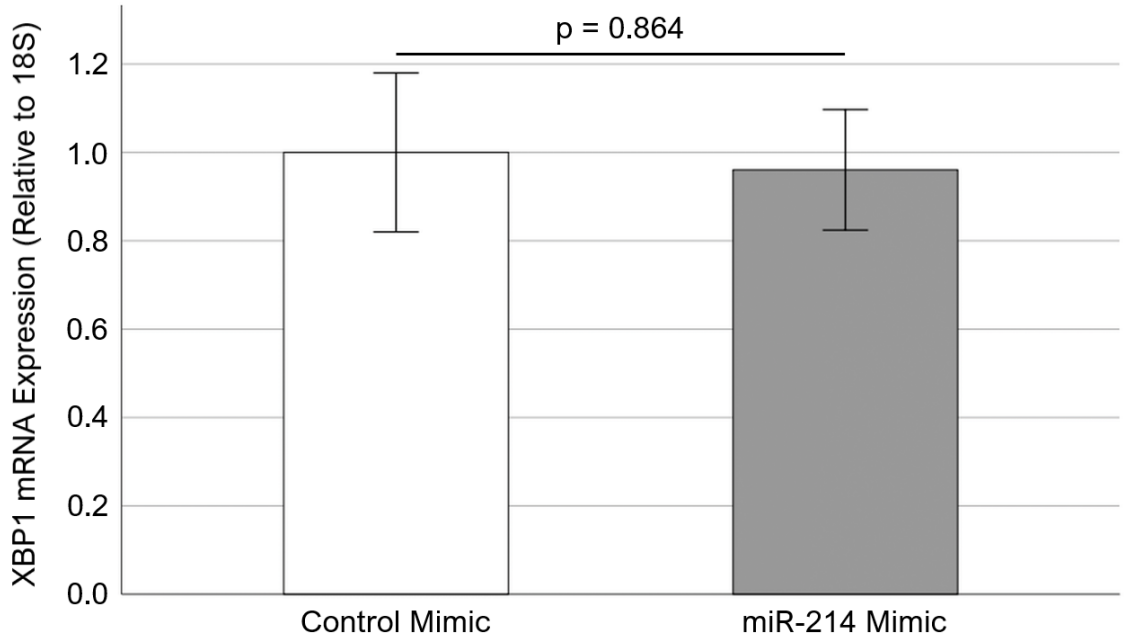

Figure 5.13.2 – Effect of miR-214 mimic (50 nM) on XBP1 mRNA expression in PAV leaflets after 2 days of static culture in osteogenic medium (n = 7 – 8). Data are presented as mean ± standard error of mean.

5.14 Effect of Cyclic Stretch on XBP1 mRNA Expression in Porcine Aortic Valves (PAVs)

Freshly obtained porcine aortic valve (PAV) leaflets were cyclically (1 Hz) stretched at 10% and 15% for 2 days in osteogenic medium. After completion of the stretch experiments, the expression of XBP1 mRNA (relative to 18S) was evaluated in the cyclically stretched tissue samples using RT-qPCR. It was found that there was no significant difference in XBP1 mRNA expression between 10% and 15% stretch (as shown in Figure 5.14).

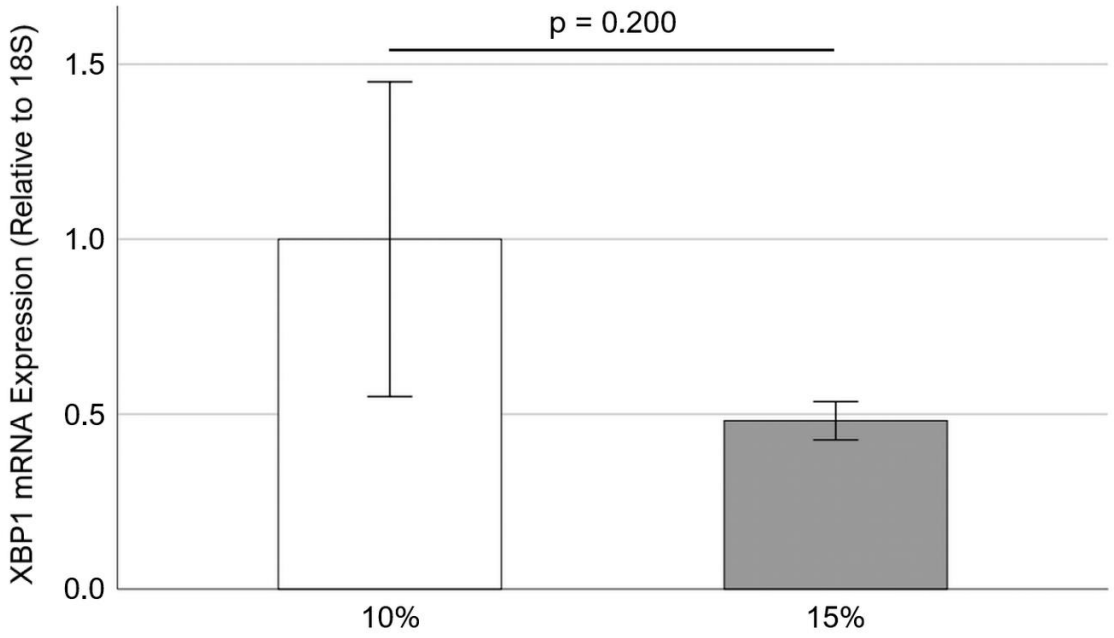

Figure 5.14 – Effect of cyclic stretch on XBP1 mRNA expression in PAV leaflets (n = 4). Data are presented as mean ± standard error of mean.

Since the expression of miR-214 is stretch-sensitive in PAV tissue (Figure 5.7), the expression of an mRNA target of miR-214 should be stretch-sensitive as well. So, it makes sense that the expression of XBP1 mRNA is not stretch-sensitive, as it is not targeted by miR-214 in PAV tissue (Figure 5.13.2).

5.15 Effect of miR-214 Overexpression on RNF111 mRNA Expression in Porcine Aortic Valves (PAVs)

Ring Finger Protein 111 (RNF111) is a nuclear RING-domain containing E3 ubiquitin ligase. RNF111 plays a key role in the induction of mesoderm during embryonic development. RNF111 enhances Transforming Growth Factor-β (TGF-β) signaling by promoting the ubiquitination and proteosomal degradation of negative regulators, such as SMAD Family Member 7 or SMAD7 (Koinuma *et al.*, 2003). In addition, RNF111 is a predicted target of miR-214 (Tokar *et al.*, 2018). Considering that Transforming Growth

Factor-β1 (TGF-β1) promotes aortic valve (AV) calcification (Jian *et al*., 2003), it will be interesting to see whether miR-214 targets RNF111 in AV tissue.

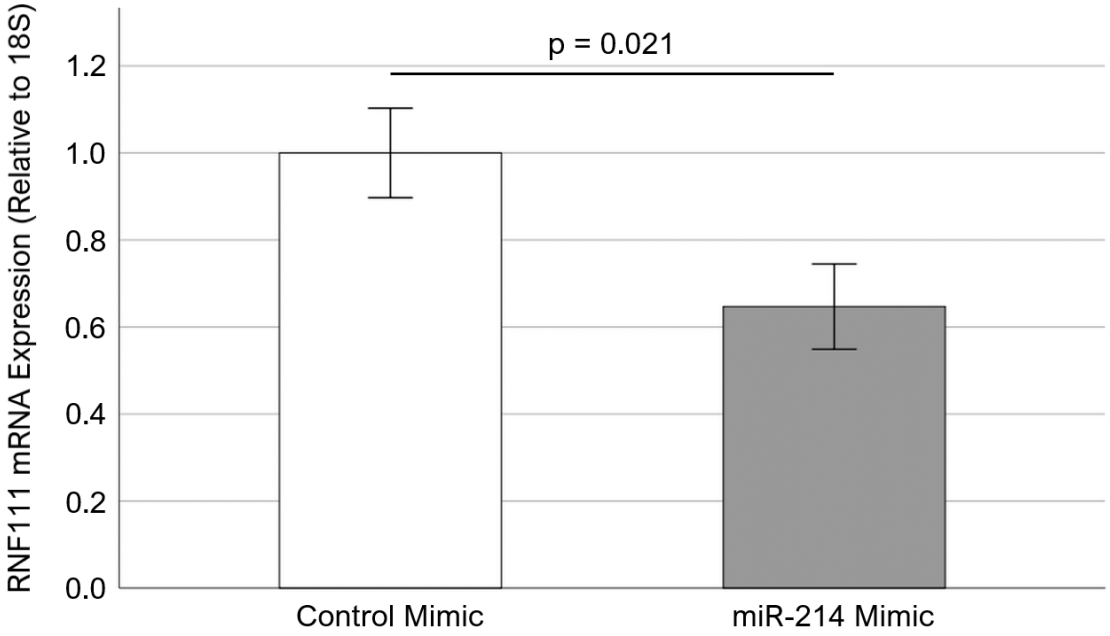

Figure 5.15 – Effect of miR-214 mimic (50 nM) on RNF111 mRNA expression in PAV leaflets after 2 days of static culture in osteogenic medium (n = 12). Data are presented as mean ± standard error of mean.

To test this hypothesis, freshly obtained porcine aortic valve (PAV) leaflets were cultured under static condition for 2 days in osteogenic medium. Overexpression of miR-214 was accomplished by using a synthetic miR-214 mimic (QIAGEN, Germantown, MD). For the control and treatment groups, the osteogenic medium was supplemented with 50 nM negative control mimic and miR-214 mimic, respectively. For both cases, Lipofectamine^{TM} 2000 (THERMO FISHER SCIENTIFIC, Waltham, MA) was used as the transfection reagent and the supplementation was done at Day 0. After completion of the static experiments, the expression of RNF111 mRNA (relative to 18S) was evaluated in the cyclically stretched tissue samples using RT-qPCR. It was found that addition of 50 nM miR-214 mimic at Day 0 resulted in a significant decrease in RNF111 mRNA

expression compared to the control case (as shown in Figure 5.15). This indicates that miR-214 targets RNF111 mRNA in PAV tissue.

5.16 Effect of Cyclic Stretch on RNF111 mRNA Expression in Porcine Aortic Valves (PAVs)

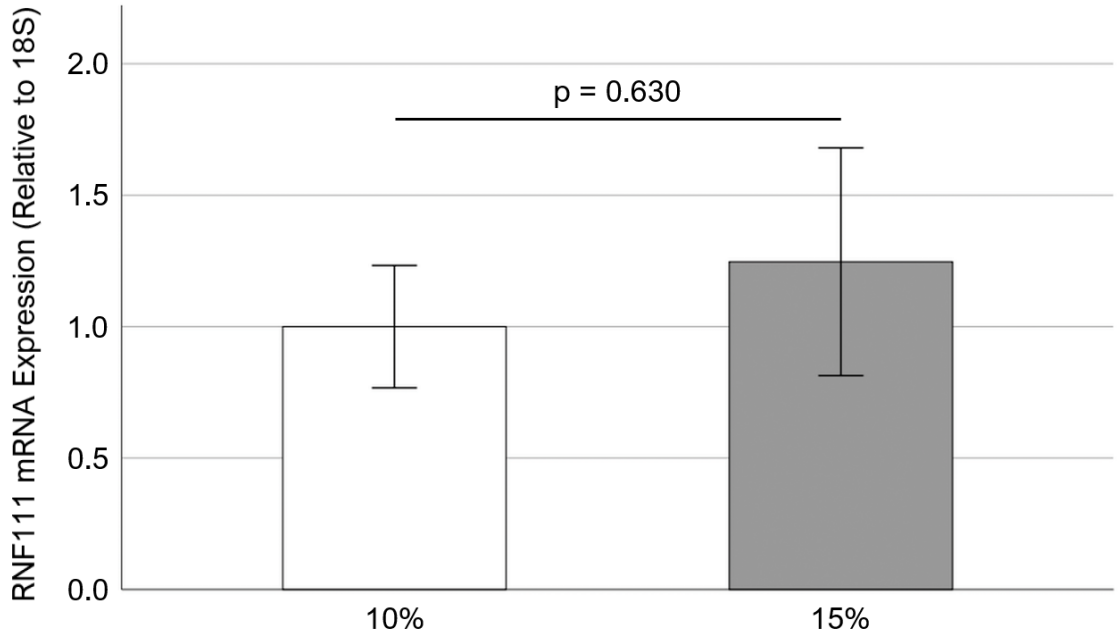

Figure 5.16 – Effect of cyclic stretch on RNF111 mRNA expression in PAV leaflets (n = 6). Data are presented as mean ± standard error of mean.

Freshly obtained porcine aortic valve (PAV) leaflets were cyclically (1 Hz) stretched at 10% and 15% for 1 week in osteogenic medium. After completion of the stretch experiments, the expression of RNF111 mRNA (relative to 18S) was evaluated in the cyclically stretched tissue samples using RT-qPCR. It was found that there was no significant difference in RNF111 mRNA expression between 10% and 15% stretch (as shown in Figure 5.16).

Since the expression of miR-214 is stretch-sensitive in PAV tissue (Figure 5.7), the expression of a major mRNA target of miR-214 should be stretch-sensitive as well. As shown in Figure 5.15, miR-214 targets RNF111 in PAV tissue; however, the expression of RNF111 mRNA is not stretch-sensitive (Figure 5.16). This implies that miR-214 may not be a strong modulator of RNF111 mRNA expression in PAV tissue.

5.17 Effect of miR-214 Overexpression on BCL2L1 mRNA Expression in Porcine Aortic Valves (PAVs)

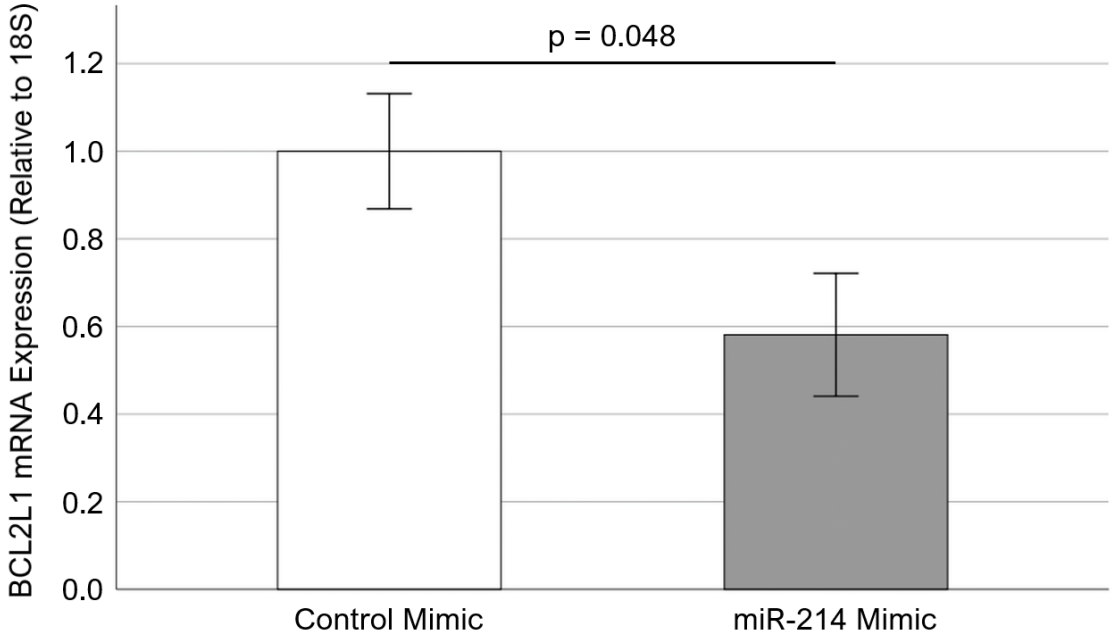

Figure 5.17 – Effect of miR-214 mimic (50 nM) on BCL2L1 mRNA expression in PAV leaflets after 2 days of static culture in osteogenic medium (n = 7 – 8). Data are presented as mean ± standard error of mean.

Bcl-2-Like Protein 1 (BCL2L1) is a member of the BCL-2 gene family. BCL-2 family members form hetero- or homodimers and act as anti- or pro-apoptotic regulators that are involved in a wide variety of cellular activities. BCL2L1 is considered to be a potent inhibitor of cell death. Interestingly, BCL2L1 is a predicted target of miR-214

(Tokar *et al*., 2018). So, it will be important to see whether miR-214 targets BCL2L1 in AV tissue.

To test this hypothesis, freshly obtained porcine aortic valve (PAV) leaflets were cultured under static condition for 2 days in osteogenic medium. Overexpression of miR-214 was accomplished by using a synthetic miR-214 mimic (QIAGEN, Germantown, MD). For the control and treatment groups, the osteogenic medium was supplemented with 50 nM negative control mimic and miR-214 mimic, respectively. For both cases, Lipofectamine^{TM} 2000 (THERMO FISHER SCIENTIFIC, Waltham, MA) was used as the transfection reagent and the supplementation was done at Day 0. After completion of the static experiments, the expression of BCL2L1 mRNA (relative to 18S) was evaluated in the cyclically stretched tissue samples using RT-qPCR. It was found that addition of 50 nM miR-214 mimic at Day 0 resulted in a significant decrease in BCL2L1 mRNA expression compared to the control case (as shown in Figure 5.17). This indicates that miR-214 targets BCL2L1 mRNA in PAV tissue.

5.18 Effect of Cyclic Stretch on BCL2L1 mRNA Expression in Porcine Aortic Valves (PAVs)

Freshly obtained porcine aortic valve (PAV) leaflets were cyclically (1 Hz) stretched at 10% and 15% for 2 days in osteogenic medium. After completion of the stretch experiments, the expression of BCL2L1 mRNA (relative to 18S) was evaluated in the cyclically stretched tissue samples using RT-qPCR. It was found that there was an almost significant decrease in BCL2L1 mRNA expression at 15% stretch compared to 10% (as shown in Figure 5.18).

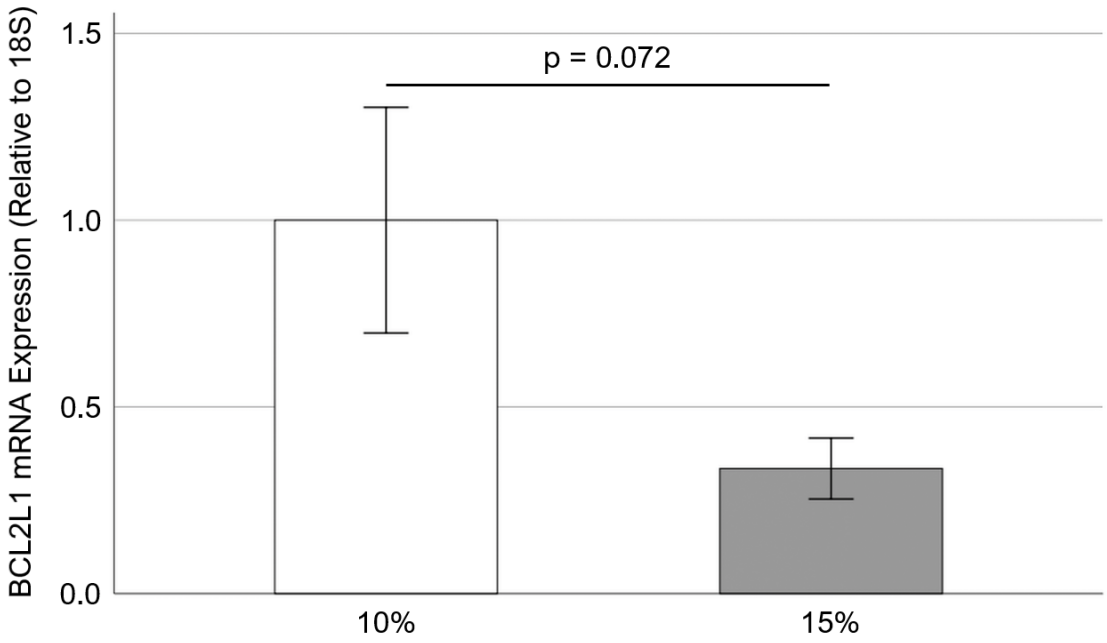

Figure 5.18 – Effect of cyclic stretch on BCL2L1 mRNA expression in PAV leaflets (n = 7 – 8). Data are presented as mean ± standard error of mean.

Since the expression of miR-214 is stretch-sensitive in PAV tissue (Figure 5.7), the expression of a major mRNA target of miR-214 should be stretch-sensitive as well. In addition, since the expression of miR-214 is downregulated at 15% stretch compared to 10%, the opposite should be observed for a major mRNA target of miR-214. As shown in Figure 5.17, miR-214 targets BCL2L1 in PAV tissue; however, the expression of BCL2L1 mRNA is downregulated at 15% stretch compared to 10% (Figure 5.18). This implies that miR-214 may not be a strong modulator of BCL2L1 mRNA expression in PAV tissue.

5.19 Effect of miR-214 Overexpression on ATF4 mRNA Expression in Porcine Aortic Valves (PAVs)

Activating Transcription Factor 4 (ATF4) binds the cAMP response element (CRE) and acts as a master transcription factor during integrated stress response (ISR). ATF4 protein expression was found to be upregulated in calcified human aortic valves (AVs)

compared to healthy ones (Wang *et al*., 2017; Cai *et al*., 2013). Functionally, ATF4 is known to promote osteogenesis (Yang *et al*., 2004; Yang *et al*., 2004). In addition, miR-214 has been shown to target ATF4 to inhibit bone formation (Wang *et al*., 2013). Hence, it will be interesting to see whether miR-214 targets ATF4 in AV tissue.

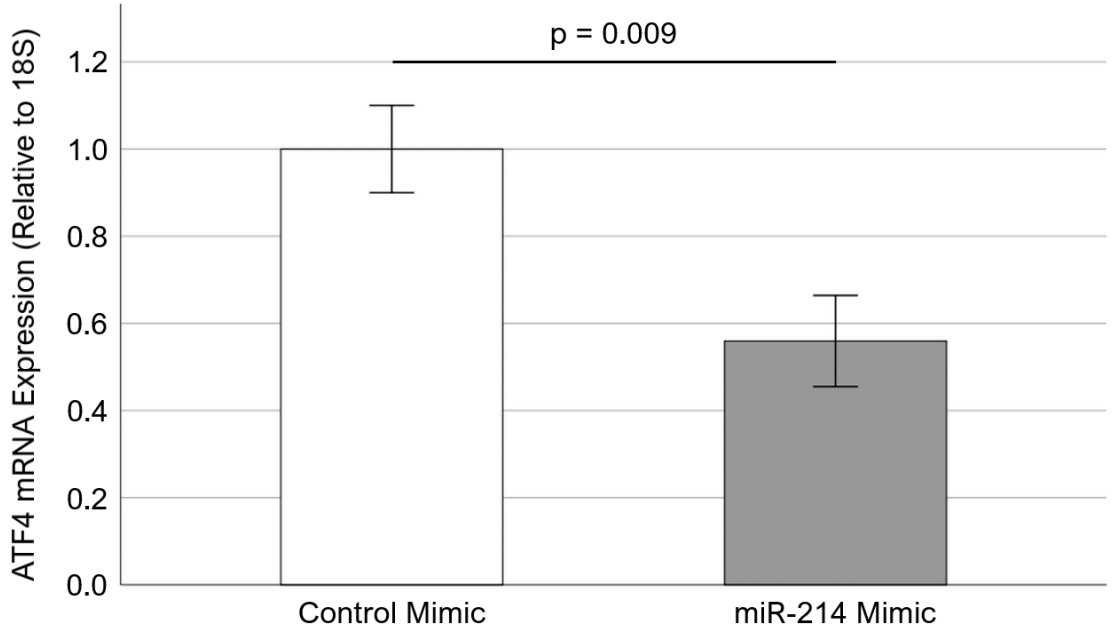

Figure 5.19 – Effect of miR-214 mimic (50 nM) on ATF4 mRNA expression in PAV leaflets after 2 days of static culture in osteogenic medium (n = 7 – 8). Data are presented as mean ± standard error of mean.

To test this hypothesis, freshly obtained porcine aortic valve (PAV) leaflets were cultured under static condition for 2 days in osteogenic medium. Overexpression of miR-214 was accomplished by using a synthetic miR-214 mimic (QIAGEN, Germantown, MD). For the control and treatment groups, the osteogenic medium was supplemented with 50 nM negative control mimic and miR-214 mimic, respectively. For both cases, Lipofectamine^{TM} 2000 (THERMO FISHER SCIENTIFIC, Waltham, MA) was used as the transfection reagent and the supplementation was done at Day 0. After completion of the static experiments, the expression of ATF4 mRNA (relative to 18S) was evaluated in the

cyclically stretched tissue samples using RT-qPCR. It was found that addition of 50 nM miR-214 mimic at Day 0 resulted in a significant decrease in ATF4 mRNA expression compared to the control case (as shown in Figure 5.19). This indicates that miR-214 targets ATF4 mRNA in PAV tissue.

5.20 Effect of Cyclic Stretch on ATF4 mRNA Expression in Porcine Aortic Valves (PAVs)

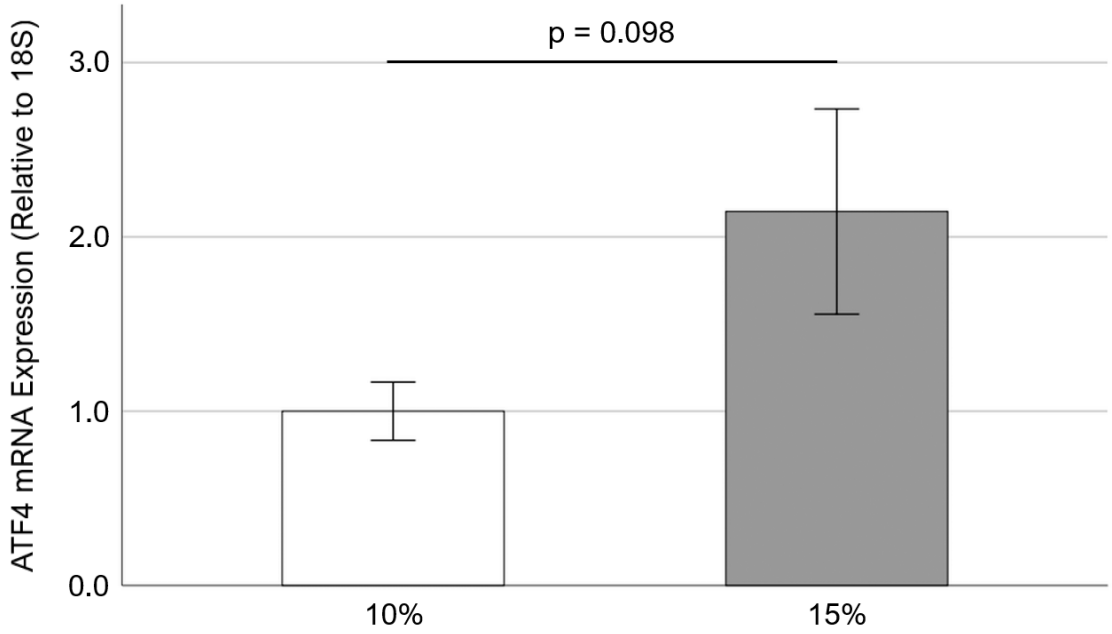

Figure 5.20 – Effect of cyclic stretch on ATF4 mRNA expression in PAV leaflets (n = 7 – 8). Data are presented as mean ± standard error of mean.

Freshly obtained porcine aortic valve (PAV) leaflets were cyclically (1 Hz) stretched at 10% and 15% for 1 week in osteogenic medium. After completion of the stretch experiments, the expression of ATF4 mRNA (relative to 18S) was evaluated in the cyclically stretched tissue samples using RT-qPCR. It was found that there was an almost significant increase in ATF4 mRNA expression at 15% stretch compared to 10% (as shown in Figure 5.20).

Since the expression of miR-214 is stretch-sensitive in PAV tissue (Figure 5.7), the expression of a major mRNA target of miR-214 should be stretch-sensitive as well. In addition, since the expression of miR-214 is downregulated at 15% stretch compared to 10%, the opposite should be observed for a major mRNA target of miR-214. As shown in Figures 5.19 and 5.20, miR-214 targets ATF4 in PAV tissue and the expression of ATF4 mRNA is upregulated at 15% stretch compared to 10%, respectively. This implies that miR-214 is a strong modulator of ATF4 mRNA expression in PAV tissue.

CHAPTER 6. SPECIFIC AIM 2 RESULTS

In this specific aim, firstly, the effect of different levels of cyclic stretch [physiological (10%) and pathological (15%)] on the relative expression of six mRNAs of interest (YAP1, SOX9, ASH2L, ROR2, ATP1A2, and UBE2C) in relation to calcific aortic valve disease (CAVD) was investigated. The associated findings are described in sections **6.1** – **6.6**. Then, the mechanistic role of one significant mRNA in relation to CAVD was examined. The associated findings are described in sections **6.7 – 6.10**.

6.1 Effect of Cyclic Stretch on YAP1 mRNA Expression in Porcine Aortic Valves (PAVs)

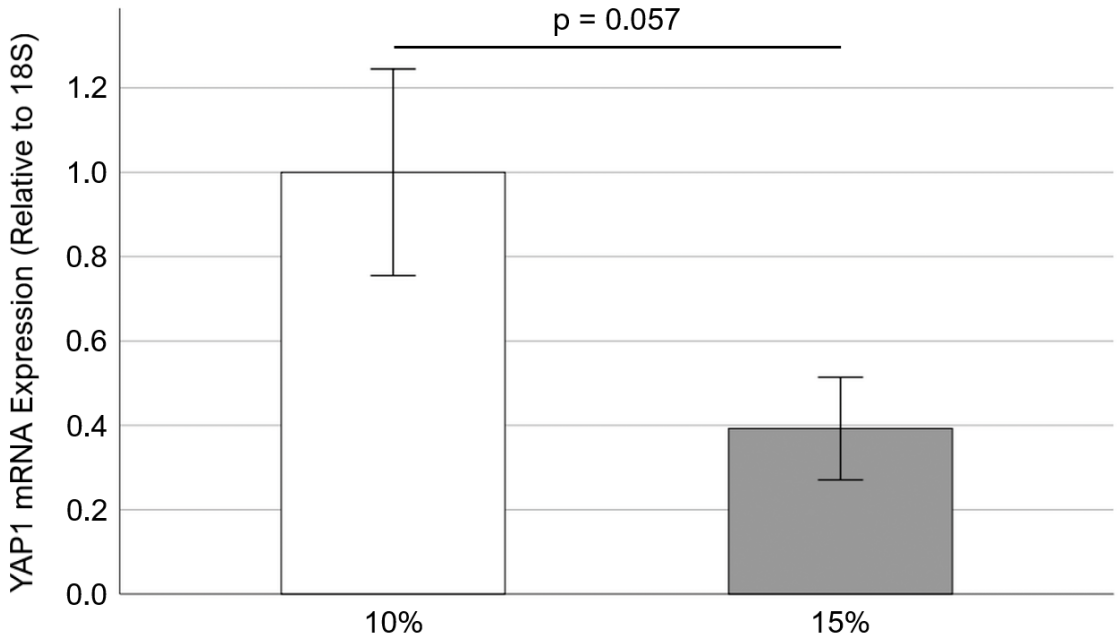

Figure 6.1 – Effect of cyclic stretch on YAP1 mRNA expression in PAV leaflets (n = 5). Data are presented as mean ± standard error of mean.

Yes Associated Protein 1 (YAP1) is a critical downstream regulatory target in the Hippo signaling pathway that plays a pivotal role in development, growth, repair, and

homeostasis. YAP-dependent transcriptional activity was found to be involved in the mechanosensing of interstitial cells (ICs) isolated from human stenotic aortic valves (AVs) (Santoro *et al*., 2018). In addition, loss of YAP has been shown to result in osteogenic differentiation of vascular smooth muscle cells (VSMCs) and vascular calcification (Wang *et al*., 2020). Hence, it will be interesting to see how cyclic stretch modulates YAP1 mRNA expression in AV tissue.

Freshly obtained porcine aortic valve (PAV) leaflets were cyclically (1 Hz) stretched at 10% and 15% for 2 days in regular medium. After completion of the stretch experiments, the expression of YAP1 mRNA (relative to 18S) was evaluated in the cyclically stretched tissue samples using RT-qPCR. It was found that there was an almost significant decrease in YAP1 mRNA expression at 15% stretch compared to 10% (as shown in Figure 6.1).

6.2 Effect of Cyclic Stretch on SOX9 mRNA Expression in Porcine Aortic Valves (PAVs)

SRY-Box Transcription Factor 9 (SOX9) is a transcription factor that plays a key role in chondrocyte differentiation and skeletal development. Reduction in SOX9 expression has been shown to promote aortic valve calcification (Peacock *et al*., 2010). In addition, SOX9 was found to repress the expression of osteogenic glycoprotein SPP1 (Secreted Phosphoprotein 1 or Osteopontin) (Peacock *et al.*, 2011). Hence, it will be interesting to see how cyclic stretch modulates SOX9 mRNA expression in AV tissue.

Freshly obtained porcine aortic valve (PAV) leaflets were cyclically (1 Hz) stretched at 10% and 15% for 3 days in regular medium. After completion of the stretch experiments, the expression of SOX9 mRNA (relative to 18S) was evaluated in the cyclically stretched

tissue samples using RT-qPCR. It was found that there was no significant difference in SOX9 mRNA expression between 10% and 15% stretch (as shown in Figure 6.2).

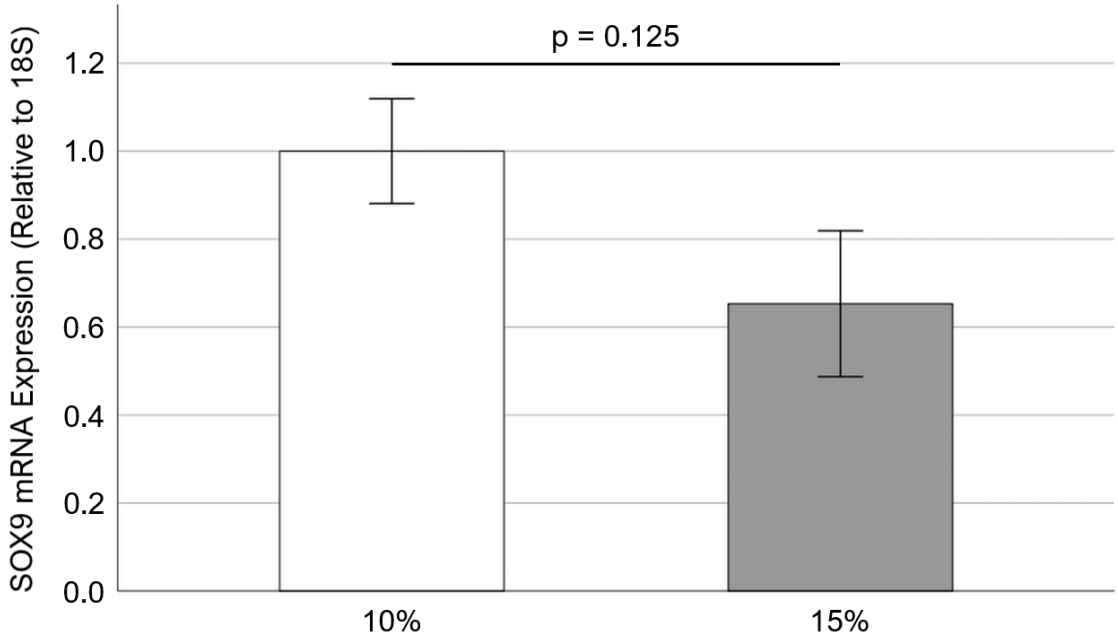

Figure 6.2 – Effect of cyclic stretch on SOX9 mRNA expression in PAV leaflets (n = 5 – 6). Data are presented as mean ± standard error of mean.

6.3 Effect of Cyclic Stretch on ASH2L mRNA Expression in Porcine Aortic Valves (PAVs)

ASH2 Like, Histone Lysine Methyltransferase Complex Subunit (ASH2L) is a component of some histone methyltransferase complexes (such as SET1/ASH2 and MLL1/MLL) which regulates transcription through recruitment of those complexes to gene promoters. Recently, it was found that disturbed flow (low, oscillatory shear stress) upregulates ASH2L mRNA expression in human aortic valve endothelial cells (HAVECs) compared to steady flow (Fernandez Esmerats *et al*., 2019). Considering that disturbed flow is known to promote aortic valve (AV) calcification (Rathan *et al*., 2011), it will be interesting to see how cyclic stretch modulates ASH2L mRNA expression in AV tissue.

Freshly obtained porcine aortic valve (PAV) leaflets were cyclically (1 Hz) stretched at 10% and 15% for 3 days in regular medium. After completion of the stretch experiments, the expression of ASH2L mRNA (relative to 18S) was evaluated in the cyclically stretched tissue samples using RT-qPCR. It was found that there was no significant difference in ASH2L mRNA expression between 10% and 15% stretch (as shown in Figure 6.3).

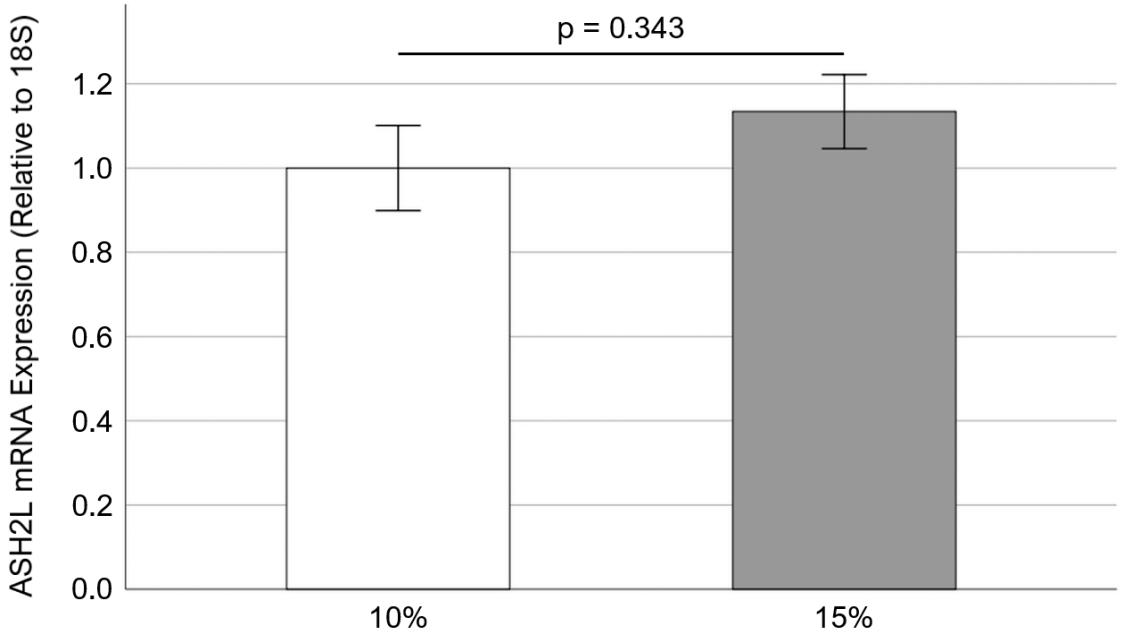

Figure 6.3 – Effect of cyclic stretch on ASH2L mRNA expression in PAV leaflets (n = 5 – 6). Data are presented as mean ± standard error of mean.

6.4 Effect of Cyclic Stretch on ROR2 mRNA Expression in Porcine Aortic Valves (PAVs)

Receptor Tyrosine Kinase Like Orphan Receptor 2 (ROR2) gene encodes a type I transmembrane protein. ROR2 may be involved in chondrogenesis, cartilage and growth plate development. ROR2 mRNA expression was found to be significantly downregulated in calcified smooth muscle cells (SMCs) compared to non-calcified ones (Xin *et al*., 2013).

Hence, it will be interesting to see how cyclic stretch modulates ROR2 mRNA expression in AV tissue.

Freshly obtained porcine aortic valve (PAV) leaflets were cyclically (1 Hz) stretched at 10% and 15% for 3 days in regular medium. After completion of the stretch experiments, the expression of ROR2 mRNA (relative to 18S) was evaluated in the cyclically stretched tissue samples using RT-qPCR. It was found that there was no significant difference in ROR2 mRNA expression between 10% and 15% stretch (as shown in Figure 6.4).

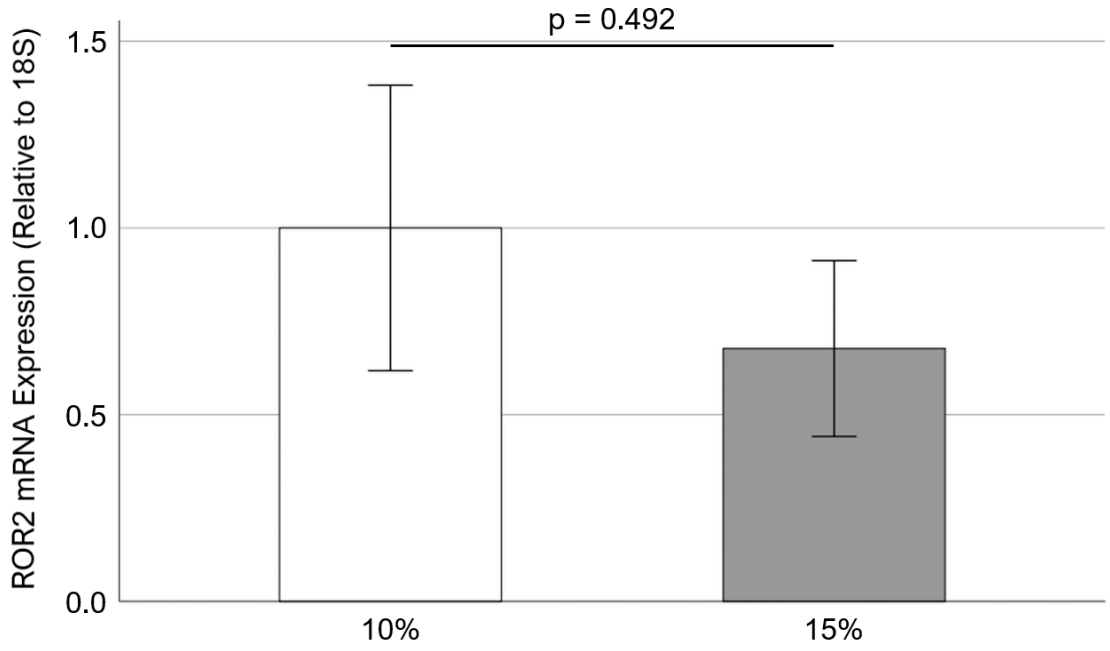

Figure 6.4 – Effect of cyclic stretch on ROR2 mRNA expression in PAV leaflets (n = 5 – 6). Data are presented as mean ± standard error of mean.

6.5 Effect of Cyclic Stretch on ATP1A2 mRNA Expression in Porcine Aortic Valves (PAVs)

ATPase Na^+/K^+ Transporting Subunit Alpha 2 (ATP1A2) gene encodes an integral membrane protein responsible for establishing and maintaining the electrochemical gradients of Na^+ and K^+ ions across the plasma membrane. These gradients are essential

for osmoregulation, for sodium-coupled transport of a variety of organic and inorganic molecules, and for electrical excitability of nerve and muscle. In a study by Bossé *et al*. (2009), ATP1A2 was found to be one of the most downregulated genes in stenotic human aortic valves (AVs) compared to healthy ones. Hence, it will be important to see how cyclic stretch modulates ATP1A2 mRNA expression in AV tissue.

Freshly obtained porcine aortic valve (PAV) leaflets were cyclically (1 Hz) stretched at 10% and 15% for 3 days in regular medium. After completion of the stretch experiments, the expression of ATP1A2 mRNA (relative to 18S) was evaluated in the cyclically stretched tissue samples using RT-qPCR. It was found that there was no significant difference in ATP1A2 mRNA expression between 10% and 15% stretch (as shown in Figure 6.5).

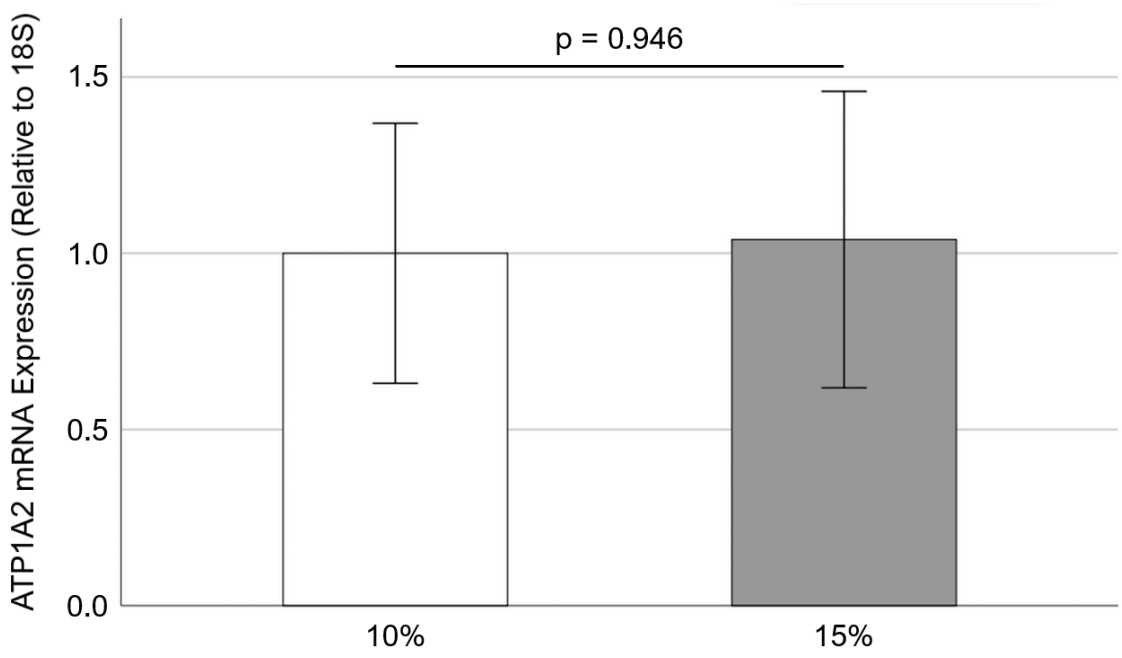

Figure 6.5 – Effect of cyclic stretch on ATP1A2 mRNA expression in PAV leaflets (n = 6). Data are presented as mean ± standard error of mean.

6.6 Effect of Cyclic Stretch on UBE2C mRNA Expression in Porcine Aortic Valves (PAVs)

Ubiquitin Conjugating Enzyme E2 C (UBE2C) gene encodes a member of the E2 ubiquitin-conjugating enzyme family. UBE2C acts as an essential factor of the anaphase promoting complex/cyclosome (APC/C), a cell cycle-regulated ubiquitin ligase that controls progression through mitosis. It initiates Lysine-11-linked polyubiquitin chains on APC/C substrates, leading to the degradation of APC/C substrates by the proteasome and promoting mitotic exit. In a recent study by Fernandez Esmerats *et al*. (2019), UBE2C was found to be shear-sensitive in human aortic valve endothelial cells (HAVECs). Hence, it will be interesting to see how cyclic stretch modulates UBE2C mRNA expression in aortic valve (AV) tissue.

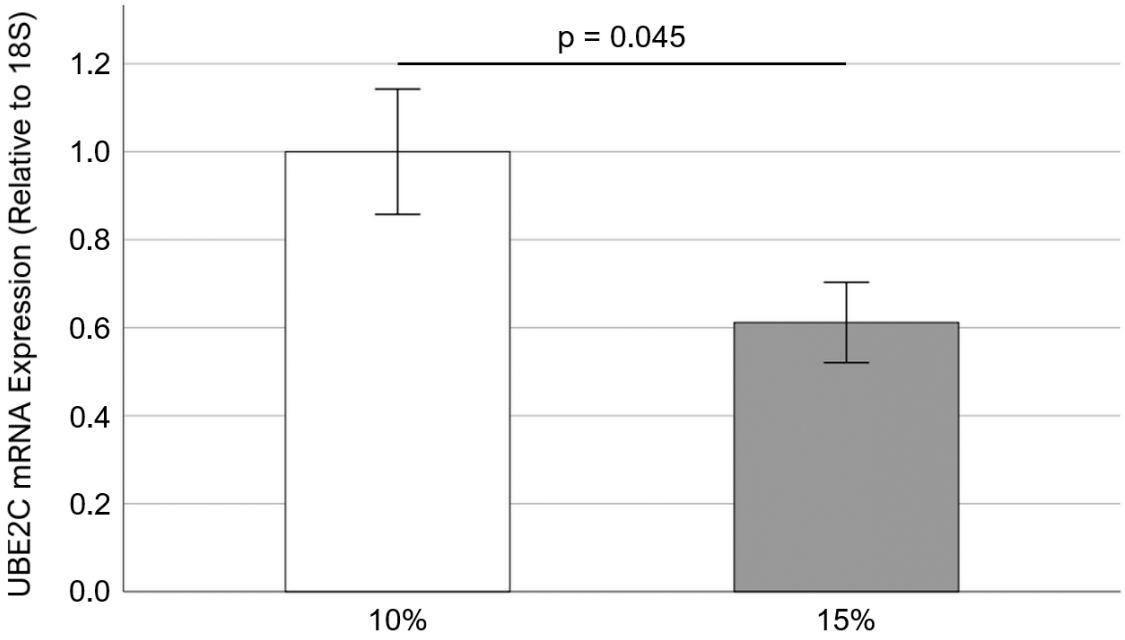

Figure 6.6 – Effect of cyclic stretch on UBE2C mRNA expression in PAV leaflets (n = 6). Data are presented as mean ± standard error of mean.

Freshly obtained porcine aortic valve (PAV) leaflets were cyclically (1 Hz) stretched at 10% and 15% for 3 days in regular medium. After completion of the stretch experiments, the expression of UBE2C mRNA (relative to 18S) was evaluated in the cyclically stretched tissue samples using RT-qPCR. It was found that there was a significant decrease in UBE2C mRNA expression at 15% stretch compared to 10% (as shown in Figure 6.6).

Going forward, it was decided to focus on the mechanistic role of UBE2C since:

1) UBE2C was found to be shear-sensitive in HAVECs (Fernandez Esmerats *et al*., 2019).
2) Among the six genes tested (sections **6.1 – 6.6**), UBE2C was the only one that was significantly stretch-sensitive in PAVs (Figure 6.6).

6.7 Effect of Cyclic Stretch on VHL mRNA Expression in Porcine Aortic Valve (PAVs)

Von Hippel-Lindau Tumor Suppressor (VHL) gene encodes VHL protein (pVHL), which binds to elongin C, elongin B, cullin-2 and Rbx1 (Ring-Box 1). This complex catalyzes the polyubiquitinylation of specific proteins and targets them for degradation by proteosomes. Interestingly, UBE2C has been shown to bind and degrade pVHL (Fernandez Esmerats *et al*., 2019). In addition, pVHL expression was found to be shear-sensitive in human aortic valve endothelial cells (HAVECs) (Fernandez Esmerats *et al.*, 2019). Hence, it will be important to see how cyclic stretch modulates VHL mRNA expression in aortic valve (AV) tissue.

Freshly obtained porcine aortic valve (PAV) leaflets were cyclically (1 Hz) stretched at 10% and 15% for 3 days in regular medium. After completion of the stretch experiments, the expression of VHL mRNA (relative to 18S) was evaluated in the cyclically stretched

tissue samples using RT-qPCR. It was found that there was no significant difference in VHL mRNA expression between 10% and 15% stretch (as shown in Figure 6.7). Since pathological (15%) stretch downregulates UBE2C mRNA expression compared to 10% (Figure 6.6), it makes sense that there is no significant difference in VHL mRNA expression between 10% and 15% stretch.

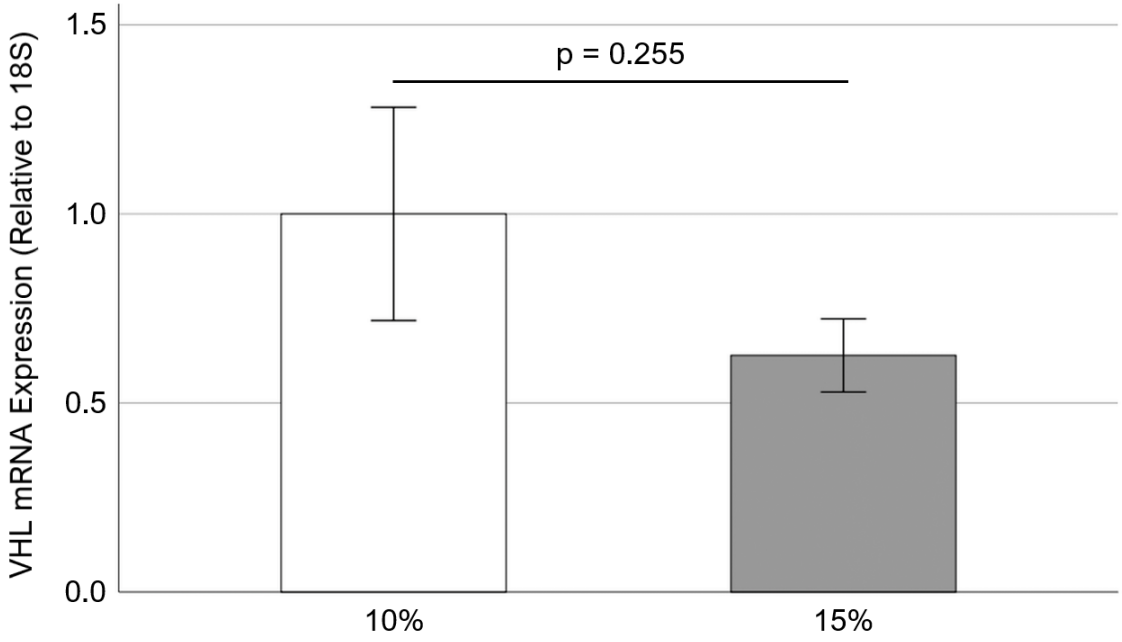

Figure 6.7 – Effect of cyclic stretch on VHL mRNA expression in PAV leaflets (n = 5 – 6). Data are presented as mean ± standard error of mean.

6.8 Effect of Cyclic Stretch on HIF1A mRNA Expression in Porcine Aortic Valves (PAVs)

Hypoxia Inducible Factor 1 Subunit Alpha (HIF1A) gene encodes the *alpha* subunit of transcription factor Hypoxia Inducible Factor 1 (HIF1), which is a heterodimer composed of an *alpha* and a *beta* subunit. HIF1 functions as a master regulator of cellular and systemic homeostatic response to hypoxia by activating transcription of many genes, including those involved in energy metabolism, angiogenesis, apoptosis, and other genes

whose protein products increase oxygen delivery or facilitate metabolic adaptation to hypoxia. HIF1 thus plays an essential role in embryonic vascularization, tumor angiogenesis and pathophysiology of ischemic disease. Interestingly, pVHL is known to degrade HIF1A (Maxwell *et al*., 1999). In addition, HIF1A expression was found to be shear-sensitive in human aortic valve endothelial cells (HAVECs) (Fernandez Esmerats *et al.*, 2019) and upregulated in stenotic human aortic valves (AVs) (Perrotta *et al*., 2015). Hence, it will be important to see how cyclic stretch modulates HIF1A mRNA expression in AV tissue.

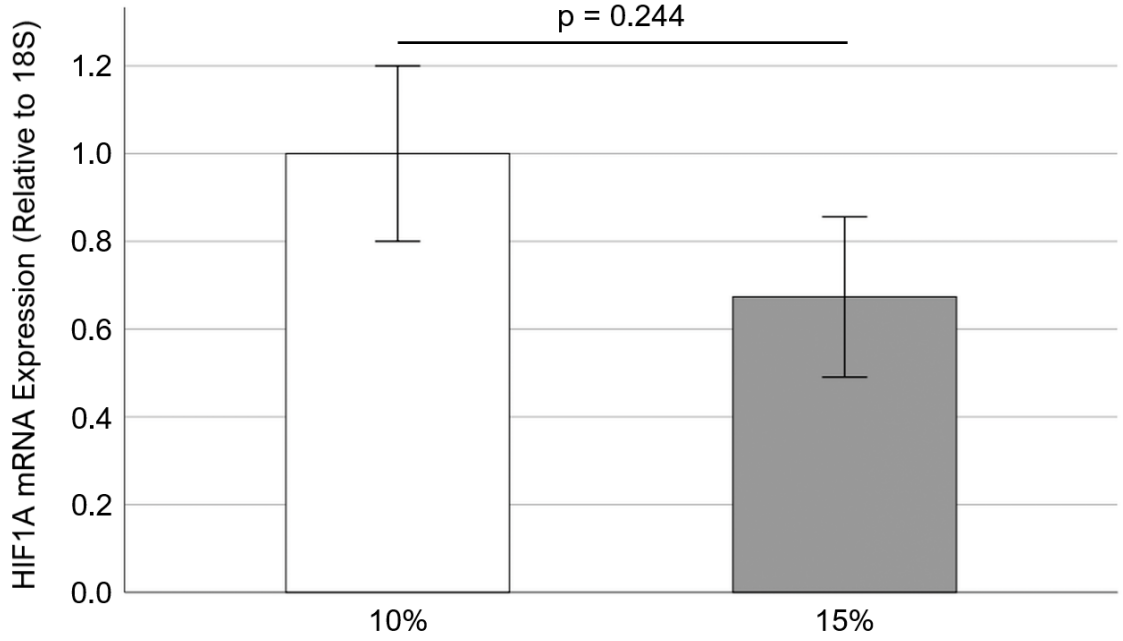

Figure 6.8 – Effect of cyclic stretch on HIF1A mRNA expression in PAV leaflets (n = 10). Data are presented as mean ± standard error of mean.

Freshly obtained porcine aortic valve (PAV) leaflets were cyclically (1 Hz) stretched at 10% and 15% for 3 days in regular medium. After completion of the stretch experiments, the expression of HIF1A mRNA (relative to 18S) was evaluated in the cyclically stretched tissue samples using RT-qPCR. It was found that there was no significant difference in HIF1A mRNA expression between 10% and 15% stretch (as shown in Figure 6.8). Since

there is no significant difference in VHL mRNA expression between 10% and 15% stretch (Figure 6.7), it makes sense that there is no significant difference in HIF1A mRNA expression between 10% and 15% stretch.

6.9 Effect of HIF1A Inhibitor PX-478 on Porcine Aortic Valve (PAV) Calcification under Pathological (15%) Stretch in Osteogenic Medium

4-[bis(2-chloroethyl)oxidoamino]-L-phenylalanine dihydrochloride, or PX-478, is a specific inhibitor of HIF1A (Koh *et al.*, 2008). This orally available pharmacological agent is currently under clinical trial as a potential treatment for metastatic cancer (ClinicalTrials.gov Identifier: NCT00522652). It was found to be well tolerated in a phase I, dose escalation study (Tibes *et al.*, 2010).

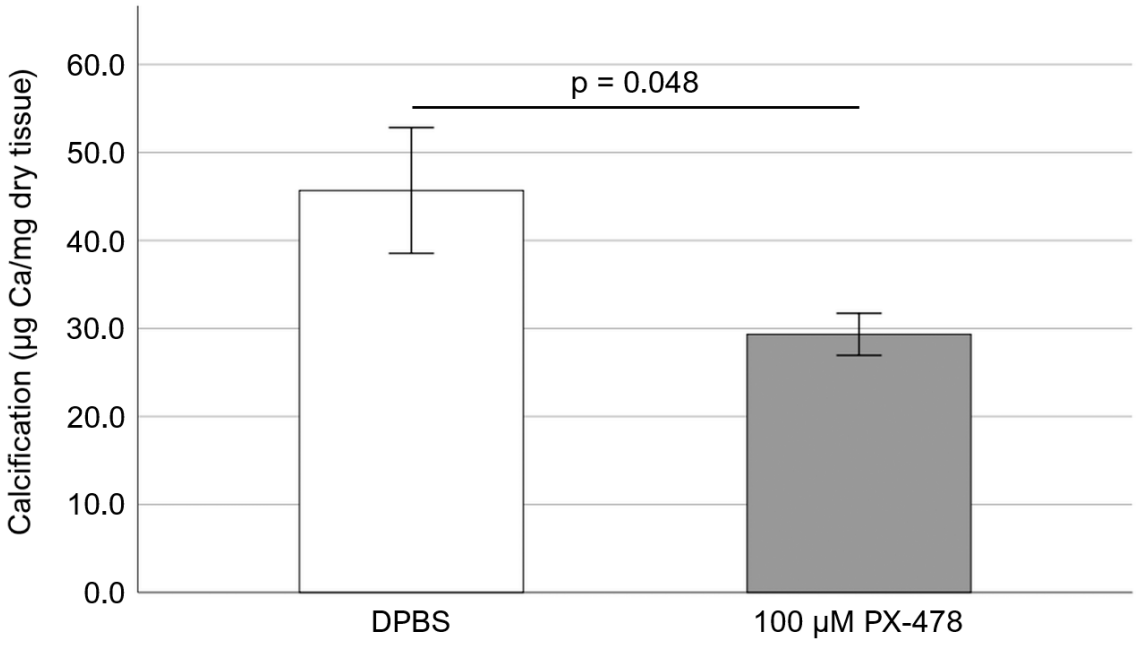

Figure 6.9.1 – Effect of PX-478 (100 µM) on PAV leaflet calcification (dry basis) after 24 days of 15% stretch in osteogenic medium, as determined by Arsenazo assay (n = 8). Data are presented as mean ± standard error of mean.

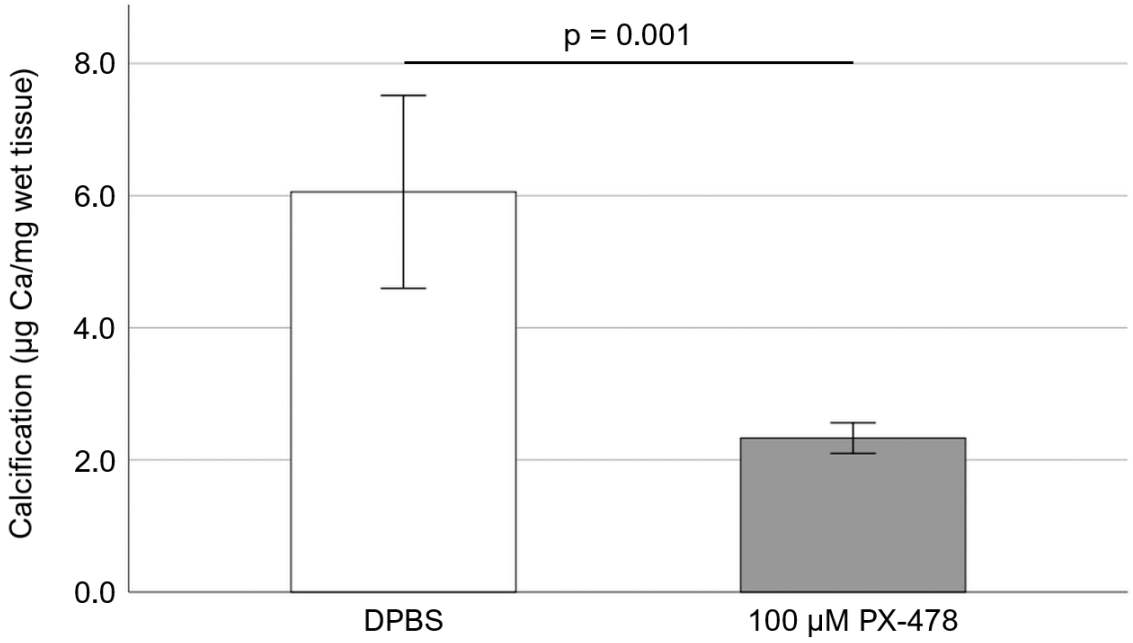

Figure 6.9.2 – Effect of PX-478 (100 µM) on PAV leaflet calcification (wet basis) after 24 days of 15% stretch in osteogenic medium, as determined by Arsenazo assay (n = 8). Data are presented as mean ± standard error of mean.

Although there was no significant difference in HIF1A mRNA expression between 10% and 15% stretch in porcine aortic valve (PAV) tissue, it was hypothesized that HIF1A inhibitor PX-478 might still have an inhibitory effect on PAV calcification under pathological (15%) stretch, since HIF1A expression was found to be upregulated in stenotic human aortic valves (AVs) (Perrotta *et al*., 2015). To test this hypothesis, freshly obtained PAV leaflets were cyclically (1 Hz) stretched at 15% for 24 days in osteogenic medium. The experiment consisted of two groups: (1) control (with Dulbecco's Phosphate-Buffered Saline or DPBS) and (2) treatment (with 100 µM PX-478). PX-478 (catalog no. 202350) was purchased from MEDKOO BIOSCIENCES (Morrisville, NC). During the experiment, the osteogenic medium was replaced every 2 – 3 days and supplemented with either DPBS or 100 µM PX-478. The PX-478 solution was made fresh each time. After completion of the stretch experiment, the degree of calcification in PAV leaflets was quantitatively

assessed by Arsenazo assay. It was found that addition of 100 µM PX-478 every 2 – 3 days resulted in a significant decrease in PAV leaflet calcification (dry basis) compared to the control case (as shown in Figure 6.9.1). Similar downregulation in PAV leaflet calcification can also be observed under wet basis (as shown in Figure 6.9.2).

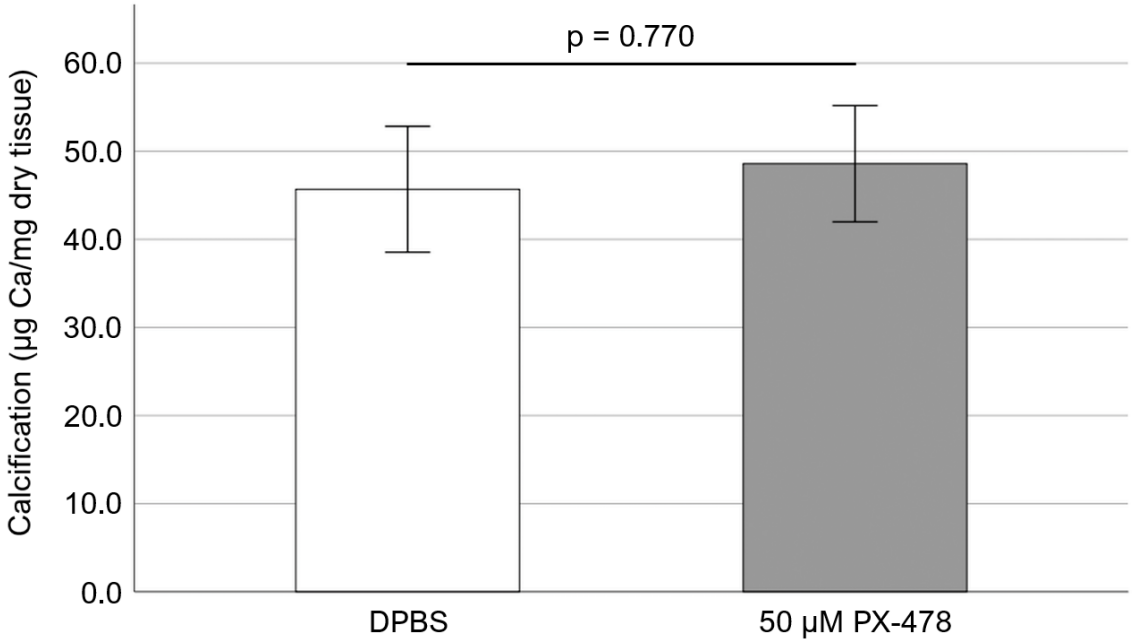

Figure 6.9.3 – Effect of PX-478 (50 µM) on PAV leaflet calcification (dry basis) after 24 days of 15% stretch in osteogenic medium, as determined by Arsenazo assay (n = 8). Data are presented as mean ± standard error of mean.

Next, it was decided to reduce the concentration of PX-478 by half (i. e. 50 µM) and see whether it can still inhibit PAV calcification under pathological (15%) stretch in osteogenic medium. To investigate that, freshly obtained PAV leaflets were cyclically (1 Hz) stretched at 15% for 24 days in osteogenic medium. The experiment consisted of two groups: (1) control (with DPBS) and (2) treatment (with 50 µM PX-478). During the experiment, the osteogenic medium was replaced every 2 – 3 days and supplemented with either DPBS or 50 µM PX-478. The PX-478 solution was made fresh each time. After completion of the stretch experiment, the degree of calcification in PAV leaflets was

quantitatively assessed by Arsenazo assay. It was found that addition of 50 μM PX-478 every 2 – 3 days did not have any significant effect on PAV leaflet calcification (dry basis) compared to the control case (as shown in Figure 6.9.3). Similar result for PAV leaflet calcification can also be observed under wet basis (as shown in Figure 6.9.4).

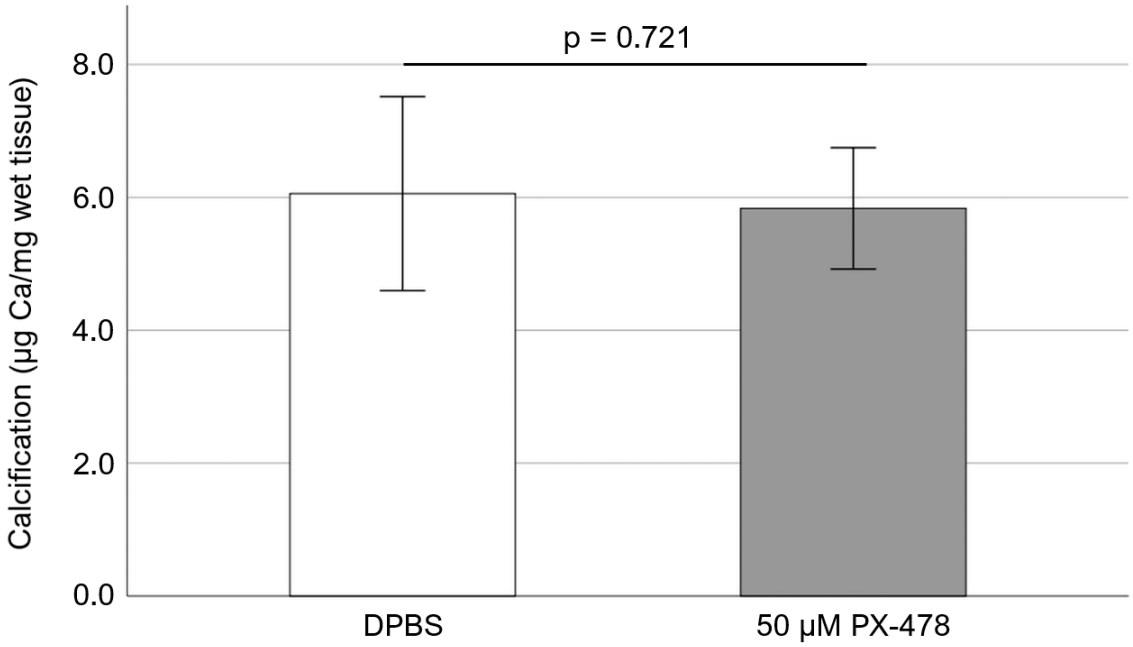

Figure 6.9.4 – Effect of PX-478 (50 μM) on PAV leaflet calcification (wet basis) after 24 days of 15% stretch in osteogenic medium, as determined by Arsenazo assay (n = 8). Data are presented as mean ± standard error of mean.

In addition, Alizarin Red stain was performed to qualitatively assess the degree of calcification in PAV leaflets after 24 days of 15% stretch in osteogenic medium (supplemented with either DPBS or 50 μM PX-478). Briefly, 10-μm frozen PAV tissue sections were hydrated and incubated in 2% Alizarin Red solution (2 g per 100 mL DI water; pH = 4.1 – 4.3) for 30 seconds to 1 minute. Alizarin Red binds to calcium and positive staining is identified as orange or red in color. In contrary to the results from Arsenazo assay (Figures 6.9.3 and 6.9.4), it was found that addition of 50 μM PX-478 every 2 – 3 days resulted in significantly lower positive staining (i. e. calcification) in PAV

leaflets compared to the control (DPBS) case, as shown in representative images in Figure 6.9.5.1.

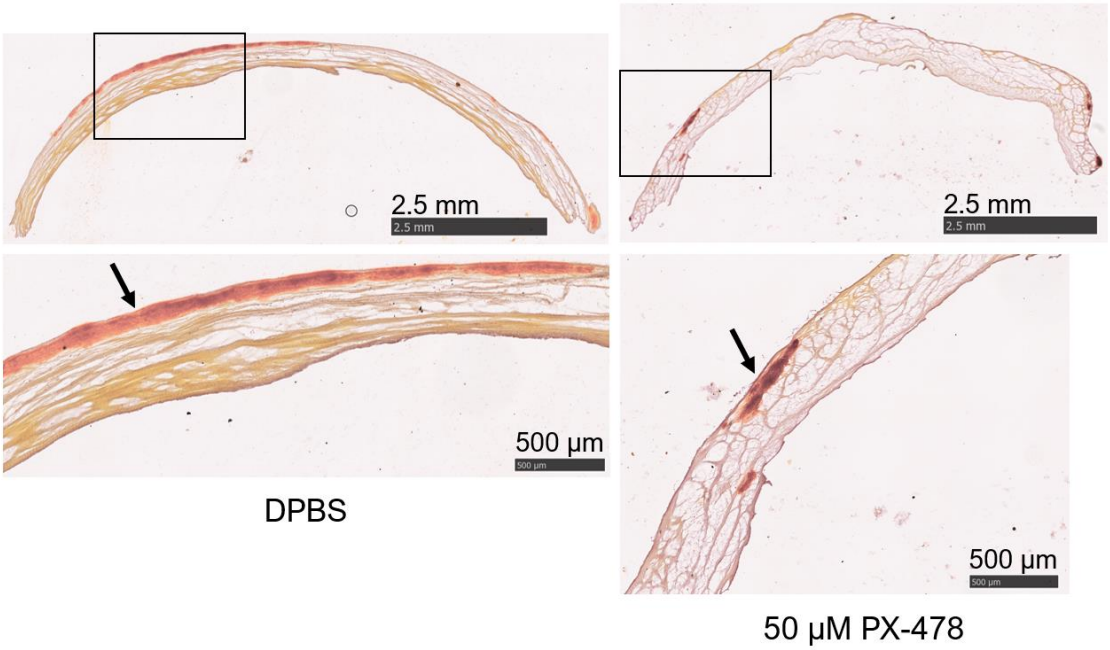

Figure 6.9.5.1 – Representative Alizarin Red staining images of PAV leaflets (top row: lower magnification, bottom row: higher magnification) after 24 days of 15% stretch in osteogenic medium. Arrows indicate areas of calcification.

ImageJ software was used to further quantify the amount of positively stained area as a percentage of total tissue area in these images. It was found that indeed, addition of 50 µM PX-478 every 2 – 3 days resulted in a significant decrease in positively stained area compared to the control (DPBS) case (as shown in Figure 6.9.5.2).

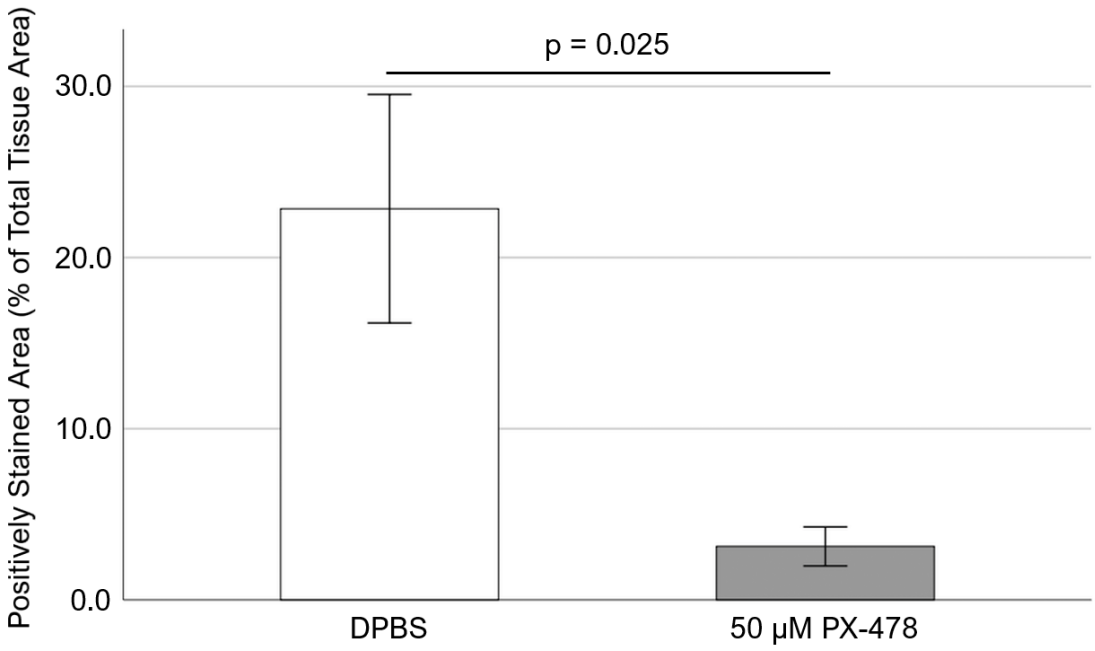

Figure 6.9.5.2 – Quantification of Alizarin Red staining images of PAV leaflets after 24 days of 15% stretch in osteogenic medium (n = 5 – 7). Data are presented as mean ± standard error of mean.

The experimental results outlined in section **6.9** indicate that a higher concentration of PX-478 (such as 100 µM) has a significant effect on inhibiting PAV calcification under pathological (15%) stretch in osteogenic medium, as shown in Figures 6.9.1 and 6.9.2. However, a lower concentration of PX-478 (such as 50 µM) may impart some level of inhibitory effect on PAV calcification under 15% stretch in osteogenic medium, as shown in Figures 6.9.5.1 and 6.9.5.2.

6.10 Effect of HIF1A Inhibitor PX-478 on Porcine Aortic Valve (PAV) Collagen Turnover under Pathological (15%) Stretch in Osteogenic Medium

Initial stages of calcific aortic valve disease (CAVD) involve pathological extracellular matrix (ECM) remodeling of aortic valve (AV) leaflets (Chen *et al.*, 2011). This is characterized by increased collagen production and a significant increase in the

ratio of immature-to-mature collagen. This maladaptive ECM remodeling ultimately results in stenotic AV leaflets that obstruct flow and compromise cardiac function. In a recent study by Villa-Roel *et al*. (2020), it was found that PX-478 significantly reduced aortic plaque burden in two chronic mouse models of atherosclerosis. This implies that PX-478 may have an inhibitory effect on aberrant collagen production. Therefore, it will be interesting to see whether PX-478 has a significant effect on collagen turnover in porcine aortic valve (PAV) leaflets under pathological (15%) stretch in osteogenic medium.

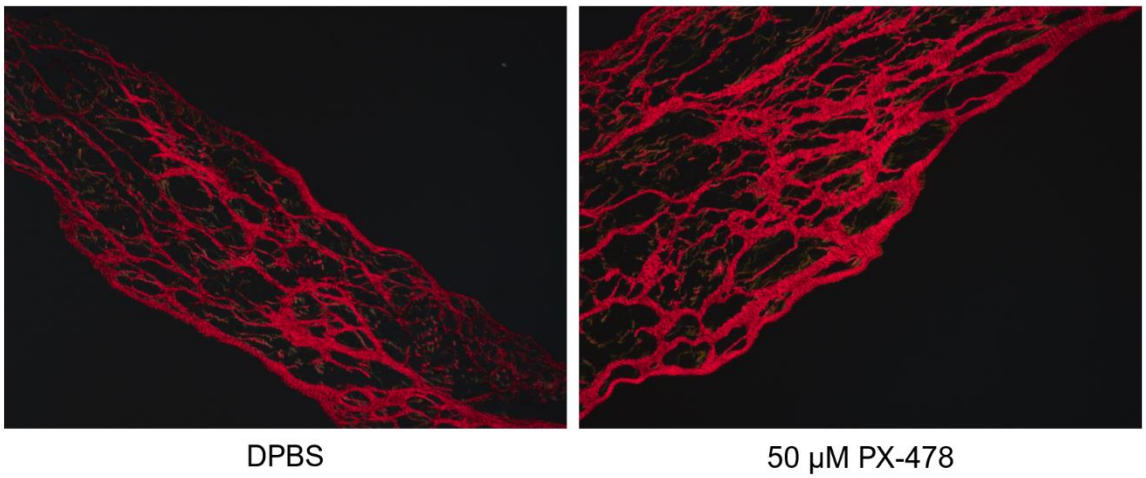

Figure 6.10.1 – Representative Picrosirius Red staining images of PAV leaflets after 24 days of 15% stretch in osteogenic medium. Red fibers indicate mature collagen; green and yellow fibers indicate immature collagen.

To test this hypothesis, freshly obtained PAV leaflets were cyclically (1 Hz) stretched at 15% for 24 days in osteogenic medium. The experiment consisted of two groups: (1) control (with DPBS) and (2) treatment (with 50 μM PX-478). During the experiment, the osteogenic medium was replaced every 2 – 3 days and supplemented with either DPBS or 50 μM PX-478. The PX-478 solution was made fresh each time. After completion of the stretch experiment, Picrosirius Red stain (catalog no. 365548, SIGMA-ALDRICH, St. Louis, MO) was performed to quantify the amount of mature and immature collagen fibers

in PAV leaflets. Briefly, 10-µm frozen PAV tissue sections were hydrated and incubated in Picrosirius Red (saturated picric acid) solution for one hour, followed by a wash in 0.5% acidified water (5 mL glacial acetic acid in 995 mL DI water). The stained PAV tissue samples were then imaged using a polarized light microscope (ZEISS, Jena, Germany). Mature collagen fibers are indicated by red color, whereas immature collagen is identified by green and yellow fibers (Rathan *et al*., 2016), as shown in Figure 6.10.1.

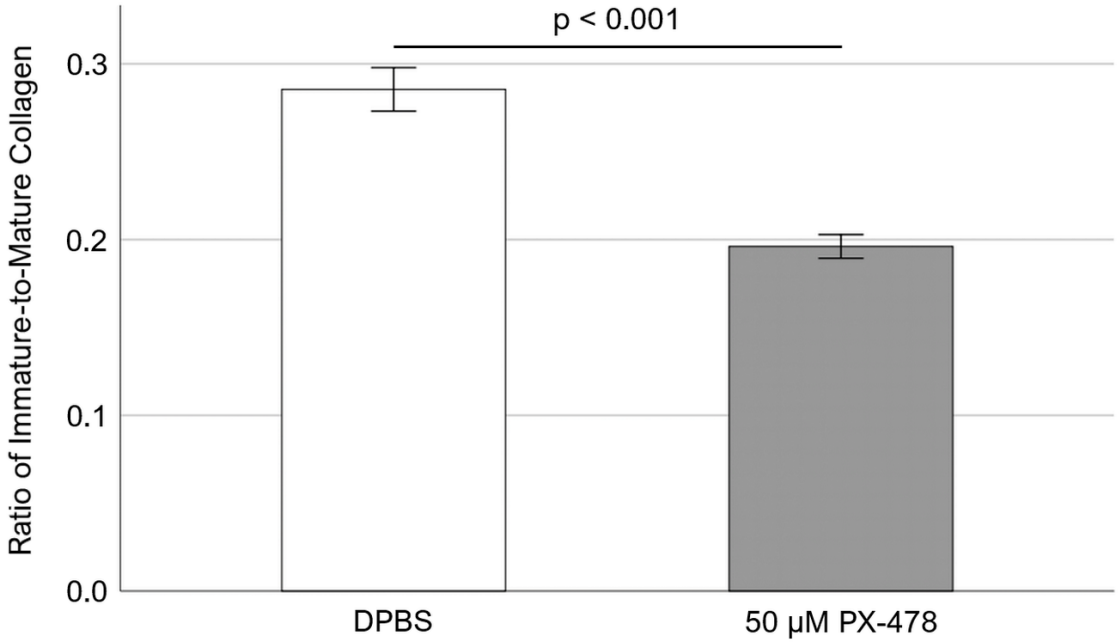

Figure 6.10.2 – Quantification of Picrosirius Red staining images of PAV leaflets after 24 days of 15% stretch in osteogenic medium (n = 7). Each sample comprises of multiple images representing multiple locations. Data are presented as mean ± standard error of mean.

ImageJ software was used to quantify the amount of mature (red fibers) and immature (green and yellow fibers) collagen in these images. It was found that addition of 50 µM PX-478 every 2 – 3 days resulted in a significant decrease in the ratio of immature-to-mature collagen in PAV leaflets compared to the control (DPBS) case (as shown in Figure 6.10.2). This implies that a lower concentration of PX-478 (such as 50 µM) can inhibit

pathological collagen turnover (quantified as the ratio of immature-to-mature collagen) in PAV leaflets under 15% stretch in osteogenic medium.

CHAPTER 7. DISCUSSION

In specific aim 1, the effect of physiological (10%) and pathological (15%) cyclic stretch on the expression of miR-21-5p, miR-483-3p, miR-181a, miR-181b, miR-199a-3p, miR-122-5p, and miR-214 in porcine aortic valve (PAV) leaflets was investigated. Then, the mechanistic role of miR-214 in modulating PAV calcification was examined. The associated findings are discussed in sections **7.1 – 7.10**:

7.1 Cyclic Stretch and miR-21-5p Expression in Porcine Aortic Valves (PAVs)

Pathological (15%) stretch was found to upregulate miR-21-5p expression in PAV leaflets compared to the physiological (10%) level (Figure 5.1). In recent studies by Coffey *et al*. (2016) and Wang *et al*. (2017), miR-21-5p expression was found to be significantly higher in calcified human aortic valves (AVs) compared to healthy ones. In addition, miR-21-5p has been shown to promote extracellular matrix (ECM) degradation and osteogenesis (Ma *et al*., 2020; Valenti *et al*., 2019). Given that elevated mechanical stretch induces pathological ECM remodeling and calcification in PAV leaflets (Balachandran *et al.*, 2009; Balachandran *et al*., 2010), it makes sense that 15% stretch upregulates miR-21-5p expression in PAV leaflets compared to 10%.

7.2 Cyclic Stretch and miR-483-3p Expression in Porcine Aortic Valves (PAVs)

Pathological (15%) stretch did not induce any significant change in miR-483-3p expression in PAV leaflets compared to the physiological (10%) level, although there was a 25% decrease in average expression (Figure 5.2). In a recent study by Fernandez Esmerats *et al*. (2019), it has been shown that low, oscillatory shear stress (i. e. disturbed flow)

significantly downregulates miR-483-3p expression in human aortic valve endothelial cells (HAVECs) compared to laminar shear stress (i. e. stable flow) and miR-483-3p overexpression inhibits PAV calcification. In addition, pulmonary arterial hypertension (PAH) is associated with a decreased level of miR-483-3p and miR-483-3p may have an inhibitory effect on PAH (Zhang *et al*., 2020). Given that both elevated mechanical stretch and disturbed flow induce calcification in PAV leaflets (Balachandran *et al*., 2010; Rathan *et al*., 2011), these imply that elevated stretch may not be a strong modulator of miR-483-3p expression in PAV leaflets compared to low, oscillatory shear stress.

7.3 Cyclic Stretch and miR-181a Expression in Porcine Aortic Valves (PAVs)

Pathological (15%) stretch was found to significantly downregulate miR-181a expression in PAV leaflets compared to the physiological (10%) level (Figure 5.3). In a recent study by Rathan *et al*. (2016), miR-181a expression has been shown to be side-specific (significantly higher on the fibrosa side compared to ventricularis) in PAV leaflets, which implies that low, oscillatory shear stress (experienced by the fibrosa side) may upregulate miR-181a expression in PAV leaflets compared to unidirectional, pulsatile shear stress (experienced by the ventricularis side). Since both elevated stretch and low, oscillatory shear stress induce calcification in PAV leaflets (Balachandran *et al*., 2010; Rathan *et al*., 2011), these imply that stretch- and shear-mediated regulation of miR-181a expression are unique in relation to AV calcification. Interestingly, overexpression of miR-181a was found to inhibit Angiotensin II (Ang II)-induced increase in Osteopontin (OPN) expression in vascular smooth muscle cells (VSMCs) (Remus *et al*., 2013). In addition, miR-181a has been shown to reduce osteogenic differentiation of human bone marrow-derived mesenchymal stem cells (BMSCs) (Tao *et al*., 2019). These indicate that elevated

stretch-mediated downregulation of miR-181a expression may have a significant role in promoting AV calcification.

7.4 Cyclic Stretch and miR-181b Expression in Porcine Aortic Valves (PAVs)

Pathological (15%) stretch was found to significantly downregulate miR-181b expression in PAV leaflets compared to the physiological (10%) level (Figure 5.4). miR-181b expression has been shown to be side-specific (significantly higher on the fibrosa side compared to ventricularis) in PAV leaflets, which implies that low, oscillatory shear stress (experienced by the fibrosa side) may upregulate miR-181b expression in PAV leaflets compared to unidirectional, pulsatile shear stress (experienced by the ventricularis side) (Rathan *et al*., 2016). In addition, low, oscillatory shear stress (i. e. disturbed flow) was found to upregulate miR-181b expression in human aortic valve endothelial cells (HAVECs) compared to laminar shear stress (i. e. stable flow) (Heath *et al*., 2018). Furthermore, miR-181b was found to target Tissue Inhibitor of Metalloproteinases 3 (TIMP3) and promote Matrix Metalloproteinases (MMP) activity in HAVECs (Heath *et al*., 2018). Since both elevated stretch and low, oscillatory shear stress induce calcification in PAV leaflets (Balachandran *et al*., 2010; Rathan *et al*., 2011), these imply that stretch- and shear-mediated regulation of miR-181b expression are unique in relation to AV calcification. Interestingly, miR-181b has been shown to target Transforming Growth Factor-β (TGF-β) in vascular smooth muscle cells (VSMCs) (Hori *et al*., 2017) and TGF-β signaling is known to promote calcification (Jian *et al.*, 2003). These indicate that elevated stretch-mediated downregulation of miR-181b may have a significant role in promoting AV calcification.

7.5 Cyclic Stretch and miR-199a-3p Expression in Porcine Aortic Valves (PAVs)

Pathological (15%) stretch was found to significantly downregulate miR-199a-3p expression in PAV leaflets compared to the physiological (10%) level (Figure 5.5). miR-199a-3p expression has been shown to be side-specific (significantly higher on the fibrosa side compared to ventricularis) in PAV leaflets, which implies that low, oscillatory shear stress (experienced by the fibrosa side) may upregulate miR-199a-3p expression in PAV leaflets compared to unidirectional, pulsatile shear stress (experienced by the ventricularis side) (Rathan *et al*., 2016). Since both elevated stretch and low, oscillatory shear stress induce calcification in PAV leaflets (Balachandran *et al*., 2010; Rathan *et al*., 2011), these imply that stretch- and shear-mediated regulation of miR-199a-3p expression are unique in relation to AV calcification. Interestingly, reduced miR-199a-3p expression was found to be associated with vascular endothelial cell injury (Wang *et al*., 2018). Moreover, miR-199a-3p has been shown to inhibit osteogenic differentiation of bone marrow-derived mesenchymal stem cells (BMSCs) (Wu *et al*., 2021). These indicate that elevated stretch-mediated downregulation of miR-199a-3p may have a significant role in promoting AV calcification.

7.6 Cyclic Stretch and miR-122-5p Expression in Porcine Aortic Valves (PAVs)

Pathological (15%) stretch did not induce any significant change in miR-122-5p expression in PAV leaflets compared to the physiological (10%) level, although there was a 41% decrease in average expression (Figure 5.6). In a recent study by Coffey *et al*. (2016), miR-122-5p expression was found to be significantly lower in calcified human aortic valves (AVs) compared to healthy ones. Interestingly, miR-122-5p has been shown to

mitigate inflammation in spinal cord injury (SCI) (Wei *et al*., 2021). Given that elevated mechanical stretch induces calcification in PAV leaflets (Balachandran *et al*., 2010), these imply that elevated stretch may not be a strong modulator of miR-122-5p expression in PAV leaflets.

7.7 Cyclic Stretch and miR-214 Expression in Porcine Aortic Valves (PAVs)

Pathological (15%) stretch was found to significantly downregulate miR-214 expression in PAV leaflets compared to the physiological (10%) level (Figure 5.7). miR-214 expression has been shown to be side-specific (significantly higher on the fibrosa side compared to ventricularis) in PAV leaflets, which implies that low, oscillatory shear stress (experienced by the fibrosa side) may upregulate miR-214 expression in PAV leaflets compared to unidirectional, pulsatile shear stress (experienced by the ventricularis side) (Rathan *et al*., 2016). Indeed, it was found that when the fibrosa side of PAV leaflets was exposed to low, oscillatory shear stress, there was a significant increase in miR-214 expression compared to unidirectional, pulsatile shear stress (Rathan *et al*., 2016). Similar result was obtained for the ventricularis side as well. Since both elevated stretch and low, oscillatory shear stress induce calcification in PAV leaflets (Balachandran *et al*., 2010; Rathan *et al*., 2011), these imply that stretch- and shear-mediated regulation of miR-214 expression are unique in relation to AV calcification. Interestingly, miR-214 expression was found to be significantly lower in calcified human aortic valves (AVs) compared to healthy ones (Coffey *et al*., 2016; Wang *et al*., 2017; Song *et al*., 2017; Li *et al*., 2020). These indicate that elevated stretch-mediated downregulation of miR-214 may have a significant role in promoting AV calcification.

7.8 miR-214 Overexpression and Porcine Aortic Valve (PAV) Calcification

miR-214 overexpression was found to significantly inhibit PAV calcification under static condition. This was observed as 40% (dry basis) and 25% (wet basis) decrease in PAV calcification with miR-214 mimic in the Arsenazo assay (Figures 5.9.1 and 5.9.2). In addition, there was 60% and 28% decrease in PAV calcification with miR-214 mimic in the Alizarin Red and Von Kossa staining, respectively (Figures 5.9.3.1, 5.9.3.2, 5.9.4.1 and 5.9.4.2). Similarly, miR-214 overexpression was found to inhibit PAV calcification under pathological (15%) stretch. This was observed as 23% (dry basis) and 32% (wet basis) decrease in PAV calcification with miR-214 mimic in the Arsenazo assay (Figures 5.11.1 and 5.11.2). In a recent study by Li *et al*. (2020), it has been shown that miR-214 inhibits osteogenic differentiation of human aortic valve interstitial cells (HAVICs). In addition, wild-type and miR-214 knockout rats were intraperitoneally injected with vitamin D_2 every 2 days for one month and also fed Western diet for 4 months. It was found that miR-214 knockout rats developed increased AV calcification, resulting in significantly higher aortic jet velocity and transvalvular pressure gradient (Li *et al*., 2020).

miR-214 has been shown to inhibit osteogenic differentiation of mesenchymal stem cells (MSCs) by targeting Fibroblast Growth Factor Receptor 1 (FGFR1) (Yang *et al*., 2016). In addition, allotransplantation of bone marrow-derived mesenchymal stem cells (BMSCs) expressing miR-214 sponges could heal bone defects in osteoporotic rats (Li *et al*., 2016). Similarly, adipose-derived stem cells (ASCs) expressing miR-214 sponges were able to improve bone healing in osteoporotic rat models (Li *et al*., 2017). Furthermore, miR-214 was found to inhibit osteogenic differentiation of human osteoblasts by targeting Baculoviral IAP Repeat Containing 7 (BIRC7) (Liu *et al*., 2017). Osteogenic

differentiation of maxillary sinus membrane stem cells (MSMSCs) was inhibited by miR-214 overexpression (Peng *et al*., 2019). Finally, silk-based orthopedic screws that incorporate antisense miR-214 (AS-miR-214) was found to promote osteogenesis in MSCs (James *et al*., 2019). Altogether, it is evident that miR-214 has an anti-osteogenic effect across different cell and tissue types.

7.9 Cyclic Stretch and TWIST1 mRNA Expression in Porcine Aortic Valves (PAVs)

Pathological (15%) stretch was found to significantly downregulate TWIST1 mRNA expression in PAV leaflets compared to the physiological (10%) level (Figure 5.12). Yin *et al.* (2010) found that TWIST1 positively regulated miR-214 expression (when there was an increase in TWIST1 expression, miR-214 expression also increased and *vice versa*) in epithelial ovarian cancer (EOC) stem cells. In addition, inhibition of TWIST1 expression activated Nuclear Factor Kappa B (NF-κB)-dependent RANTES (C-C Motif Chemokine Ligand 5 or CCL5) production induced by Tumor Necrosis Factor-α (TNF-α) treatment in type II (expressing high level of TWIST1) EOC stem cells. Interestingly, downregulation of miR-214 expression, mediated by suppressed TWIST1 expression, was found to promote fibrogenic signaling in activated hepatic stellate cells (HSCs) via upregulation of Connective Tissue Growth Factor (CTGF) (Chen *et al*., 2015). Furthermore, expression of TWIST1 and miR-214 was significantly downregulated in cardiac tissue samples from explanted hearts of dilated cardiomyopathy patients compared to healthy ones (Baumgarten *et al*., 2013). The reduction in TWIST1 expression resulted in an increase in the activity of Ubiquitin Proteosome System (UPS). Hence, it is clear that TWIST1 positively regulates miR-214 expression. In a study by Zhou *et al*. (2019), it has been shown that Methyltransferase Like 3 (MTTL3) promotes osteogenic differentiation of

human aortic valve interstitial cells (HAVICs) by inhibiting TWIST1 expression. Similarly, Zhang *et al*. (2014) showed that TWIST1 expression was downregulated in calcified human aortic valves (AVs) compared to healthy ones and TWIST1 inhibited the osteogenic differentiation of HAVICs. In addition, long noncoding RNA OIP5 Antisense RNA 1 (OIP5-AS1) has been shown to inhibit osteogenic differentiation of HAVICs by upregulating TWIST1 expression (Zheng *et al*., 2019).Therefore, elevated stretch-mediated downregulation of miR-214 expression in PAV leaflets (Figure 5.7) can be mediated by reduced TWIST1 expression under pathological (15%) stretch (Figure 5.12).

7.10 Cyclic Stretch, miR-214 Overexpression and ATF4 mRNA Expression in Porcine Aortic Valve (PAVs)

miR-214 overexpression was found to significantly inhibit Activating Transcription Factor 4 (ATF4) mRNA expression in PAV leaflets (Figure 5.19). In addition, pathological (15%) stretch was found to upregulate ATF4 mRNA expression in PAV leaflets compared to the physiological (10%) level (Figure 5.20). In a study by Wang *et al*. (2012), it was found that miR-214 directly targeted ATF4 in MC3T3-E1 preosteoblast cells. In another study by Li *et al*. (2015), it was shown that miR-214 suppressed glucose production in mouse primary hepatocytes by targeting ATF4. Similarly, Cui *et al.* (2018) discovered that long noncoding RNA GM10768 activated hepatic gluconeogenesis by repressing miR-214 expression and upregulating ATF4 expression. Yao *et al*. (2017) found that the osteogenic differentiation of human periodontal ligament stem cells (hPDLSCs) was suppressed by miR-214 by targeting ATF4. In addition, long noncoding RNA Metastasis Associated Lung Adenocarcinoma Transcript 1 (MALAT1) was found to promote osteogenic differentiation of human bone marrow stromal cells (BMSCs) by sponging miR-214

expression and upregulating ATF4 expression (Huang *et al*., 2020). Furthermore, miR-214 was shown to target ATF4 in ATDC5 chondrogenic cells (Roberto *et al*., 2018). Therefore, it is evident that the inhibiting effect of miR-214 overexpression on ATF4 mRNA expression in PAV leaflets is consistent with similar observations in different cell and tissue types. Interestingly, Wang *et al*. (2017) found that ATF4 protein expression was significantly upregulated in calcified human aortic valves (AVs) compared to healthy ones. Fu *et al*. (2019) showed that Histone Deacetylase 6 (HDAC6) protein expression was significantly downregulated in calcified human AVs compared to healthy ones and inhibition of HDAC6 expression promoted osteogenic differentiation of human aortic valve interstitial cells (HAVICs) by upregulating ATF4 expression. In addition, Cai *et al.* (2013) found that oxidized low density lipoprotein (oxLDL) induced osteogenic differentiation in porcine aortic valve interstitial cells (PAVICs) by upregulating ATF4 expression. Similarly, Tumor Necrosis Factor-α (TNF-α) promoted calcification of vascular smooth muscle cells (VSMCs) by inducing ATF4 expression. Hence, it is clear that ATF4 promotes valvular and vascular calcification. Since elevated stretch induces calcification in PAV leaflets (Balachandran *et al*., 2010), elevated stretch-mediated downregulation of miR-214 expression can promote PAV calcification via upregulation of ATF4 expression.

In specific aim 2, the effect of physiological (10%) and pathological (15%) cyclic stretch on the mRNA expression of YAP1, SOX9, ASH2L, ROR2, ATP1A2, and UBE2C in porcine aortic valve (PAV) leaflets was investigated. Then, the mechanistic role of UBE2C in modulating PAV calcification was examined. The associated findings are discussed in sections **7.11 – 7.20**:

7.11 Cyclic Stretch and YAP1 mRNA Expression in Porcine Aortic Valves (PAVs)

Pathological (15%) stretch was found to downregulate Yes Associated Protein 1 (YAP1) mRNA expression in PAV leaflets compared to the physiological (10%) level (Figure 6.1). In a study by Seo *et al*. (2013), it was shown that YAP1 inhibited Wingless-type Integration Site (Wnt) signaling and the depletion of YAP1 induced Wnt signaling. YAP1 bound β-catenin and induced Dickkopf WNT Signaling Pathway Inhibitor 1 (Dkk1), a negative regulator of Wnt signaling, to maintain stemness and prevent osteogenesis. Chen *et al*. (2017) found that knockdown of YAP1 enhanced the osteogenic differentiation of human adipose-derived mesenchymal stem cells (hASCs). Guo *et al*. (2018) showed that loss of Kindlin-2 (KIND2) induced osteogenic differentiation in mesenchymal stem cells (MSCs) via downregulation of the mRNA and protein levels of YAP1 and Tafazzin (TAZ). Interestingly, loss of YAP1 and TAZ in vascular smooth muscle cells (VSMCs) led to osteogenic differentiation and vascular calcification (Wang *et al*., 2020). On the contrary, Gao *et al*. (2021) showed that Aldo-Keto Reductase Family 1 Member B (AKR1B1) protein expression was upregulated in calcified human aortic valves (AVs) compared to healthy ones and AKR1B1 promotes calcification of human aortic valve interstitial cells (HAVICs) by inducing active-YAP1 protein expression. Santoro *et al*. (2018) found that subtle variations in matrix stiffness could regulate HAVIC activation in a YAP1-dependent

manner. Hence, it is unclear whether YAP1 has an anti- or pro-osteogenic effect considering different cell and tissue types. Given that elevated mechanical stretch induces calcification in PAV leaflets (Balachandran *et al*., 2010), elevated stretch-mediated downregulation of YAP1 mRNA expression may promote PAV calcification under pathological (15%) stretch.

7.12 Cyclic Stretch and SOX9 mRNA Expression in Porcine Aortic Valves (PAVs)

Pathological (15%) stretch did not induce any significant change in SRY-Box Transcription Factor 9 (SOX9) mRNA expression in PAV leaflets compared to the physiological (10%) level, although there was a 35% decrease in average expression (Figure 6.2). Loebel *et al*. (2015) showed that SOX9 expression was downregulated during osteogenesis of human mesenchymal stem cells (hMSCs) and inhibition of SOX9 expression increased osteogenic differentiation of hMSCs. Liao *et al*. (2014) found that SOX9 promoted Bone Morphogenetic Protein 2 (BMP2)-induced chondrogenic differentiation and inhibited BMP2-induced osteogenic differentiation in C3H10T1/2 mesenchymal stem cells (MSCs). Cheng *et al*. (2010) showed that SOX9 could inhibit the transactivation of Runt-Related Transcription Factor 2 (RUNX2) via dose-dependent degradation, which was independent of the ubiquitin-proteosome pathway. Similarly, Zhou *et al*. (2006) found that SOX9 could inhibit RUNX2 function *in vivo* in established osteoblastic lineage. Therefore, it is evident that SOX9 has an inhibitory effect on osteogenesis. In a study by Peacock *et al*. (2010), it was observed that $SOX9^{fl/+}$COL2A1-cre mice (expressing reduced level of SOX9 in heart valves) developed aortic valve (AV) calcification compared to $SOX9^{fl/+}$ littermate controls (expressing normal level of SOX9 in heart valves). Interestingly, Huk *et al*. (2015) showed that nuclear localization of SOX9

significantly decreased during porcine aortic valve interstitial cell (PAVIC) calcification. However, treatment with nuclear export signal inhibitor Leptomycin B maintained normal level of SOX9 nuclear localization and significantly reduced PAVIC calcification. In addition, SOX9 protein expression was found to be significantly downregulated in calcified human AVs compared to healthy ones. Furthermore, hypercholesterolemic *Reversa* mice (which developed AV calcification) expressed reduced level of SOX9 in AV leaflets compared to normocholesterolemic control mice (Huk *et al*., 2015). Since elevated mechanical stretch induces calcification in PAV leaflets (Balachandran *et al*., 2010), these imply that elevated stretch may not be a strong modulator of SOX9 mRNA expression in PAV leaflets.

7.13 Cyclic Stretch and ASH2L mRNA Expression in Porcine Aortic Valves (PAVs)

Pathological (15%) stretch did not induce any significant change in ASH2 Like, Histone Lysine Methyltransferase Complex Subunit (ASH2L) mRNA expression in PAV leaflets compared to the physiological (10%) level, although there was a 13% increase in average expression (Figure 6.3). Fernandez Esmerats *et al*. (2019) showed that low, oscillatory shear stress (i. e. disturbed flow) significantly upregulated ASH2L mRNA expression in human aortic valve endothelial cells (HAVECs) compared to laminar shear stress (i. e. stable flow). Chen *et al*. (2019) found that circ-ASH2L promoted tumor progression by downregulating miR-34a expression and upregulating Notch Receptor 1 (NOTCH1) expression. Interestingly, Toshima *et al*. (2020) reported that the expression of miR-34a and NOTCH1 was upregulated and downregulated, respectively, in calcified human aortic valves (AVs). Furthermore, inhibition of miR-34a expression was shown to inhibit porcine aortic valve interstitial cell (PAVIC) calcification via upregulation of

NOTCH1 expression. In a study by Qi *et al*. (2014), it was found that ASH2L induced Estrogen Receptor 1 (ESR1) expression in mammary epithelial cells via its interaction with GATA Binding Protein 3 (GATA3). Interestingly, McRobb *et al*. (2017) showed that inhibition of ESR1 expression resulted in significantly higher calcification of human coronary artery smooth muscle cells (HCASMCs). Since both elevated mechanical stretch and disturbed flow induce calcification in PAV leaflets (Balachandran *et al*., 2010; Rathan *et al*., 2011), these imply that elevated stretch may not be a strong modulator of ASH2L mRNA expression in PAV leaflets compared to low, oscillatory shear stress.

7.14 Cyclic Stretch and ROR2 mRNA Expression in Porcine Aortic Valves (PAVs)

Pathological (15%) stretch did not induce any significant change in Receptor Tyrosine Kinase Like Orphan Receptor 2 (ROR2) mRNA expression in PAV leaflets compared to the physiological (10%) level, although there was a 32% decrease in average expression (Figure 6.4). In a study by Xin *et al*. (2013), it was found that ROR2 mRNA expression was significantly downregulated in calcified smooth muscle cells (SMCs) compared to non-calcified ones. On the other hand, Zhu *et al*. (2016) reported that ROR2 mRNA expression was significantly upregulated during osteogenic differentiation of vascular smooth muscle cells (VSMCs). ROR2 is a receptor of Wnt Family Member 5A (WNT5A), which is involved in the noncanonical Wnt signaling pathway (Oishi *et al*., 2003; Mikels *et al*., 2006). Interestingly, Albanese *et al*. (2017) found that WNT5A mRNA expression was significantly upregulated in calcified human aortic valves (AVs) compared to healthy ones. Furthermore, addition of recombinant human WNT5A protein (rhWNT5A) promoted calcification in human aortic valve interstitial cells (HAVICs). Since elevated mechanical stretch induces calcification in PAV leaflets (Balachandran *et*

al., 2010), these imply that elevated stretch may not be a strong modulator of ROR2 mRNA expression in PAV leaflets.

7.15 Cyclic Stretch and ATP1A2 mRNA Expression in Porcine Aortic Valves (PAVs)

Pathological (15%) stretch did not induce any significant change in ATPase Na^+/K^+ Transporting Subunit Alpha 2 (ATP1A2) mRNA expression in PAV leaflets compared to the physiological (10%) level (Figure 6.5). Yuan *et al*. (2007) found that cyclic stretch (25% at 6 cycles/min) did not bring about any significant change in ATP1A2 mRNA expression in skeletal muscle cells compared to the control (unstretched) condition. In a study by Leite *et al*. (2020), it was reported that ATP1A2 mediated Lipopolysaccharide (LPS)-induced inflammation in astrocytes. Interestingly, Bossé *et al*. (2009) found that ATP1A2 gene expression was significantly downregulated in stenotic human aortic valves (AVs) compared to healthy ones. Furthermore, ATP1A2 gene expression was significantly lower in hypertensive and hypercholesterolemic mice (that developed severe aortic stenosis) compared to control mice (Chu *et al*., 2016). Since elevated mechanical stretch induces calcification in PAV leaflets (Balachandran *et al*., 2010), these imply that elevated stretch may not be a strong modulator of ATP1A2 mRNA expression in PAV leaflets.

7.16 Cyclic Stretch and UBE2C mRNA Expression in Porcine Aortic Valves (PAVs)

Pathological (15%) stretch was found to significantly downregulate Ubiquitin Conjugating Enzyme E2 C (UBE2C) mRNA expression in PAV leaflets compared to the physiological (10%) level (Figure 6.6). Chou *et al*. (2014) found that UBE2C mRNA expression was significantly upregulated in breast microcalcification lesions compared to non-calcified ones. In addition, knockdown of UBE2C expression promoted apoptosis in

MCF-7 (Michigan Cancer Foundation-7 MCF-7) human breast cancer cells. Guo *et al.* (2017) showed that inhibition of UBE2C expression induced autophagic death in U87-MG (Uppsala 87 Malignant Glioma) and U251 human glioma cells. In a recent study by Fernandez Esmerats *et al*. (2019), it was reported that low, oscillatory shear stress (i. e. disturbed flow) significantly upregulated UBE2C mRNA and protein expression in human aortic valve endothelial cells (HAVECs) compared to laminar shear stress (i. e. stable flow). Since both elevated stretch and low, oscillatory shear stress induce calcification in PAV leaflets (Balachandran *et al*., 2010; Rathan *et al*., 2011), these imply that stretch- and shear-mediated regulation of UBE2C mRNA expression are unique in relation to AV calcification.

7.17 Cyclic Stretch and VHL mRNA Expression in Porcine Aortic Valves (PAVs)

Pathological (15%) stretch did not induce any significant change in Von Hippel-Lindau Tumor Suppressor (VHL) mRNA expression in PAV leaflets compared to the physiological (10%) level, although there was a 38% decrease in average expression (Figure 6.7). Wang *et al*. (2017) found that overexpression of VHL by adenoviral vector significantly reduced liver fibrosis in mice. On the other hand, Zhou *et al*. (2016) reported that fibroblast-specific VHL protein (pVHL) knockout mice developed significantly lower lung fibrosis under bleomycin treatment compared to the control mice. Furthermore, Wan *et al*. (2008) found that mice lacking VHL protein (pVHL) in osteoblasts produced more bone in response to distraction osteogenesis compared to the control mice. Interestingly, Fernandez Esmerats *et al*. (2019) showed that low, oscillatory shear stress (i. e. disturbed flow) significantly downregulated VHL protein (pVHL) expression in human aortic valve endothelial cells (HAVECs) compared to laminar shear stress (i. e. stable flow); however,

there was no significant change in VHL mRNA expression. Given that elevated stretch and low, oscillatory shear stress induce calcification in PAV leaflets (Balachandran *et al*., 2010; Rathan *et al*., 2011), these imply that stretch- and shear-mediated regulation of VHL mRNA expression are similar in relation to AV calcification. Since pathological (15%) stretch downregulated UBE2C mRNA expression in PAV leaflets compared to 10% (Figure 6.6), it can be assumed that there would be downregulation of UBE2C protein expression as well. Reduction in UBE2C protein expression would result in similar VHL protein (pVHL) expression under 15% stretch compared to 10%, since UBE2C protein has been shown to degrade VHL protein (pVHL) in human embryonic kidney (HEK) cells (Fernandez Esmerats *et al*., 2019). Consequently, it would be logical to observe no significant difference in VHL mRNA expression in PAV leaflets between 10% and 15% stretch (Figure 6.7).

7.18 Cyclic Stretch and HIF1A mRNA Expression in Porcine Aortic Valves (PAVs)

Pathological (15%) stretch did not induce any significant change in Hypoxia Inducible Factor 1 Subunit Alpha (HIF1A) mRNA expression in PAV leaflets compared to the physiological (10%) level, although there was a 33% decrease in average expression (Figure 6.8). Idelevich *et al*. (2011) found that overexpression of Bone Gamma-Carboxyglutamate Protein (BGP) induced vascular calcification in a HIF1A-dependent manner. Similarly, Mokas *et al*. (2016) showed that HIF1A expression was significantly upregulated in calcifying aortas of nephrectomized (to induce chronic kidney disease) male Wistar rats on high-mineral diet (1.2% calcium and 1.2% phosphate) along with calcitriol supplementation (to induce mineral imbalance) compared to nephrectomized ones on normal diet. Zhu *et al*. (2018) reported that advanced glycation end products (AGEs)

enhanced vascular smooth muscle cell (VSMC) calcification by activating the HIF1A-Pyruvate Dehydrogenase Kinase 4 (PDK4) pathway and inhibition of PDK4 expression significantly reduced VSMC calcification. Furthermore, Balogh *et al*. (2019) showed that hypoxia (5% O_2) induced osteogenic differentiation of VSMCs in a HIF1A-dependent and mitochondria-derived reactive oxygen species (ROS)-dependent manner compared to normoxic (21% O_2) condition. Interestingly, Perrotta *et al*. (2015) found that HIF1A protein expression was significantly higher in the calcified areas of stenotic human aortic valves (AVs) compared to non-calcified areas. Parra-Izquierdo *et al*. (2019) showed that Interferon-γ (IFN-γ) and lipopolysaccharide (LPS), in combination, induced calcification of human aortic valve interstitial cells (HAVICs) under normoxic condition by activating the Signal Transducer and Activator of Transcription 1 (STAT1)/HIF1A pathway. Swaminathan *et al*. (2019) reported that both normoxic (20% O_2) and hypoxic (13% O_2) culture of aged (> 2 years) PAV tissue resulted in significant upregulation of the expression of Matrix Metalloproteinase 9 (MMP9)-Neutrophil Gelatinase-Associated Lipocalin (NGAL) complex and fragmentation of elastic fibers (in the ventricularis layer) compared to fresh ones. In addition, hypoxia (13% O_2) induced the formation of ectopic, nascent elastic fibers in the fibrosa layer of aged (> 2 years) PAV tissue compared to fresh and normoxic (20% O_2) ones, implying pathological alteration in elastic matrix composition. In a recent study by Fernandez Esmerats *et al*. (2019), it was found that low, oscillatory shear stress (i. e. disturbed flow) significantly upregulated HIF1A mRNA and protein expression in human aortic valve endothelial cells (HAVECs) compared to laminar shear stress (i. e. stable flow). Given that elevated stretch and low, oscillatory shear stress induce calcification in PAV leaflets (Balachandran *et al*., 2010; Rathan *et al*., 2011), these imply

that elevated stretch may not be a strong modulator of HIF1A mRNA expression in PAV leaflets compared to low, oscillatory shear stress. Since pathological (15%) stretch downregulated UBE2C mRNA expression in PAV leaflets compared to 10% (Figure 6.6), it can be assumed that there would be downregulation of UBE2C protein expression as well. Reduction in UBE2C protein expression would result in similar VHL protein (pVHL) expression under 15% stretch compared to 10%, since UBE2C protein has been shown to degrade VHL protein (pVHL) in human embryonic kidney (HEK) cells (Fernandez Esmerats *et al*., 2019). Similar VHL protein (pVHL) expression would result in similar HIF1A protein expression in PAV leaflets between 10% and 15% stretch, since VHL protein (pVHL) is known to degrade HIF1A protein (Maxwell *et al*., 1999). Consequently, it would be logical to observe no significant difference in HIF1A mRNA expression in PAV leaflets between 10% and 15% stretch (Figure 6.8). This is further validated in the study by Swaminathan *et al*. (2019), which showed that O_2 diffusion coefficient was essentially similar in PAV leaflets between 4.5 and 10.5 kPa pressure (i. e. different degree of leaflet stretching) under normoxic (20% O_2) condition.

7.19 HIF1A Inhibitor PX-478 and Porcine Aortic Valve (PAV) Calcification under Pathological (15%) Stretch

HIF1A inhibitor PX-478 (at 100 µM concentration) was found to significantly reduce PAV calcification under pathological (15%) stretch in osteogenic medium. This was observed as 36% (dry basis) and 62% (wet basis) decrease in PAV calcification under 15% stretch in the Arsenazo assay (Figures 6.9.1 and 6.9.2). On the other hand, when the concentration of PX-478 was reduced by half (i. e. 50 µM), it was found that there was no significant effect on PAV calcification under 15% stretch, as determined by Arsenazo assay

(Figures 6.9.3 and 6.9.4). However, Alizarin Red staining showed that 50 μM PX-478 significantly reduced PAV calcification under 15% stretch. This was observed as 86% decrease in the positively stained area (Figures 6.9.5.1 and 6.9.5.2). These imply that a higher concentration of PX-478 (such as 100 μM) had a significant effect on inhibiting PAV calcification under pathological (15%) stretch in osteogenic medium. However, a lower concentration of PX-478 (such as 50 μM) might impart some level of inhibitory effect on PAV calcification under 15% stretch. Furthermore, since there was no significant difference in HIF1A mRNA expression between 10% and 15% stretch in PAV leaflets (Figure 6.8), this indicates that PX-478 (especially at higher concentration) inhibits PAV calcification in a stretch-independent (within the 10 – 15% range) manner.

7.20 HIF1A Inhibitor PX-478 and Porcine Aortic Valve (PAV) Collagen Turnover under Pathological (15%) Stretch

HIF1A inhibitor PX-478 (at 50 μM concentration) was found to significantly reduce collagen turnover in PAV leaflets under pathological (15%) stretch in osteogenic medium. This was observed as 31% decrease in the ratio of immature-to-mature collagen fibers in PAV leaflets under 15% stretch in osteogenic medium, as determined by Picrosirius Red staining (Figures 6.10.1 and 6.10.2). Hutson *et al*. (2016) showed that there was significant alteration in the collagen fiber architecture of calcified human aortic valves (AVs) compared to healthy ones. Furthermore, immature collagen was found to be associated with regions of microcalcification in atherosclerotic plaques (Hutcheson *et al*., 2016). These imply that a lower concentration of PX-478 (such as 50 μM) could inhibit pathological collagen turnover (quantified as the ratio of immature-to-mature collagen) in PAV leaflets under 15% stretch in osteogenic medium. In addition, since there was no significant

difference in HIF1A mRNA expression between 10% and 15% stretch in PAV leaflets (Figure 6.8), this indicates that PX-478 (at lower concentration) inhibits PAV collagen turnover in a stretch-independent (within the 10 – 15% range) manner.

7.21 Overall Impact

Calcific aortic valve disease (CAVD) is one of the most prevalent heart valve diseases in the elderly population (Osnabrugge *et al*., 2013). There are no therapeutic drugs available to treat CAVD, mainly because of a lack of clear understanding of the disease mechanism. Since CAVD is complex and multifactorial in nature, one of the crucial steps in better understanding the disease mechanism is to decouple and evaluate the effects of different pathological cues on initiating and propagating CAVD. Elevated mechanical stretch, which can result from hypertension (Yap *et al*., 2010), is known to induce aortic valve (AV) calcification (Balachandran *et al*., 2010). However, the mechanobiological pathways that link elevated stretch and increased AV calcification are poorly understood. The research work presented in this dissertation shed some light on these mechanistic links by first evaluating the effects of physiological (10%) and pathological (15%) cyclic stretch on the expression levels of specific microRNAs (miRNAs) and messenger RNAs (mRNA) in relation to CAVD. Then, focused efforts were made in understanding the functional roles of one miRNA (miR-214) and one mRNA (UBE2C) in AV calcification. These, in turn, have provided us with two therapeutic targets to develop potential treatment options for CAVD. In addition, the presented work has significantly enriched our current understanding of AV mechanobiology and its relation to CAVD. Further assessment of the efficacy of miR-214 and UBE2C/HIF1A as potential therapeutic targets needs to be conducted in animal models of CAVD (Sider *et al*., 2011; Miller *et al*., 2011).

7.22 Limitations

The current work has some limitations. Firstly, healthy porcine aortic valve (PAV) leaflets were used for this research work, since it is impossible to obtain healthy human aortic valves (AVs) in sufficient number. However, the research findings should be equally applicable for human AVs since PAV is an established and widely used *ex vivo* model for studying CAVD (Balachandran *et al*., 2010). Secondly, uniaxial cyclic stretch was applied on PAV leaflets in the circumferential direction, although *in vivo* the AV experiences biaxial cyclic stretch in the radial and circumferential direction. However, the research findings should be equally significant since the AV tissue is stiffer in the circumferential direction due to preferential alignment of collagen fibers (Billiar *et al*., 2000). This implies that the AV tissue experiences significantly higher stress for a given stretch in the circumferential direction compared to the radial direction, which is more relevant in terms of modeling and studying CAVD *ex vivo*. Thirdly, protein expression was not extensively evaluated for the gene candidates in specific aim 2, although there can be difference in the mRNA and protein expression profile for a specific gene under the cyclic stretch conditions (due to post-translational modification, for example). A significant effort was made to quantify the protein expression of HIF1A; however, potentially due to its rapid degradation under normal oxygen tension, it was really difficult to quantify HIF1A protein expression in PAVs. Fourthly, there is a lack of knowledge on the exact binding mechanism (on a molecular level) and protein-drug interaction for HIF1A inhibitor PX-478, which was used in specific aim 2. This might entail some off-target effects associated with the use of PX-478. So, HIF1A-PX478 interaction studies need to be conducted on a molecular level to evaluate the exact binding mechanism and potential for off-target effects. Lastly, the *ex*

vivo experimental approach used in this dissertation might not capture the *in vivo* scenario where hypoxia may develop in a thicker (diseased) AV, resulting in an induction of HIF1A signaling. However, the goal for this dissertation research was to focus on the pathological events that precede the thickening of AV (i. e. disease). From that point-of-view, it was observed that pathological stretch did not significantly affect HIF1A mRNA expression in PAV compared to the physiological level, while there can be a difference in the protein expression (which was difficult to quantify due to its rapid degradation under normal oxygen tension).

CHAPTER 8. CONCLUSIONS AND FUTURE WORKS

8.1 Conclusions

In this dissertation, the effect of physiological (10%) and pathological (15%) cyclic stretch on the expression of specific miRNAs and mRNAs of interest [in relation to calcific aortic valve disease (CAVD)] in porcine aortic valve (PAV) leaflets was investigated. The major findings from this research work are as follows:

8.1.1 Specific Aim 1

8.1.1.1 Effect of Pathological Stretch on Different miRNA Expression

a. Pathological stretch

1. **Upregulates** miR-21-5p expression. Since elevated cyclic stretch is representative of hypertensive condition (Yap *et al*., 2010), this implies that hypertension may induce miR-21-5p expression in aortic valve (AV) compared to normotensive condition. Considering that hypertension is one of the major risk factors of CAVD (Rajamannan *et al*., 2011), this indicates that miR-21-5p may have a functional role in hypertension-induced AV pathogenesis and calcification.
2. **Significantly downregulates** miR-181a, miR-181b, miR-199a-3p and miR-214 expression. This implies that hypertension may reduce miR-181a, miR-181b, miR-199a-3p and miR-214 expression in AV compared to normotensive condition. This, in turn, indicates that miR-181a, miR-181b,

miR-199a-3p and miR-214 may have functional roles in hypertension-induced AV pathogenesis and calcification.

3. **Does not have any significant effect** on miR-122-5p and miR-483-3p expression. This implies that hypertension may not have any significant effect on miR-122-5p and miR-483-3p expression in AV compared to normotensive condition.

8.1.1.2 Effect of miR-214 Overexpression on PAV Calcification

a. miR-214 overexpression **significantly inhibits** PAV calcification under static and pathological stretch conditions. This indicates that miR-214 overexpression (using a synthetic miR-214 mimic) can be a potential therapeutic option for inhibiting hypertension-induced AV calcification, especially in the early stage of CAVD.

8.1.1.3 Effect of Pathological Stretch on TWIST1 mRNA Expression

a. Pathological stretch **significantly downregulates** TWIST1 mRNA expression, which is a positive regulator of miR-214. Since elevated cyclic stretch is representative of hypertensive condition (Yap *et al*., 2010), this implies that hypertension may reduce TWIST1 mRNA expression in AV compared to normotensive condition. Considering that hypertension is one of the major risk factors of CAVD (Rajamannan *et al*., 2011), this indicates that TWIST1 may have a functional role in hypertension-induced AV pathogenesis and calcification.

8.1.1.4 Effect of miR-214 Overexpression on Potential Target Gene Expression

a. miR-214 overexpression

1. **Significantly inhibits** the mRNA expression of its potential target genes RNF111, BCL2L1 and ATF4. This implies that three potential mechanistic pathways through which miR-214 can impart its regulatory effect on AV homeostasis and pathogenesis are via the modulation of RNF111, BCL2L1 and ATF4 mRNA expression.
2. **Does not have any significant effect** on the mRNA expression of its potential target gene XBP1. This indicates that miR-214 does not impart its regulatory effect on AV homeostasis and pathogenesis via modulation of XBP1 mRNA expression.

8.1.1.5 Effect of Pathological Stretch on Potential Target Gene Expression of miR-214

a. Pathological stretch

1. **Upregulates** ATF4 mRNA expression. Since elevated cyclic stretch is representative of hypertensive condition (Yap *et al*., 2010), this implies that hypertension may induce ATF4 mRNA expression in AV compared to normotensive condition. Considering that hypertension is one of the major risk factors of CAVD (Rajamannan *et al*., 2011), this indicates that ATF4 may have a functional role in hypertension-induced AV pathogenesis and calcification.
2. **Downregulates** BCL2L1 mRNA expression. This implies that hypertension may reduce BCL2L1 mRNA expression in AV compared to normotensive condition. This, in turn, indicates that BCL2L1 may have a functional role in hypertension-induced AV pathogenesis and calcification.

3. **Does not have any significant effect** on XBP1 and RNF111 mRNA expression. This implies that hypertension may not have any significant effect on XBP1 and RNF111 mRNA expression in AV compared to normotensive condition.

8.1.1.6 Potential Pathway

Pathological stretch significantly downregulates TWIST1 gene expression (which is anti-calcific in nature). This, in turn, significantly downregulates miR-214 expression. Downregulation of miR-214 expression results in the upregulation of its target gene ATF4 expression (which is pro-calcific in nature). This, in turn, significantly increases AV calcification under pathological stretch.

8.1.2 Specific Aim 2

8.1.2.1 Effect of Pathological Stretch on Different mRNA Expression

a. Pathological stretch

1. **Downregulates** YAP1 mRNA expression. Since elevated cyclic stretch is representative of hypertensive condition (Yap *et al*., 2010), this implies that hypertension may reduce YAP1 mRNA expression in AV compared to normotensive condition. Considering that hypertension is one of the major risk factors of CAVD (Rajamannan *et al*., 2011), this indicates that YAP1 may have a functional role in hypertension-induced AV pathogenesis and calcification.

2. **Significantly downregulates** UBE2C mRNA expression. This implies that hypertension may reduce UBE2C mRNA expression in AV compared to normotensive condition. This, in turn, indicates that UBE2C may have a functional role in hypertension-induced AV pathogenesis and calcification.
3. **Does not have any significant effect** on SOX9, ASH2L, ROR2 and ATP1A2 mRNA expression. This implies that hypertension may not have any significant effect on SOX9, ASH2L, ROR2 and ATP1A2 mRNA expression in AV compared to normotensive condition.

8.1.2.2 Effect of Pathological Stretch on VHL mRNA expression

a. Pathological stretch **does not have any significant effect** on VHL mRNA expression, which is a potential downstream target of UBE2C. This indicates that hypertension may not have any significant effect on VHL mRNA expression in AV compared to normotensive condition.

8.1.2.3 Effect of Pathological Stretch on HIF1A mRNA expression

a. Pathological stretch **does not have any significant effect** on HIF1A mRNA expression, which is a potential downstream target of VHL. This implies that hypertension may not have any significant effect on HIF1A mRNA expression in AV compared to normotensive condition.

8.1.2.4 Effect of HIF1A Inhibitor PX-478 on PAV Calcification

a. HIF1A inhibitor PX-478 **significantly reduces** PAV calcification under pathological stretch. This indicates that PX-478 can be a potential therapeutic

option for inhibiting hypertension-induced AV calcification, especially in the early stage of CAVD.

8.1.2.5 Effect of HIF1A Inhibitor PX-478 on PAV Collagen Turnover

a. HIF1A inhibitor PX-478 **significantly reduces** PAV collagen turnover under pathological stretch. This implies that PX-478 can be a potential therapeutic option for inhibiting hypertension-induced AV remodeling, especially in the early stage of CAVD.

8.1.2.6 Potential Pathway

Pathological stretch significantly downregulates UBE2C mRNA expression. However, the mRNA expression profiles of its downstream targets VHL and HIF1A are not significantly affected by pathological stretch. HIF1A inhibitor PX-478 significantly reduces PAV collagen turnover and calcification under pathological stretch. These imply that HIF1A may promote PAV calcification in a stretch-independent manner, while UBE2C may impart its stretch-dependent effect on PAV calcification via alternative stretch-sensitive downstream pathway other than VHL/HIF1A.

8.2 Future Works

Based on the abovementioned research findings, the following future works are suggested:

8.2.1 Specific Aim 1

a. Investigate the functional roles of miR-21-5p, miR-181a, miR-181b and miR-199a-3p in pathological stretch-induced AV calcification *ex vivo*

Since pathological stretch was found to upregulate miR-21-5p expression and significantly downregulate miR-181a, miR-181b, and miR-199a-3p expression in PAV compared to the physiological level, the logical next step would be to evaluate their functional role in PAV calcification. This will be accomplished by overexpression or inhibition of respective miRNA expression and evaluating their effect on PAV calcification (using Arsenazo assay and Alizarin Red staining) under 15% stretch in osteogenic medium.

b. Identify downstream regulatory pathways of miR-214 in relation to pathological stretch-induced AV calcification

It was found that miR-214 might impart its inhibitory effect on PAV calcification via downregulation of ATF4 expression. This is one potential pathway; however, there are several other genes (such as Ras-Related Protein RAB14) that miR-214 can potentially modulate (Tokar *et al*., 2018). To obtain a deeper understanding of the regulatory role of miR-214 in relation to CAVD, the effect of miR-214 on all major potential targets needs to be investigated. This will be accomplished by overexpressing miR-214 in PAVs under static culture in osteogenic medium and evaluating its effect on the mRNA expression of interest. Furthermore, the effects of physiological and pathological cyclic stretch on the expression of significant mRNA targets of miR-214 will be assessed to identify the most important ones in relation to stretch-induced AV pathogenesis.

c. Investigate the therapeutic effect of miR-214 overexpression on AV calcification *in vivo*

Since miR-214 overexpression was found to inhibit PAV calcification under both static and pathological stretch condition *ex vivo*, the logical next step would be to evaluate its effect on AV calcification and stenosis in an animal model of CAVD. Unfortunately, there is a lack of animal model of CAVD. Hence, the first effort in this direction will be to develop a good animal model of early stage CAVD. This will be attempted by inducing hypertension (via Angiotensin II infusion) in male wild-type C57BL/6J mice (Jackson Laboratory, Bar Habor, ME), which will be fed a pro-calcific diet (containing high vitamin D_3, for example).

8.2.2 Specific Aim 2

a. Investigate the functional roles of YAP1 in pathological stretch-induced AV calcification *ex vivo*

Since pathological stretch was found to downregulate YAP1 mRNA expression in PAV compared to the physiological level, the logical next step would be to evaluate its functional role in PAV calcification. This will be accomplished via inhibition of YAP1 mRNA and protein expression by Verteporfin (trade name: Visudyne; currently used in photodynamic therapy) and evaluating its effect on PAV calcification (using Arsenazo assay and Alizarin Red staining) under 15% stretch in osteogenic medium.

b. Identify downstream regulatory pathways of UBE2C in relation to pathological stretch-induced AV calcification

It was found that VHL/HIF1A pathway downstream of UBE2C was not stretch-sensitive in PAV. Since pathological stretch was found to significantly downregulate UBE2C mRNA expression in PAV compared to the physiological level, this implies that UBE2C may have other downstream pathways (such as Ubiquitin Protein Ligase E3D or UBE3D) that are significantly modulated by cyclic stretch. This will be accomplished by identifying such downstream pathways in bioinformatics databases (such as STRING database: https://string-db.org/) and evaluating the effect of UBE2C overexpression and inhibition on their mRNA and protein expression in PAV. In addition, the effects of physiological and pathological cyclic stretch on the expression of significant downstream targets of UBE2C will be assessed to identify the most important ones in relation to stretch-induced AV pathogenesis.

c. Examine the therapeutic effect of UBE2C overexpression on pathological stretch-induced AV calcification *ex vivo* and *in vivo*

Since pathological stretch was found to downregulate UBE2C mRNA expression in PAV compared to the physiological level, it will be important to evaluate its direct effect on PAV calcification. This will be accomplished via overexpression of UBE2C mRNA and protein expression by adenoviral vector and evaluating its effect on PAV calcification (using Arsenazo assay and Alizarin Red staining) under 15% stretch in osteogenic medium.

d. Investigate the therapeutic effect of HIF1A inhibition on AV calcification *in vivo*

Since HIF1A inhibitor PX-478 was found to inhibit PAV calcification under pathological stretch *ex vivo*, the logical next step would be to evaluate its effect on

AV calcification and stenosis in an animal model of CAVD. Unfortunately, there is a lack of animal model of CAVD. Hence, the first effort in this direction will be to develop a good animal model of early stage CAVD. This will be attempted by inducing hypertension (via Angiotensin II infusion) in male wild-type C57BL/6J mice (Jackson Laboratory, Bar Habor, ME), which will be fed a pro-calcific diet (containing high vitamin D_3, for example).

8.2.3 Beyond Dissertation

a. Design a robust and pulsatile organ culture system for AV that enables precise control of hemodynamic parameters, such as pressure and cardiac output

The research work presented in this dissertation focused on the effect of physiological and pathological cyclic stretch on specific miRNA and mRNA expression in relation to CAVD. However, the AV experiences different types of mechanical forces (such as tensile stretch and shear stress) simultaneously. Therefore, a robust and pulsatile organ culture system needs to be designed (using whole PAV including the aortic root, for example) that can experimentally simulate the *in vivo* functioning of AV under different hemodynamic conditions (such as hypertension, low cardiac output, high heart rate, etc.), while maintaining AV cell viability and system sterility over an extended period of time (3 – 4 weeks). Such an organ culture system will provide increased control and reproducibility over different hemodynamic parameters, as opposed to an animal model. This will be accomplished by building upon our laboratory's previous work in the area of organ culture systems.

b. Develop 3D-bioprinted AVs using human cells that can sustain the hemodynamic loads in a pulsatile organ culture system

One of the major challenges in the area of aortic valve mechanobiology in relation to CAVD is the inability to use human AV tissue for experimental purpose, since it is impossible to obtain healthy human AV tissue in sufficient number to conduct this type of studies. This can be overcome by 3D bioprinting of whole AV (including the aortic root) using healthy human AV cells (endothelial and interstitial). However, a major issue with such 3D bioprinted AVs is that these cannot withstand the hemodynamic forces as experienced by AV *in vivo*. Therefore, there is a need to engineer 3D bioprinted human AVs that are structurally similar to native AVs in terms of its ability to sustain *in vivo* type hemodynamic loads. This will be attempted, at first, by 3D bioprinting AVs comprising of collagen/elastin scaffold and human AV interstitial cells. Endothelial cells will be added separately to *line* the valve leaflet and luminal surfaces of the aortic root. The main goal will be to match the material properties of healthy human AVs while maximizing cell viability in the bioprinted valve.

c. Establish a robust animal model of CAVD that combines the effects of mechanical force (such as hypertension) and pro-calcific diet (such as high vitamin D_3)

One of the most significant problems in CAVD research is the lack of a good animal model. The author of this dissertation strongly believes that manipulation of hemodynamic loads (such as inducing hypertension) or diet (such high fat) alone is not sufficient to induce AV stenosis *in vivo* within a short period of time (3 – 4 months). However, a combination of these two factors may be able to induce and

accelerate AV disease within this period. Therefore, the underlying hypothesis here is that hypertension in combination with a pro-calcific diet can induce AV disease (at least the early stage of CAVD) in small animals. This will be accomplished by inducing hypertension (via infusion of Angiotensin II) in male (since CAVD is more prevalent in males than females) wild-type C57BL/6J mice, which will be fed a pro-calcific diet (containing high vitamin D_3).

APPENDIX

A.1 Stretch Programs (Si Programmer™ Software)

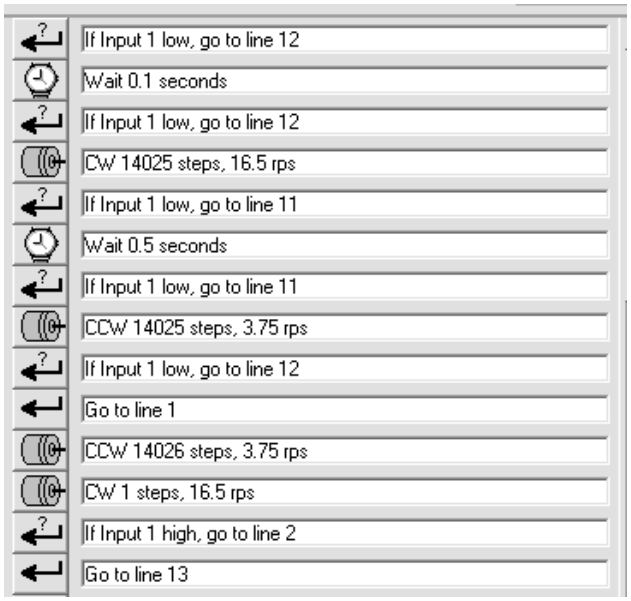

(a) 10% stretch program

(b) 15% stretch program

Figure A.1 – Stretch programs

A.2 Calcium Arsenazo Assay

A.2.1 Reagents:

- DPBS (THERMO FISHER SCIENTIFIC catalog no. 21600044)
- Acetic Acid 1 M (SIGMA ALDRICH catalog no. AX0073)
- Arsenazo III Reagent (POINTE SCIENTIFIC catalog no. C7529)
- Calcium Standard (0.5 mg/mL) (RICCA CHEMICAL COMPANY catalog no. 1799-16)

A.2.2 Procedure:

1. Measure the empty weight of each microcentrifuge tube.
2. Wash tissue samples three times with DPBS.
3. Use mortar and pestle to grind the tissue samples with liquid nitrogen and transfer each of these to a microcentrifuge tube.
4. Measure the combined weight of each microcentrifuge tube containing a wet tissue sample.
5. Incubate the tissue samples in a dryer at 37°C for 24 hours. Remember to keep the lids of the microcentrifuge tubes open.
6. Measure the combined weight of each microcentrifuge tube containing a dry tissue sample.
7. Add 500 µL of 1 M acetic acid to each microcentrifuge tube.
8. Vortex the tissue samples overnight (12 hours) in refrigerator.
9. Centrifuge the samples at 13,000xg for 10 minutes.
10. Transfer the supernatants to new microcentrifuge tubes.

11. Prepare calcium standards in 1 M acetic acid (0, 20, 40, 60, 80, 100 µg/mL).
12. Pipet 25 µL of each standard and sample in triplicate to a clear 96-well plate.
13. Add 300 µL of Arsenazo III reagent to each well (dilute sample if color change is more than that of maximum calcium standard).
14. Incubate for 30 seconds at room temperature.
15. Read the absorbance of each well in a plate reader at 650 nm (color is stable for 30 minutes).

A.3 Alizarin Red Stain

A.3.1 Reagents:

For Alizarin Red Solution:

- Alizarin Red S 2 g (SIGMA ALDRICH catalog no. A5533)
- DI water 100 mL
- 0.5% Ammonium Hydroxide (SIGMA ALDRICH catalog no. 320145)

Mix the solution, adjust the pH to 4.1 – 4.3 using 0.5% Ammonium Hydroxide. The pH is critical. Make fresh.

A.3.2 Procedure:

1. Rehydrate frozen sections in 70% ethanol.
2. Rinse with DI water at room temperature.
3. Incubate with Alizarin Red S solution for 30 seconds.
4. Shake off excess dye and blot sections using Kimwipes.

5. Dehydrate the slides in the autostainer.
6. Coverslip the slides and store at room temperature.

A.4 Von Kossa Stain

A.4.1 Reagents:

For 5% Silver Nitrate Solution (Stable for 1 year):

- Silver Nitrate 25 g (SIGMA ALDRICH catalog no. S8157)
- DI water 500 mL

Mix well, pour into a clean brown bottle and store in refrigerator at 4°C.

For 5% Sodium Thiosulfate (Make fresh):

- Sodium Thiosulfate 5 g (SIGMA ALDRICH catalog no. S7026)
- DI water 100 mL

For Nuclear Fast Red (Kernechtrot) Solution:

- Nuclear Fast Red 0.1 g (SIGMA ALDRICH catalog no. 229113)
- Aluminum Sulfate 5 g (SIGMA ALDRICH catalog no. 368458)
- DI water 100 mL
- Thymol 1 grain (SIGMA ALDRICH catalog no. T0501)

Dissolve aluminum sulfate in DI water. Add Nuclear Fast Red and slowly heat to boil and cool. Filter and add a grain of thymol as a preservative.

A.4.2 Procedure:

1. Rehydrate frozen sections in DI water at room temperature.
2. Incubate slides with 5% silver nitrate solution placed under a UV lamp. Place foil or mirror beneath the jar/tray to reflect the light. Leave for 1 hour or until calcium turns black.
3. Wash three times with DI water for 5 minutes at room temperature.
4. Wash one time with 5% sodium thiosulfate for 5 minutes at room temperature.
5. Wash one time with tap water, one time with DI water.
6. Incubate slides with Nuclear Fast Red for 5 minutes at room temperature.
7. Wash briefly with DI water.
8. Dehydrate the slides in the autostainer.
9. Coverslip the slides and store at room temperature.

A.5 Specific Aim 1 Data

Table A.5.1 – miR-21-5p expression in PAV leaflets.

Stretch	miR-21-5p Expression (Relative to U6)							
10%	0.76	1.13	2.29	0.46	0.46	1.51	0.39	
15%	9.45	18.20	8.08	11.86	0.45	0.08	0.08	0.70

Table A.5.2 – miR-483-3p expression in PAV leaflets.

Stretch	miR-483-3p Expression (Relative to U6)							
10%	1.39	1.32	1.45	1.34	0.43	0.77	0.31	
15%	1.22	0.87	1.01	1.10	0.45	0.19	0.27	0.92

Table A.5.3 – miR-181a expression in PAV leaflets.

Stretch	miR-181a Expression (Relative to U6)							
10%	0.49	0.67	2.17	0.91	0.60	0.60	1.74	0.82
15%	0.31	0.37	0.47	0.23	0.49	0.32	0.72	0.16

Table A.5.4 – miR-181b expression in PAV leaflets.

Stretch	miR-181b Expression (Relative to U6)

Table A.5.4 Continued

10%	1.15	1.22	0.90	0.53	0.66	1.54
15%	0.33	0.29	0.26	0.22	0.28	0.19

Table A.5.5 – miR-199a-3p expression in PAV leaflets.

Stretch	miR-199a-3p Expression (Relative to U6)					
10%	1.32	1.08	0.86	0.77	0.65	1.32
15%	0.35	0.42	0.33	0.16	0.20	0.15

Table A.5.6 – miR-122-5p expression in PAV leaflets.

Stretch	miR-122-5p Expression (Relative to U6)				
10%	0.39	1.09	2.05	0.47	
15%	0.89	0.08	1.02	0.39	0.55

Table A.5.7 – miR-214 expression in PAV leaflets.

Stretch	miR-214 Expression (Relative to U6)									
10%	2.11	1.45	0.79	0.57	0.57	1.98	0.27	0.74	0.53	
15%	0.65	0.18	0.50	0.08	0.36	0.38	0.12	0.22	0.32	0.08

Table A.5.8 – miR-214 expression in PAV leaflets after 2 weeks of static culture in osteogenic medium.

Mimic	miR-214 Expression (Relative to U6)							
Control	0.44	0.52	0.03	1.65	0.14	1.72	0.39	3.09
miR-214	116.48	46.69	414.78	27.93	251.68	16.59	484.29	

Table A.5.9.1 – PAV leaflet calcification (dry basis) after 2 weeks of static culture in osteogenic medium, as assessed by Arsenazo assay.

Mimic	Calcification (μg Ca/mg dry tissue)							
Control	15.57	20.35	22.88	29.72	4.78	19.80	32.23	27.17
miR-214	6.83	15.07	14.70	6.93	14.68	14.54	17.78	

Table A.5.9.2 – PAV leaflet calcification (wet basis) after 2 weeks of static culture in osteogenic medium, as assessed by Arsenazo assay.

Mimic	Calcification (μg Ca/mg wet tissue)							
Control	1.66	2.57	2.88	3.70	1.82	2.17	3.77	2.90
miR-214	1.80	1.95	2.16	2.08	2.01	1.99	2.17	

Table A.5.9.3 – Quantification of Alizarin Red staining images of PAV leaflets after 2 weeks of static culture in osteogenic medium.

Mimic	Positively Stained Area (% of Total Tissue Area)					
Control	1.70	2.07	3.26	2.88	1.64	1.74
miR-214	0.59	1.82	0.01	0.01	2.79	0.11

Table A.5.9.4 – Quantification of Von Kossa staining images of PAV leaflets after 2 weeks of static culture in osteogenic medium.

Mimic	Positively Stained Area (% of Total Tissue Area)					
Control	2.67	2.57	2.89	2.46		
miR-214	1.96	2.64	2.12	1.29	2.02	1.37

Table A.5.10 – miR-214 expression in PAV leaflets after 1 week of 15% stretch in osteogenic medium.

Mimic	miR-214 Expression (Relative to U6)						
Control	1.60	1.22	0.73	1.84	0.61	0.000019	
miR-214	7.11	6.78	12.95	9.48	4.50	8.29	11.86

Table A.5.11.1 – PAV leaflet calcification (dry basis) after 1 week of 15% stretch in osteogenic medium, as assessed by Arsenazo assay.

Mimic	Calcification (μg Ca/mg dry tissue)							
Control	37.73	18.00	30.49	24.94	27.31	29.75	38.19	27.63
miR-214	23.96	23.17	14.06	17.51	31.94	25.37	21.67	23.34

Table A.5.11.2 – PAV leaflet calcification (wet basis) after 1 week of 15% stretch in osteogenic medium, as assessed by Arsenazo assay.

Mimic	Calcification (μg Ca/mg wet tissue)							
Control	3.93	1.67	2.57	2.60	2.44	3.79	4.46	2.36
miR-214	2.52	2.55	1.28	1.15	2.92	1.99	2.03	1.87

Table A.5.12 – TWIST1 mRNA expression in PAV leaflets.

Stretch	TWIST1 mRNA Expression (Relative to 18S)							
10%	0.76	0.89	1.25	0.98	0.47	1.09	1.56	
15%	0.04	0.06	0.08	0.03	0.11	0.04	0.10	0.09

Table A.5.13.1 – miR-214 expression in PAV leaflets after 2 days of static culture in osteogenic medium.

Mimic	miR-214 Expression (Relative to U6)			
Control	2.92	0.06	0.27	0.75
miR-214	12603.12	29685.87	21714.01	570725.87

Table A.5.13.2 – XBP1 mRNA expression in PAV leaflets after 2 days of static culture in osteogenic medium.

Mimic	XBP1 mRNA Expression (Relative to 18S)							
Control	1.38	0.50	0.59	1.93	1.31	1.01	0.51	0.76
miR-214	0.53	1.43	1.01	1.28	0.71	1.19	0.57	

Table A.5.14 – XBP1 mRNA expression in PAV leaflets.

Stretch	XBP1 mRNA Expression (Relative to 18S)			
10%	2.35	0.59	0.46	0.60
15%	0.46	0.63	0.37	0.46

Table A.5.15 – RNF111 mRNA expression in PAV leaflets after 2 days of static culture in osteogenic medium.

Mimic	RNF111 mRNA Expression (Relative to 18S)					
Control	1.48	1.63	1.02	0.63	0.66	0.69
	0.44	1.16	1.09	1.24	1.04	0.92
miR-214	0.68	0.80	0.94	0.32	0.15	0.06
	0.74	0.37	0.89	1.11	0.92	0.78

Table A.5.16 – RNF111 mRNA expression in PAV leaflets.

Stretch	RNF111 mRNA Expression (Relative to 18S)					
10%	0.97	1.68	0.69	1.62	0.87	0.18
15%	2.62	1.98	1.85	0.86	0.07	0.10

Table A.5.17 – BCL2L1 mRNA expression in PAV leaflets after 2 days of static culture in osteogenic medium.

Mimic	BCL2L1 mRNA Expression (Relative to 18S)							
Control	1.25	1.22	0.47	1.45	0.67	1.08	0.85	
miR-214	0.90	0.71	1.06	1.02	0.08	0.09	0.36	0.42

Table A.5.18 – BCL2L1 mRNA expression in PAV leaflets.

Stretch	BCL2L1 mRNA Expression (Relative to 18S)							
10%	1.38	0.95	1.98	1.95	0.52	0.08	0.13	
15%	0.67	0.47	0.52	0.36	0.16	0.41	0.04	0.04

Table A.5.19 – ATF4 mRNA expression in PAV leaflets after 2 days of static culture in osteogenic medium.

Mimic	ATF4 mRNA Expression (Relative to 18S)							
Control	1.20	1.24	0.60	0.95	0.99	0.72	1.29	
miR-214	0.83	0.65	0.80	0.52	0.26	0.03	0.87	0.51

Table A.5.20 – ATF4 mRNA expression in PAV leaflets.

Stretch	ATF4 mRNA Expression (Relative to 18S)							
10%	0.73	1.16	1.74	1.39	0.56	0.81	0.61	
15%	4.07	5.04	2.64	1.94	1.21	1.24	0.53	0.49

A.6 Specific Aim 2 Data

Table A.6.1 – YAP1 mRNA expression in PAV leaflets.

Stretch	YAP1 mRNA Expression (Relative to 18S)				
10%	1.42	1.07	0.22	0.72	1.57
15%	0.73	0.12	0.13	0.39	0.60

Table A.6.2 – SOX9 mRNA expression in PAV leaflets.

Stretch	SOX9 mRNA Expression (Relative to 18S)					
10%	1.32	1.17	0.86	1.01	0.64	
15%	0.68	0.95	1.28	0.19	0.47	0.35

Table A.6.3 – ASH2L mRNA expression in PAV leaflets.

Stretch	ASH2L mRNA Expression (Relative to 18S)					
10%	0.95	0.65	1.30	1.27	0.88	0.96
15%	1.03	1.10	1.22	0.90	1.42	

Table A.6.4 – ROR2 mRNA expression in PAV leaflets.

Stretch	ROR2 mRNA Expression (Relative to 18S)					
10%	0.31	0.48	2.30	2.07	0.68	0.16

Table A.6.4 Continued

15%	0.71	0.10	1.46	0.30	0.82	

Table A.6.5 – ATP1A2 mRNA expression in PAV leaflets.

Stretch	ATP1A2 mRNA Expression (Relative to 18S)					
10%	2.48	1.00	1.35	1.06	0.07	0.05
15%	0.33	1.19	2.40	2.12	0.11	0.09

Table A.6.6 – UBE2C mRNA expression in PAV leaflets.

Stretch	UBE2C mRNA Expression (Relative to 18S)					
10%	1.37	0.64	1.07	1.11	0.52	1.29
15%	0.35	0.42	0.67	0.74	0.52	0.96

Table A.6.7 – VHL mRNA expression in PAV leaflets.

Stretch	VHL mRNA Expression (Relative to 18S)					
10%	2.27	0.38	0.83	0.60	1.28	0.64
15%	0.51	0.64	0.33	0.89	0.75	

Table A.6.8 – HIF1A mRNA expression in PAV leaflets.

Stretch	HIF1A mRNA Expression (Relative to 18S)				
10%	0.63	0.27	0.62	0.36	0.77

Table A.6.8 Continued

	0.79	2.20	1.38	1.81	1.18
15%	0.25	0.76	0.35	0.04	0.93
	1.92	0.77	0.35	1.23	0.14

Table A.6.9.1 – PAV leaflet calcification (dry basis) after 24 days of 15% stretch in osteogenic medium, as assessed by Arsenazo assay.

Group	Calcification (µg Ca/mg dry tissue)							
DPBS	25.35	65.61	30.30	30.58	44.64	84.57	47.04	37.37
PX-478 (100 µM)	18.02	27.50	35.09	35.23	27.98	23.53	28.82	38.51

Table A.6.9.2 – PAV leaflet calcification (wet basis) after 24 days of 15% stretch in osteogenic medium, as assessed by Arsenazo assay.

Group	Calcification (µg Ca/mg wet tissue)							
DPBS	3.66	11.79	3.48	2.80	4.36	13.35	5.66	3.35
PX-478 (100 µM)	1.24	2.30	2.65	2.89	2.47	1.72	2.08	3.30

Table A.6.9.3 – PAV leaflet calcification (dry basis) after 24 days of 15% stretch in osteogenic medium, as assessed by Arsenazo assay.

Group	Calcification (μg Ca/mg dry tissue)							
DPBS	25.35	65.61	30.30	30.58	44.64	84.57	47.04	37.37
PX-478 (50 μM)	45.38	30.62	30.64	59.45	55.89	36.05	44.14	86.50

Table A.6.9.4 – PAV leaflet calcification (wet basis) after 24 days of 15% stretch in osteogenic medium, as assessed by Arsenazo assay.

Group	Calcification (μg Ca/mg wet tissue)							
DPBS	3.66	11.79	3.48	2.80	4.36	13.35	5.66	3.35
PX-478 (50 μM)	4.18	4.05	2.93	8.67	6.78	4.13	5.59	10.35

Table A.6.9.5 – Quantification of Alizarin Red staining images of PAV leaflets after 24 days of 15% stretch in osteogenic medium.

Group	Positively Stained Area (% of Total Tissue Area)						
DPBS	1.00	1.83	14.68	40.21	39.10	40.74	22.40
PX-478 (50 μM)	0.79	5.31	2.47	6.26	0.80		

Table A.6.10 – Quantification of Picrosirius Red staining images of PAV leaflets after 24 days of 15% stretch in osteogenic medium.

Group	Sample	Ratio of Immature-to-Mature Collagen			
DPBS	1	0.31	0.42	0.50	0.48
		0.44	0.44	0.33	0.33
		0.35	0.15	0.39	0.39
		0.31	0.47	0.46	0.42
		0.57	0.44	0.56	0.46
	2	0.26	0.30	0.28	0.47
		0.49	0.42	0.34	0.28
		0.15			
	3	0.20	0.17	0.15	0.16
		0.14	0.12	0.16	0.18
		0.23			
	4	0.19	0.24	0.24	0.28
		0.24	0.30	0.22	0.23
		0.28			
	5	0.19	0.20	0.22	0.33
		0.34	0.30	0.32	0.39
		0.42	0.43	0.37	0.33
		0.34	0.28	0.18	0.23
		0.15			
	6	0.26	0.29	0.22	0.23

Table A.6.10 Continued

		0.19	0.15	0.18	0.19
		0.20	0.21		
	7	0.20	0.18	0.23	0.26
		0.22	0.16	0.15	0.20
		0.22	0.08		
PX-478 (50 µM)	1	0.21	0.14	0.24	0.26
		0.21	0.21	0.33	0.19
	2	0.11	0.14	0.14	0.20
		0.14	0.14	0.18	0.12
		0.15			
	3	0.23	0.22	0.14	0.14
		0.20	0.19	0.17	0.16
		0.23	0.21	0.24	0.15
		0.20	0.15	0.23	0.18
		0.22	0.10		
	4	0.04	0.13	0.19	0.23
		0.21	0.24	0.18	0.10
	5	0.31	0.29	0.29	0.20
		0.23			
	6	0.15	0.25	0.14	0.19
		0.18	0.21	0.21	0.22
		0.17	0.18		
	7	0.29	0.19	0.28	0.28

Table A.6.10 Continued

		0.21	0.26	0.20	0.26
		0.16			

REFERENCES

1. Albanese, I., Yu, B., Al-Kindi, H., Barratt, B., Ott, L., Al-Refai, M., ... & Schwertani, A. (2017). Role of noncanonical Wnt signaling pathway in human aortic valve calcification. Arteriosclerosis, thrombosis, and vascular biology, 37(3), 543-552.
2. Baden, L. R., El Sahly, H. M., Essink, B., Kotloff, K., Frey, S., Novak, R., ... & Zaks, T. (2021). Efficacy and safety of the mRNA-1273 SARS-CoV-2 vaccine. New England Journal of Medicine, 384(5), 403-416.
3. Balachandran, K. (2010). Aortic valve mechanobiology-the effect of cyclic stretch (Doctoral dissertation, Georgia Institute of Technology).
4. Balachandran, K., Sucosky, P., & Yoganathan, A. P. (2011). Hemodynamics and mechanobiology of aortic valve inflammation and calcification. International journal of inflammation, 2011.
5. Balachandran, K., Sucosky, P., Jo, H., & Yoganathan, A. P. (2009). Elevated cyclic stretch alters matrix remodeling in aortic valve cusps: implications for degenerative aortic valve disease. American Journal of Physiology-Heart and Circulatory Physiology, 296(3), H756-H764.
6. Balachandran, K., Sucosky, P., Jo, H., & Yoganathan, A. P. (2010). Elevated cyclic stretch induces aortic valve calcification in a bone morphogenic protein-dependent manner. The American journal of pathology, 177(1), 49-57.
7. Balogh, E., Tóth, A., Méhes, G., Trencsényi, G., Paragh, G., & Jeney, V. (2019). Hypoxia Triggers Osteochondrogenic Differentiation of Vascular Smooth Muscle Cells in an HIF-1 (Hypoxia-Inducible Factor 1)–Dependent and Reactive Oxygen

Species–Dependent Manner. Arteriosclerosis, thrombosis, and vascular biology, 39(6), 1088-1099.

8. Baumgarten, A., Bang, C., Tschirner, A., Engelmann, A., Adams, V., Von Haehling, S., ... & Springer, J. (2013). TWIST1 regulates the activity of ubiquitin proteasome system via the miR-199/214 cluster in human end-stage dilated cardiomyopathy. International journal of cardiology, 168(2), 1447-1452.
9. Billiar, K. L., & Sacks, M. S. (2000). Biaxial mechanical properties of the natural and glutaraldehyde treated aortic valve cusp—part I: experimental results. J. Biomech. Eng., 122(1), 23-30.
10. Billiar, K. L., & Sacks, M. S. (2000). Biaxial mechanical properties of the native and glutaraldehyde-treated aortic valve cusp: part II—a structural constitutive model. J. Biomech. Eng., 122(4), 327-335.
11. Bossé, Y., Miqdad, A., Fournier, D., Pépin, A., Pibarot, P., & Mathieu, P. (2009). Refining molecular pathways leading to calcific aortic valve stenosis by studying gene expression profile of normal and calcified stenotic human aortic valves. Circulation: Cardiovascular Genetics, 2(5), 489-498.
12. Butcher, J. T., & Nerem, R. M. (2006). Valvular endothelial cells regulate the phenotype of interstitial cells in co-culture: effects of steady shear stress. Tissue engineering, 12(4), 905-915.
13. Butcher, J. T., Penrod, A. M., García, A. J., & Nerem, R. M. (2004). Unique morphology and focal adhesion development of valvular endothelial cells in static and fluid flow environments. Arteriosclerosis, thrombosis, and vascular biology, 24(8), 1429-1434.

14. Butcher, J. T., Tressel, S., Johnson, T., Turner, D., Sorescu, G., Jo, H., & Nerem, R. M. (2006). Transcriptional profiles of valvular and vascular endothelial cells reveal phenotypic differences: influence of shear stress. Arteriosclerosis, thrombosis, and vascular biology, 26(1), 69-77.
15. Cai, Z., Li, F., Gong, W., Liu, W., Duan, Q., Chen, C., ... & Wang, D. W. (2013). Endoplasmic reticulum stress participates in aortic valve calcification in hypercholesterolemic animals. Arteriosclerosis, thrombosis, and vascular biology, 33(10), 2345-2354.
16. Cao, K., Bukač, M., & Sucosky, P. (2016). Three-dimensional macro-scale assessment of regional and temporal wall shear stress characteristics on aortic valve leaflets. Computer methods in biomechanics and biomedical engineering, 19(6), 603-613.
17. Chakraborty, S., Wirrig, E. E., Hinton, R. B., Merrill, W. H., Spicer, D. B., & Yutzey, K. E. (2010). Twist1 promotes heart valve cell proliferation and extracellular matrix gene expression during development in vivo and is expressed in human diseased aortic valves. Developmental biology, 347(1), 167-179.
18. Charitos, E. I., & Sievers, H. H. (2013). Anatomy of the aortic root: implications for valve-sparing surgery. Annals of cardiothoracic surgery, 2(1), 53.
19. Chen, J. H., & Simmons, C. A. (2011). Cell–matrix interactions in the pathobiology of calcific aortic valve disease: critical roles for matricellular, matricrine, and matrix mechanics cues. Circulation research, 108(12), 1510-1524.
20. Chen, L., Chen, R., Kemper, S., Charrier, A., & Brigstock, D. R. (2015). Suppression of fibrogenic signaling in hepatic stellate cells by Twist1-dependent microRNA-214

expression: Role of exosomes in horizontal transfer of Twist1. American Journal of Physiology-Gastrointestinal and Liver Physiology, 309(6), G491-G499.

21. Chen, S. I., Zheng, Y., Zhang, S., Jia, L., & Zhou, Y. (2017). Promotion effects of miR-375 on the osteogenic differentiation of human adipose-derived mesenchymal stem cells. Stem Cell Reports, 8(3), 773-786.
22. Chen, Y., Li, Z., Zhang, M., Wang, B., Ye, J., Zhang, Y., ... & Wang, S. (2019). Circ-ASH2L promotes tumor progression by sponging miR-34a to regulate Notch1 in pancreatic ductal adenocarcinoma. Journal of Experimental & Clinical Cancer Research, 38(1), 1-15.
23. Cheng, A., & Genever, P. G. (2010). SOX9 determines RUNX2 transactivity by directing intracellular degradation. Journal of Bone and Mineral Research, 25(12), 2680-2689.
24. Choi, B., Lee, S., Kim, S. M., Lee, E. J., Lee, S. R., Kim, D. H., ... & Song, J. K. (2017). Dipeptidyl peptidase-4 induces aortic valve calcification by inhibiting insulin-like growth factor-1 signaling in valvular interstitial cells. Circulation, 135(20), 1935-1950.
25. Chou, C. P., Huang, N. C., Jhuang, S. J., Pan, H. B., Peng, N. J., Cheng, J. T., ... & Chang, T. H. (2014). Ubiquitin-conjugating enzyme UBE2C is highly expressed in breast microcalcification lesions. PLoS One, 9(4), e93934.
26. Chu, Y., Lund, D. D., Doshi, H., Keen, H. L., Knudtson, K. L., Funk, N. D., ... & Heistad, D. D. (2016). Fibrotic aortic valve stenosis in hypercholesterolemic/hypertensive mice. Arteriosclerosis, thrombosis, and vascular biology, 36(3), 466-474.

27. Coffey, S., Williams, M. J., Phillips, L. V., Galvin, I. F., Bunton, R. W., & Jones, G. T. (2016). Integrated microRNA and messenger RNA analysis in aortic stenosis. Scientific reports, 6(1), 1-10.
28. Cowell, S. J., Newby, D. E., Prescott, R. J., Bloomfield, P., Reid, J., Northridge, D. B., & Boon, N. A. (2005). A randomized trial of intensive lipid-lowering therapy in calcific aortic stenosis. New England Journal of Medicine, 352(23), 2389-2397.
29. Cui, X., Tan, J., Shi, Y., Sun, C., Li, Y., Ji, C., ... & Liu, C. (2018). The long non-coding RNA Gm10768 activates hepatic gluconeogenesis by sequestering microRNA-214 in mice. Journal of Biological Chemistry, 293(11), 4097-4109.
30. Dahal, S., Huang, P., Murray, B. T., & Mahler, G. J. (2017). Endothelial to mesenchymal transformation is induced by altered extracellular matrix in aortic valve endothelial cells. Journal of Biomedical Materials Research Part A, 105(10), 2729-2741.
31. DECK, J. D. (1986). Endothelial cell orientation on aortic valve leaflets. Cardiovascular research, 20(10), 760-767.
32. Deng, X. S., Meng, X., Venardos, N., Song, R., Yamanaka, K., Fullerton, D., & Jaggers, J. (2017). Autophagy negatively regulates pro-osteogenic activity in human aortic valve interstitial cells. journal of surgical research, 218, 285-291.
33. Duan, Q., Wang, X., Gong, W., Ni, L., Chen, C., He, X., ... & Wang, D. W. (2012). ER stress negatively modulates the expression of the miR-199a/214 cluster to regulates tumor survival and progression in human hepatocellular cancer. PloS one, 7(2), e31518.
34. Duan, Q., Yang, L., Gong, W., Chaugai, S., Wang, F., Chen, C., ... & Wang, D. W. (2015). MicroRNA-214 is upregulated in heart failure patients and suppresses XBP1-

mediated endothelial cells angiogenesis. Journal of cellular physiology, 230(8), 1964-1973.

35. El Accaoui, R. N., Gould, S. T., Hajj, G. P., Chu, Y., Davis, M. K., Kraft, D. C., ... & Weiss, R. M. (2014). Aortic valve sclerosis in mice deficient in endothelial nitric oxide synthase. American Journal of Physiology-Heart and Circulatory Physiology, 306(9), H1302-H1313.
36. Fernandez Esmerats, J., Villa-Roel, N., Kumar, S., Gu, L., Salim, M. T., Ohh, M., ... & Jo, H. (2019). Disturbed flow increases UBE2C (Ubiquitin E2 Ligase C) via loss of miR-483-3p, inducing aortic valve calcification by the pVHL (von Hippel-Lindau Protein) and HIF-1α (Hypoxia-Inducible Factor-1α) pathway in endothelial cells. Arteriosclerosis, thrombosis, and vascular biology, 39(3), 467-481.
37. Fu, Z., Li, F., Jia, L., Su, S., Wang, Y., Cai, Z., & Xiang, M. (2019). Histone deacetylase 6 reduction promotes aortic valve calcification via an endoplasmic reticulum stress-mediated osteogenic pathway. The Journal of thoracic and cardiovascular surgery, 158(2), 408-417.
38. Gao, C., Hu, W., Liu, F., Zeng, Z., Zhu, Q., Fan, J., ... & Liu, X. (2021). Aldo-keto reductase family 1 member B induces aortic valve calcification by activating hippo signaling in valvular interstitial cells. Journal of Molecular and Cellular Cardiology, 150, 54-64.
39. Ge, L., & Sotiropoulos, F. (2010). Direction and magnitude of blood flow shear stresses on the leaflets of aortic valves: is there a link with valve calcification?. Journal of biomechanical engineering, 132(1).

40. Guo, L., Cai, T., Chen, K., Wang, R., Wang, J., Cui, C., ... & Wu, C. (2018). Kindlin-2 regulates mesenchymal stem cell differentiation through control of YAP1/TAZ. Journal of Cell Biology, 217(4), 1431-1451.
41. Guo, L., Ding, Z., Huang, N., Huang, Z., Zhang, N., & Xia, Z. (2017). Forkhead Box M1 positively regulates UBE2C and protects glioma cells from autophagic death. Cell Cycle, 16(18), 1705-1718.
42. Ha, M., & Kim, V. N. (2014). Regulation of microRNA biogenesis. Nature reviews Molecular cell biology, 15(8), 509-524.
43. Heath, J. M., Esmerats, J. F., Khambouneheuang, L., Kumar, S., Simmons, R., & Jo, H. (2018). Mechanosensitive microRNA-181b regulates aortic valve endothelial matrix degradation by targeting TIMP3. Cardiovascular engineering and technology, 9(2), 141-150.
44. Hjortnaes, J., Shapero, K., Goettsch, C., Hutcheson, J. D., Keegan, J., Kluin, J., ... & Aikawa, E. (2015). Valvular interstitial cells suppress calcification of valvular endothelial cells. Atherosclerosis, 242(1), 251-260.
45. Holliday, C. J., Ankeny, R. F., Jo, H., & Nerem, R. M. (2011). Discovery of shear-and side-specific mRNAs and miRNAs in human aortic valvular endothelial cells. American Journal of Physiology-Heart and Circulatory Physiology, 301(3), H856-H867.
46. Hori, D., Dunkerly-Eyring, B., Nomura, Y., Biswas, D., Steppan, J., Henao-Mejia, J., ... & Das, S. (2017). miR-181b regulates vascular stiffness age dependently in part by regulating TGF-β signaling. PloS one, 12(3), e0174108.

47. Huang, X. Z., Huang, J., Li, W. Z., Wang, J. J., Song, D. Y., & Ni, J. D. (2020). LncRNA-MALAT1 promotes osteogenic differentiation through regulating ATF4 by sponging miR-214: implication of steroid-induced avascular necrosis of the femoral head. Steroids, 154, 108533.
48. Huk, D. J., Austin, B. F., Horne, T. E., Hinton, R. B., Ray, W. C., Heistad, D. D., & Lincoln, J. (2016). Valve endothelial cell–derived Tgfβ1 signaling promotes nuclear localization of Sox9 in interstitial cells associated with attenuated calcification. Arteriosclerosis, thrombosis, and vascular biology, 36(2), 328-338.
49. Hutcheson, J. D., Aikawa, E., & Merryman, W. D. (2014). Potential drug targets for calcific aortic valve disease. Nature Reviews Cardiology, 11(4), 218.
50. Hutcheson, J. D., Goettsch, C., Bertazzo, S., Maldonado, N., Ruiz, J. L., Goh, W., ... & Aikawa, E. (2016). Genesis and growth of extracellular-vesicle-derived microcalcification in atherosclerotic plaques. Nature materials, 15(3), 335-343.
51. Hutson, H. N., Marohl, T., Anderson, M., Eliceiri, K., Campagnola, P., & Masters, K. S. (2016). Calcific aortic valve disease is associated with layer-specific alterations in collagen architecture. PloS one, 11(9), e0163858.
52. Idelevich, A., Rais, Y., & Monsonego-Ornan, E. (2011). Bone Gla protein increases HIF-1α–dependent glucose metabolism and induces cartilage and vascular calcification. Arteriosclerosis, thrombosis, and vascular biology, 31(9), e55-e71.
53. James, E. N., Van Doren, E., Li, C., & Kaplan, D. L. (2019). Silk biomaterials-mediated miRNA functionalized orthopedic devices. Tissue Engineering Part A, 25(1-2), 12-23.
54. Jian, B., Narula, N., Li, Q. Y., Mohler III, E. R., & Levy, R. J. (2003). Progression of aortic valve stenosis: TGF-β1 is present in calcified aortic valve cusps and promotes

aortic valve interstitial cell calcification via apoptosis. The Annals of thoracic surgery, 75(2), 457-465.

55. Kodali, S. K., Williams, M. R., Smith, C. R., Svensson, L. G., Webb, J. G., Makkar, R. R., ... & Leon, M. B. (2012). Two-year outcomes after transcatheter or surgical aortic-valve replacement. New England Journal of Medicine, 366(18), 1686-1695.
56. Koh, M. Y., Spivak-Kroizman, T., Venturini, S., Welsh, S., Williams, R. R., Kirkpatrick, D. L., & Powis, G. (2008). Molecular mechanisms for the activity of PX-478, an antitumor inhibitor of the hypoxia-inducible factor-1α. Molecular cancer therapeutics, 7(1), 90-100.
57. Koinuma, D., Shinozaki, M., Komuro, A., Goto, K., Saitoh, M., Hanyu, A., ... & Miyazono, K. (2003). Arkadia amplifies TGF-β superfamily signalling through degradation of Smad7. The EMBO journal, 22(24), 6458-6470.
58. Kvitting, J. P. E., Ebbers, T., Wigström, L., Engvall, J., Olin, C. L., & Bolger, A. F. (2004). Flow patterns in the aortic root and the aorta studied with time-resolved, 3-dimensional, phase-contrast magnetic resonance imaging: implications for aortic valve–sparing surgery. The Journal of thoracic and cardiovascular surgery, 127(6), 1602-1607.
59. Langille, B. L., & Adamson, S. L. (1981). Relationship between blood flow direction and endothelial cell orientation at arterial branch sites in rabbits and mice. Circulation research, 48(4), 481-488.
60. Lee, R. C., Feinbaum, R. L., & Ambros, V. (1993). The C. elegans heterochronic gene lin-4 encodes small RNAs with antisense complementarity to lin-14. cell, 75(5), 843-854.

61. Lee, Y. B., Bantounas, I., Lee, D. Y., Phylactou, L., Caldwell, M. A., & Uney, J. B. (2009). Twist-1 regulates the miR-199a/214 cluster during development. Nucleic acids research, 37(1), 123-128.

62. Leite, J. A., Isaksen, T. J., Heuck, A., Scavone, C., & Lykke-Hartmann, K. (2020). The α_2 Na^+/K^+-ATPase isoform mediates LPS-induced neuroinflammation. Scientific reports, 10(1), 1-21.

63. Leon, M. B., Smith, C. R., Mack, M. J., Makkar, R. R., Svensson, L. G., Kodali, S. K., ... & Webb, J. G. (2016). Transcatheter or surgical aortic-valve replacement in intermediate-risk patients. New England Journal of Medicine, 374(17), 1609-1620.

64. Leopold, J. A. (2012). Cellular mechanisms of aortic valve calcification. Circulation: Cardiovascular Interventions, 5(4), 605-614.

65. Li, F., Yao, Q., Ao, L., Cleveland, J. C., Dong, N., Fullerton, D. A., & Meng, X. (2017). Klotho suppresses high phosphate-induced osteogenic responses in human aortic valve interstitial cells through inhibition of Sox9. Journal of Molecular Medicine, 95(7), 739-751.

66. Li, K. C., Chang, Y. H., Hsu, M. N., Lo, S. C., Li, W. H., & Hu, Y. C. (2017). Baculovirus-mediated miR-214 knockdown shifts osteoporotic ASCs differentiation and improves osteoporotic bone defects repair. Scientific reports, 7(1), 1-13.

67. Li, K. C., Chang, Y. H., Yeh, C. L., & Hu, Y. C. (2016). Healing of osteoporotic bone defects by baculovirus-engineered bone marrow-derived MSCs expressing MicroRNA sponges. Biomaterials, 74, 155-166.

68. Li, K., Zhang, J., Yu, J., Liu, B., Guo, Y., Deng, J., ... & Guo, F. (2015). MicroRNA-214 suppresses gluconeogenesis by targeting activating transcriptional factor 4. Journal of Biological Chemistry, 290(13), 8185-8195.
69. Li, N., Bai, Y., Zhou, G., Ma, Y., Tan, M., Qiao, F., ... & Xu, Z. (2020). miR-214 attenuates aortic valve calcification by regulating osteogenic differentiation of valvular interstitial cells. Molecular Therapy-Nucleic Acids, 22, 971-980.
70. Liao, J., Hu, N., Zhou, N., Lin, L., Zhao, C., Yi, S., ... & Huang, W. (2014). Sox9 potentiates BMP2-induced chondrogenic differentiation and inhibits BMP2-induced osteogenic differentiation. PloS one, 9(2), e89025.
71. Liu, A. C., Joag, V. R., & Gotlieb, A. I. (2007). The emerging role of valve interstitial cell phenotypes in regulating heart valve pathobiology. The American journal of pathology, 171(5), 1407-1418.
72. Liu, J., Li, Y., Luo, M., Yuan, Z., & Liu, J. (2017). MicroRNA-214 inhibits the osteogenic differentiation of human osteoblasts through the direct regulation of baculoviral IAP repeat-containing 7. Experimental cell research, 351(2), 157-162.
73. Loebel, C., Czekanska, E. M., Bruderer, M., Salzmann, G., Alini, M., & Stoddart, M. J. (2015). In vitro osteogenic potential of human mesenchymal stem cells is predicted by Runx2/Sox9 ratio. Tissue Engineering Part A, 21(1-2), 115-123.
74. Ma, H., Killaars, A. R., DelRio, F. W., Yang, C., & Anseth, K. S. (2017). Myofibroblastic activation of valvular interstitial cells is modulated by spatial variations in matrix elasticity and its organization. Biomaterials, 131, 131-144.

75. Ma, S., Zhang, A., Li, X., Zhang, S., Liu, S., Zhao, H., ... & Zhao, H. (2020). MiR-21-5p regulates extracellular matrix degradation and angiogenesis in TMJOA by targeting Spry1. Arthritis research & therapy, 22, 1-17.
76. Mabry, K. M., Payne, S. Z., & Anseth, K. S. (2016). Microarray analyses to quantify advantages of 2D and 3D hydrogel culture systems in maintaining the native valvular interstitial cell phenotype. Biomaterials, 74, 31-41.
77. Mahler, G. J., Frendl, C. M., Cao, Q., & Butcher, J. T. (2014). Effects of shear stress pattern and magnitude on mesenchymal transformation and invasion of aortic valve endothelial cells. Biotechnology and bioengineering, 111(11), 2326-2337.
78. Markl, M., Draney, M. T., Miller, D. C., Levin, J. M., Williamson, E. E., Pelc, N. J., ... & Herfkens, R. J. (2005). Time-resolved three-dimensional magnetic resonance velocity mapping of aortic flow in healthy volunteers and patients after valve-sparing aortic root replacement. The Journal of thoracic and cardiovascular surgery, 130(2), 456-463.
79. Maxwell, P. H., Wiesener, M. S., Chang, G. W., Clifford, S. C., Vaux, E. C., Cockman, M. E., ... & Ratcliffe, P. J. (1999). The tumor suppressor protein VHL targets hypoxia-inducible factors for oxygen-dependent proteolysis. Nature, 399(6733), 271-275.
80. McManus, D. D., & Freedman, J. E. (2015). MicroRNAs in platelet function and cardiovascular disease. Nature Reviews Cardiology, 12(12), 711.
81. McRobb, L. S., McGrath, K. C., Tsatralis, T., Liong, E. C., Tan, J. T., Hughes, G., ... & Heather, A. K. (2017). Estrogen receptor control of atherosclerotic calcification and smooth muscle cell osteogenic differentiation. Arteriosclerosis, thrombosis, and vascular biology, 37(6), 1127-1137.

82. Mikels, A. J., & Nusse, R. (2006). Purified Wnt5a protein activates or inhibits β-catenin–TCF signaling depending on receptor context. PLoS Biol, 4(4), e115.
83. Miller, J. D., Weiss, R. M., & Heistad, D. D. (2011). Calcific aortic valve stenosis: methods, models, and mechanisms. Circulation research, 108(11), 1392-1412.
84. Mokas, S., Larivière, R., Lamalice, L., Gobeil, S., Cornfield, D. N., Agharazii, M., & Richard, D. E. (2016). Hypoxia-inducible factor-1 plays a role in phosphate-induced vascular smooth muscle cell calcification. Kidney international, 90(3), 598-609.
85. Nkomo, V. T., Gardin, J. M., Skelton, T. N., Gottdiener, J. S., Scott, C. G., & Enriquez-Sarano, M. (2006). Burden of valvular heart diseases: a population-based study. The Lancet, 368(9540), 1005-1011.
86. Oishi, I., Suzuki, H., Onishi, N., Takada, R., Kani, S., Ohkawara, B., ... & Minami, Y. (2003). The receptor tyrosine kinase Ror2 is involved in non-canonical Wnt5a/JNK signalling pathway. Genes to Cells, 8(7), 645-654.
87. Olson, E. N. (2014). MicroRNAs as therapeutic targets and biomarkers of cardiovascular disease. Science translational medicine, 6(239), 239ps3.
88. Osnabrugge, R. L., Mylotte, D., Head, S. J., Van Mieghem, N. M., Nkomo, V. T., LeReun, C. M., ... & Kappetein, A. P. (2013). Aortic stenosis in the elderly: disease prevalence and number of candidates for transcatheter aortic valve replacement: a meta-analysis and modeling study. Journal of the American College of Cardiology, 62(11), 1002-1012.
89. Parra-Izquierdo, I., Castaños-Mollor, I., López, J., Gómez, C., San Román, J. A., Crespo, M. S., & García-Rodríguez, C. (2019). Lipopolysaccharide and interferon-γ team up to activate HIF-1α via STAT1 in normoxia and exhibit sex differences in

human aortic valve interstitial cells. Biochimica et Biophysica Acta (BBA)-Molecular Basis of Disease, 1865(9), 2168-2179.

90. Peacock, J. D., Huk, D. J., Ediriweera, H. N., & Lincoln, J. (2011). Sox9 transcriptionally represses Spp1 to prevent matrix mineralization in maturing heart valves and chondrocytes. PloS one, 6(10), e26769.
91. Peacock, J. D., Levay, A. K., Gillaspie, D. B., Tao, G., & Lincoln, J. (2010). Reduced sox9 function promotes heart valve calcification phenotypes in vivo. Circulation research, 106(4), 712.
92. Peng, W., Zhu, S., Chen, J., Wang, J., Rong, Q., & Chen, S. (2019). Hsa_circRNA_33287 promotes the osteogenic differentiation of maxillary sinus membrane stem cells via miR-214-3p/Runx3. Biomedicine & Pharmacotherapy, 109, 1709-1717.
93. Perrotta, I., Moraca, F. M., Sciangula, A., Aquila, S., & Mazzulla, S. (2015). HIF-1α and VEGF: immunohistochemical profile and possible function in human aortic valve stenosis. Ultrastructural pathology, 39(3), 198-206.
94. Polack, F. P., Thomas, S. J., Kitchin, N., Absalon, J., Gurtman, A., Lockhart, S., ... & Gruber, W. C. (2020). Safety and efficacy of the BNT162b2 mRNA Covid-19 vaccine. New England Journal of Medicine, 383(27), 2603-2615.
95. Qi, J., Huo, L., Zhu, Y. T., & Zhu, Y. J. (2014). Absent, small or homeotic 2-like protein (ASH2L) enhances the transcription of the estrogen receptor α gene through GATA-binding protein 3 (GATA3). Journal of Biological Chemistry, 289(45), 31373-31381.

96. Quiat, D., & Olson, E. N. (2013). MicroRNAs in cardiovascular disease: from pathogenesis to prevention and treatment. The Journal of clinical investigation, 123(1), 11-18.

97. Rajamannan, N. M., Evans, F. J., Aikawa, E., Grande-Allen, K. J., Demer, L. L., Heistad, D. D., ... & Otto, C. M. (2011). Calcific aortic valve disease: Not simply a degenerative process a review and agenda for research from the National Heart and Lung and Blood Institute Aortic Stenosis Working Group. Circulation, 124(16), 1783.

98. Rathan, S. (2016). Aortic valve mechanobiology-role of altered hemodynamics in mediating aortic valve inflammation and calcification (Doctoral dissertation, Georgia Institute of Technology).

99. Rathan, S., Ankeny, C. J., Arjunon, S., Ferdous, Z., Kumar, S., Esmerats, J. F., ... & Jo, H. (2016). Identification of side-and shear-dependent microRNAs regulating porcine aortic valve pathogenesis. Scientific reports, 6(1), 1-16.

100. Rathan, S., Yap, C. H., Morris, E., Arjunon, S., Jo, H., & Yoganathan, A. P. (2011, June). Low and unsteady shear stresses upregulate calcification response of the aortic valve leaflets. In Summer Bioengineering Conference (Vol. 54587, pp. 245-246). American Society of Mechanical Engineers.

101. Remus, E. W., Lyle, A. N., Weiss, D., Landàzuri, N., Weber, M., Searles, C., & Taylor, W. R. (2013). miR181a protects against angiotensin II-induced osteopontin expression in vascular smooth muscle cells. Atherosclerosis, 228(1), 168-174.

102. Roberto, V. P., Gavaia, P., Nunes, M. J., Rodrigues, E., Cancela, M. L., & Tiago, D. M. (2018). Evidences for a New Role of miR-214 in Chondrogenesis. Scientific reports, 8(1), 1-16.

103. Romaine, S. P., Tomaszewski, M., Condorelli, G., & Samani, N. J. (2015). MicroRNAs in cardiovascular disease: an introduction for clinicians. Heart, 101(12), 921-928.

104. Ross Jr, J., & Braunwald, E. (1968). Aortic stenosis. Circulation, 38(1s5), V-61.

105. Rupaimoole, R., & Slack, F. J. (2017). MicroRNA therapeutics: towards a new era for the management of cancer and other diseases. Nature reviews Drug discovery, 16(3), 203.

106. Sacks, M. S., & Yoganathan, A. P. (2007). Heart valve function: a biomechanical perspective. Philosophical Transactions of the Royal Society B: Biological Sciences, 362(1484), 1369-1391.

107. Sahin, U., Karikó, K., & Türeci, Ö. (2014). mRNA-based therapeutics—developing a new class of drugs. Nature reviews Drug discovery, 13(10), 759-780.

108. Santoro, R., Scaini, D., Severino, L. U., Amadeo, F., Ferrari, S., Bernava, G., ... & Pesce, M. (2018). Activation of human aortic valve interstitial cells by local stiffness involves YAP-dependent transcriptional signaling. Biomaterials, 181, 268-279.

109. Seo, E., Basu-Roy, U., Gunaratne, P. H., Coarfa, C., Lim, D. S., Basilico, C., & Mansukhani, A. (2013). SOX2 regulates YAP1 to maintain stemness and determine cell fate in the osteo-adipo lineage. Cell reports, 3(6), 2075-2087.

110. Shah, M. Y., Ferrajoli, A., Sood, A. K., Lopez-Berestein, G., & Calin, G. A. (2016). microRNA therapeutics in cancer—an emerging concept. EBioMedicine, 12, 34-42.

111. Shapero, K., Wylie-Sears, J., Levine, R. A., Mayer Jr, J. E., & Bischoff, J. (2015). Reciprocal interactions between mitral valve endothelial and interstitial cells reduce

endothelial-to-mesenchymal transition and myofibroblastic activation. Journal of molecular and cellular cardiology, 80, 175-185.

112. Shen, W., Zhou, J., Wang, C., Xu, G., Wu, Y., & Hu, Z. (2017). High mobility group box 1 induces calcification of aortic valve interstitial cells via toll-like receptor 4. Molecular medicine reports, 15(5), 2530-2536.

113. Sider, K. L., Blaser, M. C., & Simmons, C. A. (2011). Animal models of calcific aortic valve disease. International journal of inflammation, 2011.

114. Smith, C. R., Leon, M. B., Mack, M. J., Miller, D. C., Moses, J. W., Svensson, L. G., ... & Pocock, S. J. (2011). Transcatheter versus surgical aortic-valve replacement in high-risk patients. New England Journal of Medicine, 364(23), 2187-2198.

115. Song, R., Fullerton, D. A., Ao, L., Zhao, K. S., Reece, T. B., Cleveland Jr, J. C., & Meng, X. (2017). Altered Micro RNA Expression Is Responsible for the Pro-Osteogenic Phenotype of Interstitial Cells in Calcified Human Aortic Valves. Journal of the American Heart Association, 6(4), e005364.

116. Sucosky, P., Balachandran, K., Elhammali, A., Jo, H., & Yoganathan, A. P. (2009). Altered shear stress stimulates upregulation of endothelial VCAM-1 and ICAM-1 in a BMP-4–and TGF-β1–dependent pathway. Arteriosclerosis, thrombosis, and vascular biology, 29(2), 254-260.

117. Sun, W., Julie Li, Y. S., Huang, H. D., Shyy, J. Y., & Chien, S. (2010). microRNA: a master regulator of cellular processes for bioengineering systems. Annual review of biomedical engineering, 12, 1-27.

118. Swaminathan, G., Krishnamurthy, V. K., Sridhar, S., Robson, D. C., Ning, Y., & Grande-Allen, K. J. (2019). Hypoxia stimulates synthesis of neutrophil gelatinase-

associated lipocalin in aortic valve disease. Frontiers in cardiovascular medicine, 6, 156.

119. Tao, G., Mao, P., Guan, H., Jiang, M., Chu, T., Zhong, C., & Liu, J. (2019). Effect of miR-181a-3p on osteogenic differentiation of human bone marrow-derived mesenchymal stem cells by targeting BMP10. Artificial cells, nanomedicine, and biotechnology, 47(1), 4159-4164.

120. Taylor, P. M., Batten, P., Brand, N. J., Thomas, P. S., & Yacoub, M. H. (2003). The cardiac valve interstitial cell. The international journal of biochemistry & cell biology, 35(2), 113-118.

121. Thubrikar, M. J., Aouad, J., & Nolan, S. P. (1986). Comparison of the in vivo and in vitro mechanical properties of aortic valve leaflets. The Journal of Thoracic and Cardiovascular Surgery, 92(1), 29-36.

122. Thubrikar, M. J., Nolan, S. P., Aouad, J., & Deck, J. D. (1986). Stress sharing between the sinus and leaflets of canine aortic valve. The Annals of thoracic surgery, 42(4), 434-440.

123. Thubrikar, M., Bosher, L. P., & Nolan, S. P. (1979). The mechanism of opening of the aortic valve. The Journal of thoracic and cardiovascular surgery, 77(6), 863-870.

124. Tibes, R. F. G. S., Falchook, G. S., Von Hoff, D. D., Weiss, G. J., Iyengar, T., Kurzrock, R., ... & Herbst, R. S. (2010). Results from a phase I, dose-escalation study of PX-478, an orally available inhibitor of HIF-1α. Journal of Clinical Oncology, 28(15_suppl), 3076-3076.

125. Tokar, T., Pastrello, C., Rossos, A. E., Abovsky, M., Hauschild, A. C., Tsay, M., ... & Jurisica, I. (2018). mirDIP 4.1—integrative database of human microRNA target predictions. Nucleic acids research, 46(D1), D360-D370.

126. Toshima, T., Watanabe, T., Narumi, T., Otaki, Y., Shishido, T., Aono, T., ... & Watanabe, M. (2020). Therapeutic inhibition of microRNA-34a ameliorates aortic valve calcification via modulation of Notch1-Runx2 signalling. Cardiovascular research, 116(5), 983-994.

127. Valenti, M. T., Deiana, M., Cheri, S., Dotta, M., Zamboni, F., Gabbiani, D., ... & Mottes, M. (2019). Physical exercise modulates miR-21-5p, miR-129-5p, miR-378-5p, and miR-188-5p expression in progenitor cells promoting osteogenesis. Cells, 8(7), 742.

128. Van der Ven, C. F., Wu, P. J., Tibbitt, M. W., Van Mil, A., Sluijter, J. P., Langer, R., & Aikawa, E. (2017). In vitro 3D model and miRNA drug delivery to target calcific aortic valve disease. Clinical Science, 131(3), 181-195.

129. Villa-Roel, N., Gu, L., Fernandez Esmerats, J., Kang, D. W., Kumar, S., & Jo, H. (2020). Hypoxia Inducible Factor-1α Inhibitor, PX-478, Reduces Atherosclerosis in vivo. Arteriosclerosis, Thrombosis, and Vascular Biology, 40(Suppl_1), A366-A366.

130. Wan, C., Gilbert, S. R., Wang, Y., Cao, X., Shen, X., Ramaswamy, G., ... & Clemens, T. L. (2008). Activation of the hypoxia-inducible factor-1α pathway accelerates bone regeneration. Proceedings of the National Academy of Sciences, 105(2), 686-691.

131. Wang, B., Cai, Z., Liu, B., Liu, Z., Zhou, X., Dong, N., & Li, F. (2017). RAGE deficiency alleviates aortic valve calcification in ApoE−/− mice via the inhibition of

endoplasmic reticulum stress. Biochimica et Biophysica Acta (BBA)-Molecular Basis of Disease, 1863(3), 781-792.

132. Wang, H., Shi, J., Li, B., Zhou, Q., Kong, X., & Bei, Y. (2017). MicroRNA expression signature in human calcific aortic valve disease. BioMed research international, 2017.

133. Wang, H., Wang, Z., & Tang, Q. (2018). Reduced expression of microRNA-199a-3p is associated with vascular endothelial cell injury induced by type 2 diabetes mellitus. Experimental and therapeutic medicine, 16(4), 3639-3645.

134. Wang, J., Lu, Z., Xu, Z., Tian, P., Miao, H., Pan, S., ... & Jiang, H. (2017). Reduction of hepatic fibrosis by overexpression of von Hippel–Lindau protein in experimental models of chronic liver disease. Scientific reports, 7(1), 1-13.

135. Wang, L., Chennupati, R., Jin, Y. J., Li, R., Wang, S., Günther, S., & Offermanns, S. (2020). YAP/TAZ are required to suppress osteogenic differentiation of vascular smooth muscle cells. Iscience, 23(12), 101860.

136. Wang, X., Guo, B., Li, Q., Peng, J., Yang, Z., Wang, A., ... & Li, Y. (2013). miR-214 targets ATF4 to inhibit bone formation. Nature medicine, 19(1), 93-100.

137. Warnock, J. N., Nanduri, B., Pregonero Gamez, C. A., Tang, J., Koback, D., Muir, W. M., & Burgess, S. C. (2011). Gene profiling of aortic valve interstitial cells under elevated pressure conditions: modulation of inflammatory gene networks. International journal of inflammation, 2011.

138. Wei, Z., Liu, J., Xie, H., Wang, B., Wu, J., & Zhu, Z. (2021). MiR-122-5p Mitigates Inflammation, Reactive Oxygen Species and SH-SY5Y Apoptosis by Targeting

CPEB1 After Spinal Cord Injury Via the PI3K/AKT Signaling Pathway. Neurochemical Research, 1-14.

139. Wiltz, D., Arevalos, C. A., Balaoing, L. R., Blancas, A. A., Sapp, M. C., Zhang, X., & Grande-Allen, K. J. (2013). Extracellular matrix organization, structure, and function. Calcific aortic valve disease, 3-30.

140. Wu, J. C., Sun, J., Xu, J. C., Zhou, Z. Y., & Zhang, Y. F. (2021). Downregulated microRNA-199a-3p enhances osteogenic differentiation of bone marrow mesenchymal stem cells by targeting Kdm3a in ovariectomized rats. Biochemical Journal.

141. Xin, H., Xin, F., Zhou, S., & Guan, S. (2013). The Wnt5a/Ror2 pathway is associated with determination of the differentiation fate of bone marrow mesenchymal stem cells in vascular calcification. International journal of molecular medicine, 31(3), 583-588.

142. Yang, L., Ge, D., Cao, X., Ge, Y., Chen, H., Wang, W., & Zhang, H. (2016). MiR-214 attenuates osteogenic differentiation of mesenchymal stem cells via targeting FGFR1. Cellular Physiology and Biochemistry, 38(2), 809-820.

143. Yang, X., & Karsenty, G. (2004). ATF4, the osteoblast accumulation of which is determined post-translationally, can induce osteoblast-specific gene expression in non-osteoblastic cells. Journal of Biological Chemistry, 279(45), 47109-47114.

144. Yang, X., Matsuda, K., Bialek, P., Jacquot, S., Masuoka, H. C., Schinke, T., ... & Karsenty, G. (2004). ATF4 is a substrate of RSK2 and an essential regulator of osteoblast biology: implication for Coffin-Lowry syndrome. Cell, 117(3), 387-398.

145. Yao, Q., Song, R., Ao, L., Cleveland Jr, J. C., Fullerton, D. A., & Meng, X. (2017). Neurotrophin 3 upregulates proliferation and collagen production in human aortic valve

interstitial cells: a potential role in aortic valve sclerosis. American Journal of Physiology-Cell Physiology, 312(6), C697-C706.

146. Yao, S., Zhao, W., Ou, Q., Liang, L., Lin, X., & Wang, Y. (2017). MicroRNA-214 suppresses osteogenic differentiation of human periodontal ligament stem cells by targeting ATF4. Stem cells international, 2017.

147. Yap, C. H., Kim, H. S., Balachandran, K., Weiler, M., Haj-Ali, R., & Yoganathan, A. P. (2010). Dynamic deformation characteristics of porcine aortic valve leaflet under normal and hypertensive conditions. American Journal of Physiology-Heart and Circulatory Physiology, 298(2), H395-H405.

148. Yap, C. H., Saikrishnan, N., & Yoganathan, A. P. (2012). Experimental measurement of dynamic fluid shear stress on the ventricular surface of the aortic valve leaflet. Biomechanics and modeling in mechanobiology, 11(1), 231-244.

149. Yap, C. H., Saikrishnan, N., Tamilselvan, G., & Yoganathan, A. P. (2012). Experimental measurement of dynamic fluid shear stress on the aortic surface of the aortic valve leaflet. Biomechanics and modeling in mechanobiology, 11(1), 171-182.

150. Yin, G., Chen, R., Alvero, A. B., Fu, H. H., Holmberg, J., Glackin, C., ... & Mor, G. (2010). TWISTing stemness, inflammation and proliferation of epithelial ovarian cancer cells through MIR199A2/214. Oncogene, 29(24), 3545-3553.

151. Yuan, X., Lin, Z., Luo, S., Ji, G., Yuan, C., & Wu, Y. (2007). Effects of different magnitudes of cyclic stretch on Na^+-K^+-ATPase in skeletal muscle cells in vitro. Journal of cellular physiology, 212(2), 509-518.

152. Yutzey, K. E., Demer, L. L., Body, S. C., Huggins, G. S., Towler, D. A., Giachelli, C. M., ... & Aikawa, E. (2014). Calcific aortic valve disease: a consensus summary

from the Alliance of Investigators on Calcific Aortic Valve Disease. Arteriosclerosis, thrombosis, and vascular biology, 34(11), 2387-2393.

153. Zeng, Q., Song, R., Fullerton, D. A., Ao, L., Zhai, Y., Li, S., ... & Meng, X. (2017). Interleukin-37 suppresses the osteogenic responses of human aortic valve interstitial cells in vitro and alleviates valve lesions in mice. Proceedings of the National Academy of Sciences, 114(7), 1631-1636.

154. Zhang, J., He, Y., Yan, X., Chen, S., He, M., Lei, Y., ... & Shyy, J. Y. J. (2020). Micro RNA-483 amelioration of experimental pulmonary hypertension. EMBO molecular medicine, 12(5), e11303.

155. Zhang, X. W., Zhang, B. Y., Wang, S. W., Gong, D. J., Han, L., Xu, Z. Y., & Liu, X. H. (2014). Twist-related protein 1 negatively regulated osteoblastic transdifferentiation of human aortic valve interstitial cells by directly inhibiting runt-related transcription factor 2. The Journal of thoracic and cardiovascular surgery, 148(4), 1700-1708.

156. Zheng, D., Wang, B., Zhu, X., Hu, J., Sun, J., Xuan, J., & Ge, Z. (2019). LncRNA OIP5-AS1 inhibits osteoblast differentiation of valve interstitial cells via miR-137/TWIST11 axis. Biochemical and biophysical research communications, 511(4), 826-832.

157. Zhou, G., Zheng, Q., Engin, F., Munivez, E., Chen, Y., Sebald, E., ... & Lee, B. (2006). Dominance of SOX9 function over RUNX2 during skeletogenesis. Proceedings of the National Academy of Sciences, 103(50), 19004-19009.

158. Zhou, Q., Chen, T., Zhang, W., Bozkanat, M., Li, Y., Xiao, L., ... & Zhou, G. (2016). Suppression of von Hippel-Lindau protein in fibroblasts protects against

bleomycin-induced pulmonary fibrosis. American journal of respiratory cell and molecular biology, 54(5), 728-739.

159. Zhou, S. S., Jin, J. P., Wang, J. Q., Zhang, Z. G., Freedman, J. H., Zheng, Y., & Cai, L. (2018). miRNAS in cardiovascular diseases: potential biomarkers, therapeutic targets and challenges. Acta Pharmacologica Sinica, 39(7), 1073-1084.

160. Zhou, T., Han, D., Liu, J., Shi, J., Zhu, P., Wang, Y., & Dong, N. (2019). Factors influencing osteogenic differentiation of human aortic valve interstitial cells. The Journal of thoracic and cardiovascular surgery.

161. Zhu, M. E., Fang, X., Zhou, S., Li, W., & Guan, S. (2016). Indirect co-culture of vascular smooth muscle cells with bone marrow mesenchymal stem cells inhibits vascular calcification and downregulates the Wnt signaling pathways. Molecular medicine reports, 13(6), 5141-5148.

162. Zhu, Y., Ma, W. Q., Han, X. Q., Wang, Y., Wang, X., & Liu, N. F. (2018). Advanced glycation end products accelerate calcification in VSMCs through HIF-1α/PDK4 activation and suppress glucose metabolism. Scientific reports, 8(1), 1-12.